BIOSYNTHESIS OF ZINC SULPHIDE (ZnS) NANOPARTICLES FROM ENDOPHYTIC FUNGUS *ASPERGILLUS FLAVUS* FOR DEGRADATION OF ORGANIC POLLUTANTS

Thesis

Submitted in partial fulfillment of the requirements for the degree of

DOCTOR OF PHILOSOPHY

by

U. PRIYANKA
(148021CH14F09)

DEPARTMENT OF CHEMICAL ENGINEERING

NATIONAL INSTITUTE OF TECHNOLOGY KARNATAKA,

SURATHKAL, MANGALORE - 575025

March, 2019

D E C L A R A T I O N

I hereby *declare* that the Research thesis entitled **"Biosynthesis of Zinc Sulphide (ZnS) nanoparticles from endophytic fungus *Aspergillus flavus* for degradation of organic pollutants"** which is being submitted to the **National Institute of Technology Karnataka, Surathkal** in partial fulfillment of the requirements for the award of the Degree of **Doctor of Philosophy** in Chemical Engineering is a *bonafide report of the research work carried out by me*. The material contained in this **Research Thesis** has not been submitted to any University or Institution for the award of any degree.

<div align="right">

PRIYANKA U.

Register No. CH14F09

Department of Chemical Engineering

National Institute of Technology Karnataka, Surathkal

</div>

Place: NITK-Surathkal

Date:

C E R T I F I C A T E

This is to *certify* that the Research Thesis entitled **"Biosynthesis of Zinc Sulphide (ZnS) nanoparticles from endophytic fungus *Aspergillus flavus* for degradation of organic pollutants"** submitted by **Priyanka U.** (Register Number: CH14F09) as the record of the research work carried out by him*, is accepted as the Research Thesis submission* in partial fulfillment of the requirements for the award of degree of **Doctor of Philosophy**.

Research Guide

Dr. Raj Mohan B

Chairman – DRPC

ACKNOWLEDGEMENTS

ABSTRACT

Wastewater treatment is adopted from ages but the efficiency, time constraint, environmental friendliness and cost-effectiveness are the key aspects for applicability of any technique. Globally, large amounts of wastewater containing organic pollutants from various industries are being discharged into the environment. These emerging contaminants are persistently released into the oceanic environment majorly from manufacturing industries, consumers utility and effluent treatment plants. In this aspect naophotocatalysis with the amalgamation of a biological source has been explored where ZnS nanoparticles have been synthesized by endophytic fungal isolate *Aspergillus flavus* via a medicinal plant *Nothapodytes foetida*. Significant findings from the characterization study include the formation of spherical particles with an average diameter of about 18 nm by TEM and hydrodynamic diameter of 58.9 nm. Optical properties confirm the quantum confinement effect and the functional groups present on the surface of the nanoparticles, further the stability of nanoparticles is accessed by UV–Vis spectrometer, zeta potential and cyclic voltammeter. XRD reveals the phase structure and the crystallinity indicating the hexagonal phase of ZnS and diffraction peaks at 28.45º, 47.54º, 57º (2θ). The degradation efficiency of ZnS nanoparticles for methyl violet/ 2,4-dichlorophenoxyacetic acid / paracetamol are 87 % in 2 h, 33 % in 4.5 h and 51 % in 4 h respectively and the impact of various parameters on the photocatalytic activity is also investigated. The experimental results of COD and TOC are 78 % and 74 % for methyl violet; 55.5 % and 57.2 % for 2,4- dichlorophenoxyacetic acid; 47.6% and 44.5% for paracetamol respectively. Moreover, the plausible mechanism on the radical generation from ZnS nanoparticles upon irradiation for the degradation process is hypothesized based on the mass spectrum. In addition, the interaction between organic pollutants and ZnS nanoparticles is also elucidated based on AFM and fluorescence spectrum. Investigations reveal that the mechanism involved is extracellular based on micrographs/chromatogram and the peaks at 149, 301 and 579 (m/z) corresponds to proteins such as metallothioneins and phytochelatins. The formation of nanoparticles production is obtained at optimum inoculum volume of 10 % (w/v) at working volume of 1 L and agitation speed 80 rpm. XRD and TEM analysis confirmed the hexagonal phase of nanoparticles with the average diameter of 10-15 nm at an optimum concentration of 30 mM for 72 h.

Keywords: 2,4- dichlorophenoxyacetic acid, *Aspergillus flavus,* endophytic fungi, methyl violet, *Nothapodytes foetida*, paracetamol, ZnS nanoparticles

CONTENTS

LIST OF TABLES

LIST OF FIGURES

LIST OF ABBREVATIONS

TITLE	ABBREVIATION
Advanced oxidation processes	AOPs
Atomic Force Microscope	AFM
Chemical oxygen demand	COD
Dynamic light scattering	DLS
Diffuse reflectance spectroscopy	DRS
Economic Co-operation and Development	OECD
Environmental Protection Act	EPA
Energy Dispersive Analyses of X-rays	EDAX
Fourier Transfer Infra-Red Spectrometer	FTIR
High-performance liquid chromatography	HPLC
International Center for Diffraction Data	ICDD
Lethal dosage	LD_{50}
Liquid chromatography-Mass spectrometry	LC-MS
Methyl violet	MV
Nanoparticles	NPs
Paracetamol	PARA
Potato Dextrose Agar	PDA
Potato Dextrose Broth	PDB
Reactive oxygen species	ROS
Scanning Electron Microscope	SEM
Transmission Electron Microscopy	TEM
Total organic carbon	TOC
Ultraviolet-visible spectrophotometer	UV-Vis

United State Environmental Protection Agency	USEPA
World Health Organization	WHO
X-ray diffraction	XRD
Zinc sulphide	ZnS
2,4- dichlorophenoxy acetic acid	2,4-D

CHAPTER 1

1. INTRODUCTION

1. 1.   Background

Pollution can be characterized as an undesirable change in the aspects of physical, chemical and biological characteristics of the environment. The introduction of harmful substances into the environment by man's activities cause ecological damage or interfere with legitimate use of the environment. Due to the Industrial Revolution, innovation grew rapidly, science became advanced, technological age came into view and humans were able to advance further into the 21st century. This led to an increase in the environmental pollution over years inflicting an irreparable damage to the world. Waterborne contaminants entering rivers and streams are one of the most crucial environmental problems which are causing tremendous devastation. Despite the water contamination occurred by natural phenomenon through characteristic procedures, it is generally a consequence of human activities resulting in health risks for millions of people. As quoted by Alanis Obomsawin *"When the last tree is cut, the last fish is caught and the last river is polluted; when to breathe the air is sickening, you will realize, too late, the wealth is not in bank accounts and that you can't eat money"* this statement gives a view that there is a urgent need to mitigate the pollution.

Industries generate huge quantities of wastewaters containing dyes, detergents, petrochemicals, fertilizers, pesticides, plasticizers, pharmaceuticals, etc. which pose a major threat to the ecosystems as they contain chemicals which are highly toxic and structurally complex. Most of the industrial wastewaters that are released into the environment without any appropriate treatment had resulted in adverse effects on aquatic biota and human life. These lead to a drastic change in many of the aquatic systems across the world. Effluents generated from various industries contain complex organic pollutants out of which synthetic dyes contribute around 7,00,000 tons annually around the world and 20 % of them are unloaded as industrial wastes without proper treatment (Nezamzadeh-Ejhieh and Banan 2012; El-Gamal et al. 2015; Bogireddy et al. 2016). Significant quantities of triarylmethane dyes such as crystal violet and malachite green were found in the sediments and water of Buffalo River, New York, USA. These chemicals have been suggested to be responsible for the promotion of tumor growths in several scavenger species of fishes. Methyl violet (MV) dye is classified as cationic triarylmethane dye and it is a major ingredient of inks used in printings, ballpoint pens, paints,

cartridges, etc. MV has high color intensity causing inhibition of sunlight penetrating through water (Shamsipur and Rajabi 2014). The dye waters are impervious to aerobic biodegradation and their half-lives under sunlight are more noteworthy than 2000 h affecting the development of aquatic plants (Singh et al. 2011; Jafari et al. 2012; Soltani and Entezari 2013). Prolonged exposure of dyes causes numerous problems such as damage to organs, skin cancer, cell lysis etc. due to their mutagenic nature (Jeyasubramanian et al. 2015).

Similarly, effluents from agricultural residues and pharmaceutical industries containing phenols are considered as hazardous pollutants as they include endocrine disrupting chemicals due to the presence of chlorinated and nitro-substituted phenolic compounds (Akpan and Hameed 2011; Chauhan et al. 2013). Phenolic components are one of the priority pollutants present in the water bodies and are considered as major toxic pollutants by United State Environmental Protection Agency (USEPA) (Boruah et al. 2017) with a permissible limit less than 0.5 mg/L.
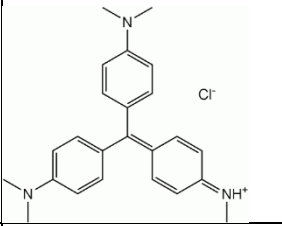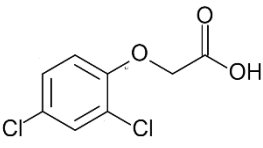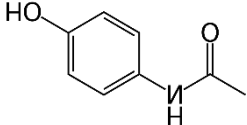
In the agricultural lands, there is a need to eradicate undesirable herbs/pests which destroy the farmland to protect the crop harvests, in this regard, pesticides/herbicides are the commonly used industrial chemicals to protect them. Reports demonstrated that herbicide, 2,4-dichlorophenoxyacetic acid (2,4-D) is one of the primary ingredients among 1500 pesticides for specific control of weeds in yard nurseries and farmlands. 2,4-D is one of the globally used herbicide since 1968 which is often present in soil, food and water resources due to their large applications in agricultural fields (Conte et al. 2016; Luna et al. 2012). The 2,4-D is used in Brazilian farming to dispense with wide leaf weeds in sugar cane crops and it is further regarded as the second most utilized herbicide in Argentina. As these herbicides are used regularly, their concentration in the water bodies is increasing tremendously. Moreover, at any point of rainfall, it is eroded into the water channels and groundwater damaging the horticultural zones and ends up scattered in the oceanic condition by means of horticultural streams or leaching. In view of the medical issues related to 2,4-D, Environmental Protection Act (EPA) reported it as a toxin and the World Health Organization (WHO) considered this it as a class II sensibly destructive herbicide. It is evaluated that the normal yearly pesticide used in Organisation for Economic Co-operation and Development (OECD) part nations is 0.22 t/km^2. Furthermore, International Agency for Research on Cancer (IARC) declared 2,4-D as class 2B carcinogen, due to its lethal dosage (LD$_{50}$) of 100 and 500 mg/kg (Chen et al. 2016; Samir et al. 2015).

The presence of active pharmaceuticals ingredients in aquatic environments was reported in the 1980's (Juan et al. 2010). Phenol is a vital industrial crude material utilized as often as possible in the production of pharmaceutical compounds, such as diclofenac, amoxicillin and

paracetamol. Pharmaceuticals are subclasses of organic contaminants that have been recognized as emerging pollutants in wastewaters and surface waters all through the world which are consistently brought into the aquatic environment by several emissions from manufacturing facilities, consumer utility and hospital disposal sites. Despite the fact that the identified fixations are regularly in the range of ng to µg per L, it cannot be excluded that the molecules designed to be biologically active affect the sensitive aquatic organisms even at such low concentrations. Most of these substances are suspected to have adverse environmental and health effects, additionally, some pharmaceutical compounds create multi-resistant strains in microorganisms, causing toxic effects on the endocrine system of aquatic organisms. Paracetamol (PARA) is recorded as the widely used analgesic/anti-inflammatory all over the world. The average consumption rate of pharmaceuticals containing PARA is reported to be 15 g per capita per year globally and 50-150 g per capita per year specifically in the developed countries. PARA is often found in the hospital sewages accounting to 6 gL^{-1} in European sewage treatment plant effluents and 10 gL^{-1} in natural waters in USA (Jallouli et al. 2017; Rad et al. 2015). Table 1.1 gives the details summarizing the properties of three organic pollutants

Table 1.1: Summary of the details of the organic pollutants MV, 2,4-D and PARA

	MV	2,4-D	PARA
Full forms	Methyl violet	2,4-dichlorophenoxyaceti acid	Paracetamol
Classification	dye	herbicide	drug
Scientific name	Pentamethyl pararosaniline chloride	(2,4-Dichlorophenoxy) acetic acid	acetaminophen
Major uses	Used for textiles, colors in paint and ink	To inhibit uncontrolled growth of many terrestrial and aquatic broadleaf weeds	Widely used antipyretic
Molecular formula	$C_{24}H_{28}N_3Cl$	$C_8H_6Cl_2O_3$	$C_8H_9NO_2$
Molecular weight	393.9 g/mol	221 g/mol	151 g/mol

Molecular structure			
Peak wave length	570 nm	280 nm	248 nm

The treatment methods for water treatment include mixing, flocculation, coagulation, sedimentation, filtration and disinfection. Most of the conventional methods are ineffective due to the large degree of aromatics/phenols present in dye molecules and phenolic compounds. Advanced oxidation processes (AOPs) are extensively used in wastewater treatment techniques where the persistent chemicals are degraded into smaller molecular weight compounds by means of reactive oxygen species (ROS). AOPs such as fenton oxidation, catalytic ozonation, electrochemical processes, ozonation, ozone/ ultraviolet light (UV) irradiation, hydrogen peroxide/UV irradiation and photocatalytic process can effectively eliminate emerging contaminants without producing secondary waste in the environment. Existing methods require high operational and maintenance costs, therefore concern lies with the treatment of effluents by economically viable methodologies (Han et al. 2015; Saharan et al. 2015).

With the advent of nanoscience and technology, various strategies of nanophotocatalysis came into picture implementing the role of molecular machinery. Nanotechnology is an interdisciplinary field of science combining biology, chemistry, physics and material science where the size of the material is designed such that it is smaller than 100 nm or at least one of its dimension is in nm range (Kim 2013). In 1986 Kim Eric Drexler in his book, *Engines of Creation: The Coming Era of Nanotechnology*, introduced the fundamental technology objective about using machines that work at the molecular scale to structure matter from the bottom up. These materials offer new solutions in various fields by manipulating certain characteristic of nanoparticles (NPs) by improving the surface, stability, homogeneity and surface to volume ratio (Moritz and Geszke-moritz 2013).

When the particle size is reduced to the atomic level, the energy levels are broken into various discrete levels leading to the increase in the band gap of the material. In this scenario, the emission and absorption wavelength become limited therefore as the size of the particle decreases the band gap increases. To reduce the surface energy, the surface has to reconstruct, which leads to the formation of energy levels in the forbidden gap of the semiconductor, further, electrical and optical properties of the material are changed by these traps. The

absorption peak corresponding to the threshold for the absorption of light in the nanoparticles (NPs) is blue shifted on decreasing size. Similarly, the photoluminescence peak position of NPs also shows a blue-shift with respect to that of bulk materials (Sandana and Rose 2014).

Solar photocatalysis is one type of AOPs driven by natural sunlight and has been demonstrated to be a promising technology for degradation and inactivation of hazardous chemical compounds in water (Ayodhya et al. 2016; Velmurugan et al. 2013) where the light source activates the oxidation and reduction process to degrade the contaminants. In the photocatalytic pathway, the NPs are activated by a certain light source that initiates a series of chemical reactions and establishes a redox atmosphere in aqueous solutions containing highly ROS that eventually mineralize the pollutants. The degradation mechanism involves the utility of the light source where the electrons are excited by the electrons leaving holes in the valence band as they tend to move from valence band to conduction band. The efficiency of the catalyst is determined when water reacts with the holes in the valence band and it generates the electron-hole pairs. These are further converted to free radicals ($^\bullet$OH) which are capable of undergoing secondary reactions. The electrons can be absorbed by oxygen to form superoxide or they can react with oxygen along with hydrogen to create hydrogen peroxide. Subsequently, these electrons react with hydrogen peroxide to create hydroxyl radicals and ions (Ibhadon and Fitzpatrick 2013; Qutub et al. 2015) (Figure 1.1).
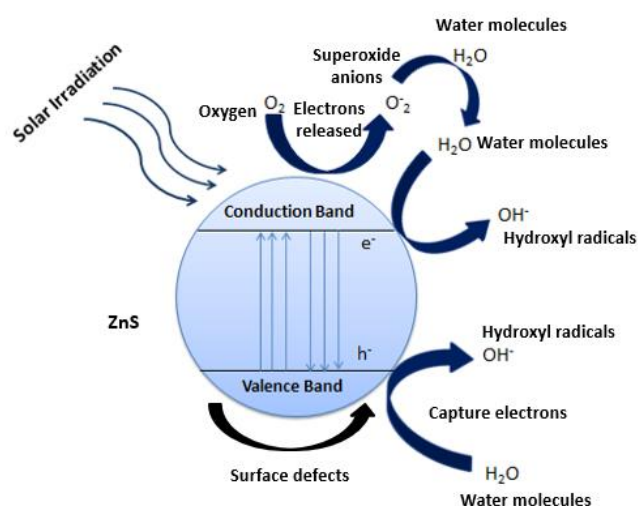
Figure 1.1: Schematic diagram of the degradation reaction mechanism over the surface of ZnS NPs

Among the most extensively studied Group II–VI semiconductor NPs, ZnS is well-known for its nontoxic multifunctional semiconductor property which is capable of rapidly generating

surplus amounts of electron-hole pairs on photoexcitation due to its direct wide band gap. It has high negative reduction capability of energized electrons because of its higher conduction band position in aqueous solutions when compared with other broadly studied semiconductor photocatalysts and it shows great photocatalytic activity because of trapped holes emerging from surface defects on the sulphides (Mansur et al. 2014). Zinc sulphide (ZnS) has enormous consideration among II–VI semiconductors due to their applications in distinct fields such as catalyzators (catalytic agent), optical sensitizers, optical sensors, UV sensors, chemical sensors, biosensors, nanogenerators, electroluminescent materials, field emitters and field effect transistors (Onwudiwe et al. 2014; Prasanth et al. 2015). It is considered to be a suitable candidate because of its distinguishing properties such as crystalline phosphor and finds its role in environmental applications as an absorbent for the uptake of pollutants, photo catalyst for the degradation of organic pollutants and solar energy conversion (El-Kemary and El-Shamy 2009).

Encapsulation of the proteins to the NPs help in providing stability and enhancing their characteristics. Fungi compared to other biological entities such as plant and bacteria, secrete huge amounts of proteins which directly influence their productivity. They exhibit monodispersity with well-defined dimensions utilizing minimal media requirements and ease to scale up becomes an added advantage to this fungi synthesized NPs (Mohanpuria et al. 2008). The microbes residing in the internal parts of plant tissues called Endophytes constitute a group of plant symbionts of microbial diversity. They are known to secrete rich source of metabolites and reported to perform multiple activities in the field of medicine, agriculture and industry potentials. The utility of endophytes for the synthesis of nanomaterials is explored for the production of NPs (Baker and Satish 2015). Owing to the above advantages, an attempt has been made to detect and degrade organic pollutants using biologically synthesized ZnS NPs from an endophytic fungus *Aspergillus flavus* to perform dual role of sensing and photocatalysis.

1. 2.   Scope and objectives of the study

The aim of the present research work is to biologically synthesize ZnS NPs using an endophytic fungus isolated from a medicinal plant *Nothapodytes foetida* that is tolerant to precursor solutions containing zinc and sulphides. These ZnS NPs potential will evaluated for it detection and degradation potentials on certain common and hazardous pollutant in aquatic systems will be evaluated.

The following are the specific objectives:

1. To isolate, identify and screen zinc and sulphide tolerant endophytic fungal species from a medicinal plant, *Nothapodytes foetida*.

2. To synthesize, optimize and postulate the possible mechanism involved in the synthesis of zinc sulphide NPs by the endophytic fungus (*Aspergillus flavus*).

3. To study the structural, morphological, optical, electrochemical and stability characteristics of the biologically synthesized ZnS NPs.

4. To estimate the degradation potential of ZnS NPs for common environmental organic pollutants such as MV, 2,4-D and PARA at different concentrations.

5. To study the fundamental mechanism involved in the degradation process of MV, 2, 4-D and PARA.

6. To produce the ZnS NPs in a stirred tank reactor and to optimize the parameters like inoculum volume, precursor concentration and incubation time that influence the yield of the ZnS NPs.

1. 3.   Organization of the thesis

The research study is presented and explained in five chapters as given below:

Chapter 1 introduces about the scenario of water pollution and highlights the utility of nanomaterials for the wastewater treatment. Further, it explains the importance of endophytic fungi in biological nanomaterials**.**

Chapter 2 encompasses the literature review that includes the overview of the synthesis of NPs and biosynthesis through endophytic fungi. The importance of the biological synthesis in general and synthesis of ZnS NPs were discussed. Moreover, the studies on degradation potential of ZnS NPs on MV, 2, 4-D and PARA were discussed in addition, the production of NPs in bioreactors is also illustrated.

Chapter 3 includes the materials and methods required to achieve the objectives followed in the synthesis and analysis of the ZnS NPs. This section includes the collection of samples, isolation, screening and identification of metal tolerant fungal species from endophytic fungi. Further, it comprises of the preparation of the stock solutions for the synthesis and optimization

of ZnS NPs, reaction concentrations and measurement techniques of the pollutants MV, 2, 4-D and PARA under study.

Chapter 4 The results confirming the significant characteristic properties like optical, structural, morphological thermal and stability were illustrated. Synthesis, possible mechanism and optimization of ZnS NPs protocol for the extracellular biosynthesis of ZnS NPs were demonstrated. The results confirming the degradation of MV, 2,4-D and PARA utilizing ZnS NPs as catalyst, the degradation mechanism and their characterization were demonstrated. This section includes the large-scale production of NPs in the stirred tank reactor.

Chapter 5 gives a summary of this dissertation as well as discusses directions for future work. The encapsulation on ZnS NPs via endophytic fungi isolated from the medicinal plant *Nothapodytes foetida* offered a promising scope for fungal nano-catalysts to exploit their degradation potential. Thus, it can be concluded that these biological nano-catalysts provided a novel catalytic and biological model in the field of material science that could help to mitigate environmental pollution.

CHAPTER 2

2.   REVIEW OF LITERATURE

2. 1.   Endophytic fungi

In 1866, De Bary introduced the term "Endophyte" which means, microorganisms that reside in the intercellular / intracellular regions of healthy plants at a particular time of their life cycle (Ryan et al. 2008; Pimentel et al. 2011; Devi and Joshi 2015). Usually, endophytes have a symbiotic relationship with their plant host and act as induced systemic resistance defense for the plants against foreign phytopathogens. It is reported that more than a million different endophytic strains inhibit in 3,00,000 different plant species. Endophytic fungi are the ecological and polyphyletic group of exceptionally various organisms, for the most of it belonging to ascomycetes and anamorphic fungi. They can colonize in internal plant tissues of healthy leaves, petioles, stems, twigs, bark, root, fruit, flower and seeds without causing any damage or pathogenic to disease their host plants. The plant host is likewise profited by the endophytes by their natural resistance from soil contaminants, their ability to degrade xenobiotics or their action as vectors to present degradative qualities with plants, which significantly assist in phytoremediation (Pimentel et al. 2011; Kaul et al. 2012).

They have been accounted for their co-production of the bioactive compounds. Two of the most contemplated and biggest classes of optional metabolites are the polyketides and non-ribosomal peptides. Various bioactive compounds are co-produced which include anticancer drug camptothecin, podophyllotoxin and natural insecticide azadirachtin. Numerous extracellular compounds like pectinases, cellulases, lipases, amylases, laccases and proteinases are produced by fungal endophytes (Jalgaonwala et al. 2011; Saikkonen et al. 2016). Different mechanisms have been proposed for the simultaneous generation of the biological compounds for instance, in case of gibberellins, the biosynthetic system of a similar compound evolves independently in plants and their microbial counterparts, on the other hand, the quality exchange between the plant host and its endophytes have been speculated, though this procedure has just been appeared to happen with microbial endophytes (Alvin et al. 2014; Nisa et al. 2015). Natural products such as taxoids, alkaloids, color curcumin, betulinic and betulonic acids were examined for their capacity to biotransformation. The vast majority of the endophytes have the ability to experience xenobiotic degradation; moreover, they can likewise be utilized as degradative characteristics which help in enhancing phytoremediation. The endophytic protection from metals/antimicrobials might be because of their introduction to various associates in the plant/soil species and these help in the natural degradation process.

Bjerkandera sp, *Ceratobasidium stevensii Neotyphodium coenophialum* and *Neotyphodium uncinatum* were subjected for wood and polyaromatic compounds biodegradation and for bioaugmentation of total petroleum hydrocarbons and polycyclic aromatic compounds removal.

The interference of endophytes and nanomaterials is a moderately new research zone that has pulled in unequivocal consideration. Owing to the fact that the endophytic fungi provide a broad variety of bioactive secondary metabolites with unique structures they could be the explored for their ability to the biosynthesis of NPs to develop an efficient environment friendly process. Synthesis of NPs from endophytic fungi have been quoted for various species and reported in Table 2.1 gives an overview of synthesis of NPs from endophytic fungi.

Table 2.1: Overview of synthesis of NPs from endophytic fungi

Sl. No	Fungal species	Source	Characteristics	Reference
1.	*Pestalotia sp.*	Leaves of *Syzygium cumini*	The absorption peak is at observed 415 nm. Silver NPs of TEM diameter 10-40 nm are synthesized and its antimicrobial activity is studied.	(Raheman et al. 2011)
2.	*Pencillium sp.*	*Curcuma longa*	Surface plasmon peaks were also located at 425 nm. Silver NPs of TEM diameter 25 nm. Antimicrobial activity is studied.	(Singh et al. 2013)
3.	*Epicoccum nigrum*	-	TEM results indicate that silver NPs size from 1 to 25 nm. The absorption peak is at 424 nm. Activity against pathogenic fungi is studied.	(Qian et al. 2013)

4.	*Fusarium solani*	*Nothapodytes foetida*	TEM results indicate that silver NPs size as 10 nm further optimization is carried out based on mathematical models	(Musavi and Balakrishnan 2014)
5.	*Penicillium sp.*	*Curcuma longa*	The absorption peak is at observed 420–425 nm. Silver NPs of TEM diameter 25 nm and 30 nm. Antimicrobial activity is also studied.	(Singh et al. 2013)
6.	*Aspergillus niger* PFR6 *Penicillium ochrochloron* PFR8 *Aspergillus tamarii* PFL2	*Potentilla fulgens* L	Silver NPs synthesized TEM results indicate that *A. tamarii* PFL2, *A. niger* PFR6 and *P. ochrochloron* PFR8 was found to have the particle size 3.5 nm ,8.7 nm and 7.7 nm and the absorbance peak at around 420 nm.	(Devi and Joshi 2015)
7.	*Pseudomonas veronii* AS 41G	*Annona squamosa* L	Maximum absorption was seen at 560 nm. TEM results indicate that gold NPs size 5-25 nm and its antibacterial activity is studied.	(Baker and Satish 2015)

2. 2.   Biological synthesis of NPs

Fungal strains such as *Fusarium*, *Penicillium* and *Aspergillus* species have been reported multiple times for the synthesis of several different kinds of nanoparticles. Fungal cultures possess some additional attributes with respect to their bacterial counterparts. For instance, the optimization for scale-up of fungal cultures has revealed that fungal mycelia can withstand the culturing fluctuations of the scale-up treatment in the bioreactor which perhaps plant and bacterial based extracts cannot. Moreover, fungal species also possess a fastidious nature of growth and this is a very vital aspect in the nanoparticle formation through the use of fungal species. This is so because this enables the release of very vital enzymes and proteins in

sufficient concentrations that in turn enables easier bioreduction of corresponding metal salts to form the biochemically reduced metallic ions as zero-valent nanoparticles. Their fast growth and prompt participation in the overall nanoparticle synthesis also eliminate the technical hurdles of the downstream processing involved. Fungal species, till date, have been explored for both extracellular and intracellular synthesis of nanoparticles. For large-scale biogenesis of nanoparticles, fungi possess unique advantages over other microorganisms. They have several advantages over bacteria for biosynthesis as they secrete large amounts of extracellular proteins with diverse functions. The so-called secretome includes all of the secreted proteins into the extracellular space. Most fungi also have a very high wall-binding capacity as well as intracellular metal uptake capacities (Mohanpuria et al. 2008). They produce large amount of enzymes per unit biomass. The use of specific enzymes such as reductase secreted by fungi opens up exciting possibilities of designing a rational biosynthesis strategy for metal nanoparticles of different chemical compositions. A number of different genera of fungi have been investigated for biotechnological process research, and it has been shown that fungi are extremely good candidates in the synthesis of nanoparticles (Sadhasivam et al. 2010). The high concentration of the fungal secretome has been used for industrial production of homologous and heterologous proteins. For example, the expression of a functionally active class I fungal hydrophobin from the entomopathogenic fungus Beauveria bassiana has been reported (Kirkland et al. 2011). The tripeptide glutathione is a well-known reducing agent involved in metal reduction and is known to participate in cadmium sulfide (CdS) biosynthesis in yeasts and fungi. Since the nanoparticles are produced outside the cell extracellularly in most of the cases, they are easy to purify and can be directly used in various applications. Fungal mycelial mesh can withstand flow pressure and other conditions in bioreactors or other chambers as compared to plant material or bacteria. Recently, fungi have gained much importance, as the extracellular secretion of enzymes has an added advantage in the downstream processing and handling of biomass (Gade et al. 2008), when compared to the bacterial fermentation process which involves use of sophisticated instruments to obtain clear filtrate from the colloidal broth (Sastry et al. 2003). Moreover, fungi are excellent secretors of protein compared to bacteria and actinomycetes, results into higher yield of nanoparticles (Rai et al. 2009).

Several fungi have already been exploited for the synthesis of silver, gold, zirconium, silica, titanium, iron and platinum nanoparticles (Krumov et al. 2009). Fungi have a number of advantages for both intra- or extracellular synthesis of nanoparticle over other organisms including plants (Narayanan et al. 2010). Due to slower kinetics, they offer better manipulation and control over crystal growth and their stabilization (Vaidyanathan et al. 2009). Fungal

mycelia can withstand flow pressure, agitation and other conditions in bioreactors or other chambers compared to plants and bacteria (Saha et al. 2010). Many of the enzymes secreted by fungi are capable of reducing metal ions quickly through non-hazardous processes and allow a controlled synthesis of nanoparticles with well defined size and shape (Moaveni et al. 2011). Moreover, large scale extracellular secretions of their reductive proteins helps in outside precipitation of nanoparticles, minimizes the unnecessary cellular components and hence, aiding direct use in various applications. Therefore, fungi could be regarded as natural biofactories for biosynthesis of nanoparticles. In 2012, Ahmad and Syed showed that extracellular platinum nanoparticles with the size ranged between 5-30 nm were obtained when the *Fusarium oxysporum* incubated with hexachloroplatinic acid (H_2PtCl_6). The nanoparticles were stabilized by proteins (Syed et al. 2012). They also investigated for the first time the biosynthesis of CdTe nanoparticles by *Fusarium oxysporum*. The CdTe quantum dots were highly fluorescent and capped by proteins secreted by the fungus. They showed antibacterial activity against Gram negative bacteria and Gram positive bacteria (Syed et al. 2013). Almost the same time, Bakhtiari's group reported the biosynthesis of spherical ZnS nanoparticles with the average size of 42 nm using the *Fusarium oxysporum* (Mirzadeh et al 2013). Some other *Fusarium sp.* such as *Fusarium acuminatum* and *Fusarium semitectum* (Ingle et al., 2008) could be used to synthesize extracellular silver nanoparticles. There are also reports about the biosynthesis of gold nanoparticles by fungi. In 2014, Castillo's group achieved the formation of gold nanoparticles using the fungus *Botrytis cinerea* for the first time. The nanoparticles were in different shapes such as spherical, pyramidal, hexagonal, triangular and decahedral of sizes ranging between 1-100 nm. They confirmed the molecules secreted by the fungus participated in the production of gold nanoparticles, but the specific mechanism remains to be elucidated (Castro et al., 2014). Others such as *Verticillium* (Mukherjee et al., 2001), *Aspergillus fumigates* (Gupta et al., 2013), *Aspergillus flavus* (Das et al., 2009) and *Copidosoma floridanum* (Narayanan et al., 2013) have also been reported about the ability to biosynthesize gold nanoparticles.

2.3. Quantum confinement effects

For a semiconducting material, a quantum dot structure is a small box with sides comparable to or smaller than the de Broglie wavelength which is surrounded by a wider band-gap semiconductor material. This box behaves as a three-dimensional potential well for carriers (electrons in the conduction band and the holes in the valence band) (Figure 2.1). In a quantum dot, carriers are narrowly confined in all three directions along each side of the box l_x, l_y, and l_z along the *x*- axis, the *y*- axis, and the *z*-axis, respectively. Therefore, the energy is quantized

along all three directions and can be written for electrons in the conduction band as equation 2.1 and for holes in the valence band as equation 2.2 (Klaus et al. 2011)

$$E = E_C + E_{nx} + E_{ny} + E_{nz} \ \ldots\ldots..(2.1)$$

$$E = E_v - [E_{nx} + E_{ny} + E_{nz}]\ldots\ldots..(2.2)$$
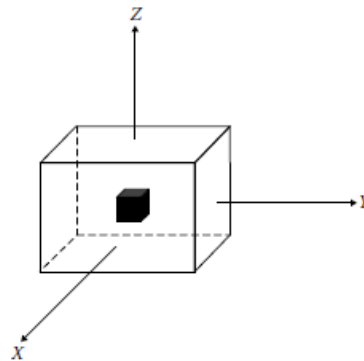
Figure 2.1: A typical geometry of a quantum dot

Where $E_{nx} = n^2_x \prod h^2/2 \ m^* \ l^2_x$, $E_{ny} = n^2_y \prod h^2/2 \ m^* \ l^2_y$, $Enz = n^2_z \prod h^2/2 \ m^* \ l^2_z$

n_x ,n_y ,n_z = 1, 2, 3,…, *h* is Planck's constant and *m** is the mass of the carriers (the electrons in the conduction band and the holes in the valence band).

The energy levels are discrete and well separated. As the carrier (the electrons in the conduction band and the holes in the valence band) motion is restricted, the conduction band and the valence band split into sub bands which become narrower with the increasing restriction in more dimensions. Finally, the density of states will be represented by the delta functions where, the carrier motion is restricted in all three directions as in the case of the quantum dot.

The quantum confinement effects in low dimensional semiconductor systems were studies based on quantum confinement effects of various semiconductors with emphasis on the optical properties, including absorption and luminescence. Obviously, the confinement of an electron and hole in nanocrystals significantly depend on the material properties, namely, on the Bohr radius a_B. One of the most important consequences of the spatial confinement effect is an increase in the energy of the band-to-band excitation peaks (blue shift), as the radius 'R' of a microcrystalline semiconductor is reduced in relation with the Bohr radius 'a_B'.

Theoretically, the regimes of quantum confinement differ in their main electron-hole interaction energy, i.e., the Coulomb term and the confinement energy of the electron and hole and kinetic energy. (Sagadevan et al. 2013; Koole et al. 2014).

2.3.1. *Weak Confinement Regime*

To observe this regime, the radius R of a crystallite should be greater than the bulk exciton Bohr radius a_B. In this region of weak confinement, the dominant energy is the Coulomb term and there already occurs a size quantization of the exciton motion. The exciton energy states are shifted to higher energies by confinement and the shift in energy ΔE is proportional to $1/R^2$. The shift 'ΔE' of the exciton ground state is given approximately by

$$\Delta E \approx [\ \textstyle\prod^2 h^2/\ 2MR^2]\ldots\ldots(2.3)$$

where, *M* is the mass of the exciton and it is given by $M = m_e^* + m_h^*$ with m_e^* and m_h^* being the effective masses of the electron and hole respectively.

2.3.2. *Moderate Confinement Regime*

The moderate confinement regime occurs when $R \approx a_B$ and $a_h < R < a_e$, where, a_h and a_e are the hole and electron Bohr radii, respectively. In II-VI semiconductors, this region is well observable in small QDs. Its characteristic feature is the well restricted motion of a photoexcited hole.

2.3.3. *Strong Confinement Regime*

Finally, the size of a QD can be decreased in such a way that $R \ll a_B$ and $R \ll a_h$ and a_e in the strong confinement regime. The Coulomb term of electron-hole interaction is now small and can be ignored or treated as perturbation. The electrons and holes can now be thought of as confinement independent particles. So excitons are not formed and the separate size quantization of an electron and hole is the dominant factor. The optical spectra consist also of a series of lines due to the transition between sub-bands. This factor was confirmed experimentally and the simple model gives the shift in energy as a function of crystallite size as

$$\Delta E \approx [\ \textstyle\prod^2 h^2/\ 2\ \mu\ R^2]\ldots\ldots(2.4)$$

in which the exciton mass M is replaced by the reduced exciton mass μ, where,
$1/\mu = 1/\ m_e^* + 1/\ m_h^*$. The electrons and holes in QDs are treated as independent particles and for the excited state there exists a ladder of discrete energy levels, as in molecular systems.

Quantum dots are semiconductor NPs which have quantum confinement property. They are crystalline structures whose dimensions are sufficiently small enough that its electronic states begin to resemble like those of an atom or particle instead of those of the bulk crystal. For a semiconducting material, a quantum dot structure is a small box with sides similar to or smaller than the de Broglie wavelength which is encompassed by the extensive band-gap semiconductor material. Energy levels are discrete and well separated when the carrier motion is restricted where the conduction and valence band is split into sub-bands which narrows down with the increased limitations in most of the dimensions (Figure 2.2).

By reducing the particle size of the catalyst one could see an increase in surface area in Figure 2.1 deduces that the diminishing in the size brought about increment in the surface area. Because of the quantum confinement effect, quantum dots showed diverse behavior in the electronics, optical and magnetic behavior by size tuning. The essential two major differentiation between the bulk size and the nanomaterial is that large surface area to volume ratio of NPs and the three-dimensional quantum confinement of their charge carriers this happens when NPs size is smaller than the exciton Bohr range of the bulk semiconductor. In quantum dots, as the electrons are limited to a point in space, they have no change in any measurement and electrons are said to be restricted at a point, suggesting that every direction changes their properties. When the size of the material reduces to the atomic level, they tend to breakdown into discrete levels therefore, it can be concluded that the size of the nanoparticle is the function of the band gap of the material. Further, it can be inferred that the size and composition of the materials can be altered by manipulating the size of the material.
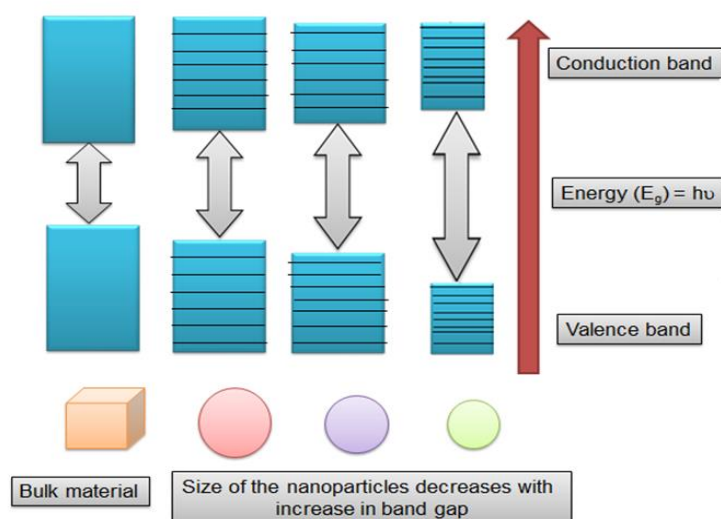
Figure 2.2: Schematic representation of decreasing size with the increasing band gap

2.4.   ZnS NPs chemical and biosynthesis

Among the most comprehensively considered II–VI semiconductors, ZnS is a remarkable multifunctional material in view of the wide band gap. This material has been shown as a prevalent photocatalyst as a result of the rapid generation of electron-hole pairs with photoexcitation as it is a direct wide band gap semiconductor material. Further, it has high negative reduction capability of energized electrons because of its higher conduction band position in aqueous solution when related to other broadly examined photocatalysts. Likewise, this material shows great photocatalytic activity because of trapped holes emerging from surface defects on the sulfides. It has additionally been used in UV detectors because of its high resistivity at encompassing conditions and quick switching time upon UV light enlightenment, along these lines showing the most astounding potential for a UV light illumination. Therefore, cadmium-free nanomaterials, for example, zinc (Zn^{2+}) compounds, are extremely encouraging options because of their ecological wealth and natural presence in the human body. The increased concern over the toxicity of cadmium has brought about numerous groups searching for less harmful metals such as zinc chalcogenides (Mansur et al. 2014).

In 1994, Bhargava et al for the first time detailed the nanosize luminescent ZnS materials and manganese-doped nanocrystals of ZnS by synthetic precipitation technique system. Due to the huge surface to volume ratio, ZnS NPs recently showed progress as a result of their quantum size effect, size and shape-dependent photoemission and superior luminescent characteristics. Biological synthesis has not been explored, hence, these procedures have gained significance in the amalgamation of NPs. Therefore, a wide array of biological entities such as microorganisms, yeast, parasites, plant biomass and extracts have been utilized for synthesis of NPs (Moritz and Małgorzata 2013). In 2002, Dubertret et al. have used NPs as biological probes in clinic examinations, this inspired the researchers to synthesize biological ZnS NPs. Later in 2006, Mandal et al. synthesized 2–5 nm sphalerite ZnS particles form sulfate-reducing bacteria under anaerobic conditions. In the recent years, various bacterial sources such as *Rhodobacter sphaeroides, Serratia nematodiphila* and *Shewanella oneidensis* were employed for synthesis and the TEM diameter is recorded to be 8 nm, 80 nm and 5 nm respectively (Bai et al. 2006; Malarkodi et al. 2013; Xiao et al. 2015). NPs synthesized from fungal source *Fusarium oxysporum*, showed TEM diameter of 42 nm and it exhibited surface plasmon resonance at 280– 320 nm (Mirzadeh et al. 2013). *Saccharomyces cerevisiae* yeast yielded NPs of diameter 30– 40 nm and indicated surface plasmon resonance band at 302.6 nm

(Sandana and Rose 2014). Further *Jatropha* latex and *Corymbia citriodora* plant source produced NPs of diameter 10 nm and 45 nm respectively (Hudlikar et al. 2012; Chen et al. 2016).

Due to large surface to volume ratio ZnS nanoparticles in recent years are becoming more and more attractive due to their quantum size effect, size- and shape-dependent photoemission and superior luminescent characteristics. One of the important properties of ZnS nanoparticles is the luminescence property. For ZnS nanoparticles to have wider applications in optoelectronics, they must possess a strong luminescence property. One of the methods to improve the luminescence property of ZnS nanoparticles is to introduce certain dopants into ZnS nanoparticles. Elements such as Mn, Cu , Al , Te , Eu, Mg, Fe, Pb and Cr have been doped into ZnS nanoparticles and improved luminescence has been observed. (Chen et al. 2014). During the last two decades, number of synthesis methods has been reported in the literature for the preparation of semiconductor nanoparticles namely chemical method, mechanochemical method, hydrothermal process, sol–gel method, electro-spinning technique, reverse micelle method and ultrasonic radiation method etc. Recently nanomaterials are of great interest because of their electro-optical properties and applications as reported by the researchers (Onwudiweet al. 2014).

The first report on nanosize luminescent ZnS materials was given by Bhargava et al in 1994. Manganese-doped nanocrystals of zinc sulfide were synthesized by chemical precipitation method. The nanomaterials had external photoluminescence quantum efficiency of 18 %. The synthesis involved reaction of diethyl zinc with hydrogen sulfide in toluene. The dopant manganese is added as ethylmanganese in tetrahydrfuran solvent to the parent solution of zinc salt before precipitation reaction. Surfactant methacrylic acid was used to maintain separation between the particles formed. The dried material was further subjected to ultraviolet curing for possible polymerization of surfactant methacrylate capping film on the surface of Mn doped ZnS nano cluster for imparting true quantum confinement. The enhancement of efficiency has been explained on the basis of surface passivation of the nanocrystals due to photopolymerization of the surfactant. The photoluminescent (PL) and photoluminescence excitation (PLE) spectra of the nanophosphor have been compared with bulk ZnS: Mn. The PL is slightly shifted and there is a larger linewidth in the nanophosphor as compared to bulk. Table 2.2 gives an overview of the

Table 2.2: Overview of the synthesis of ZnS nanoparticles

S. no	Method of preparation	Characteristics	Reference
1.	Glycoside in the aqueous crude extract of *Stevia rebaudiana*	TEM diameter size 8.35 nm. The peaks are observed at 3414.82 cm^{-1} which corresponds to -OH groups	Alijani et al. 2019
2.	Low-cost aqueous method using solvent oxalic acid	Photoluminescence peak is observed at 370 nm exhibiting blue-green emission. TEM diameter size 8–20 nm	Florence and Can, 2018
3.	Solid state reaction method	TEM diameter size 15.32–19.04 nm. ZnS:Ni nanoparticles, a green emission peak around 585 nm was observed	Jothibas et al. 2018
4.	Chemical bath deposition, co-precipitation and spin coating	Cubic phase of ZnS thin films crystallized nanoparticles with an average size of 150 nm and pores of 40 nm	Akhtar et al. 2017
5.	Hydrothermal process in combination with the co-precipitation route.	Hybrid reduced graphene oxide (RGO)/CoFe$_2$O$_4$/ZnS nanocomposites ZnS quantum dots and cobalt ferrite (CoFe$_2$O$_4$) nanoparticles with an average diameter of 3–8 nm and 10–20 nm.	Zhang et al. 2017
6.	Hydrothermal method	Cubic sphalerite phase with an average size is about 20 nm	Yin et al 2016
7.	Hydrothermal process	Cubic sphalerite phase with asize 20–60 nm	Younes et al 2016
8.	Chemical Precipitation method	Ni doped ZnS quantum dots of TEM size 2.3 – 3.6 nm. Absorption edge is located around 320–340 nm. Photoluminescence spectrum emission peak centered at around 612nm	Kumar et al. 2015

12.	Hydrothermal process	TEM diameter of diameter 200 nm. Crystalline hollow ZnS nanospheres	Han et al. 2015
13.	Solvothermal method	ZnS of wurzite with the particle size of about 3 to 10 nm	Prakasam et al. 2015
14.	Wet chemical synthesis	Fe doping TEM diameter of 5–10 nm. Photoluminescence spectra is exhibited at 290 nm with excitation wavelength 330 nm on doping Fe ions that the pristine ZnS NPs showed at 275 nm, on doping it is red shifted in between 285 and 290 nm.	Dixit et al. 2015
15.	Chemical precipitation	Absorption spectra is exhibited inbetween 250–500 nm. Photoluminescence emission spectra of Mn doped ZnS NPs in the range 350–800 nm.	Kaur et al. 2015
16.	Electro deposition method	Zinc sulfide thin films are polycrystalline with cubic crystal structure. Absorption peak at 320–340 nm. From XRD the average crystallite size of zinc sulfide was found to increases from 21 to 54 nm	Patil et al. 2015
17.	One-step Chemical Vapor Deposition method	ZnS nanobelts -The thickness difference between the two segments is about 45 nm. UV emission at approximately 338 nm and a weak and broad green emission band centered at 524 nm.	Wang et al. 2014
18.	Laser assisted solid state reaction from metal xanthate	TEM diameter is 4.8 nm Laser pulses with a peak wavelength of 355 nm	Onwudiwe et al. 2014
19.	Solid-state reaction	Chlorine and oxygen co-doped ZnS NPs Average crystallite size of about 4.28–5.08 nm. Two excitation bands in the ultraviolet (UV) range with their maxima at about 270 and 323 nm can be clearly seen.	Chen et al. 2014

20.	Microwave irradiation	ZnS with cubic structure and absorption peak at 310 nm	Rasoul et al. 2014

2.5. Mechanism of synthesis of NPs

There are two possible mechanisms for the biosynthesis of NPs, postulated as: (i) biomolecules discharged by fungal mycelium into the outer medium help in the reduction of ions to NPs and/or (ii) NPs formed inside the cell are secreted outside. In the extracellular synthesis of NPs, the proteins and reducing agents are secreted by the fungi where a minimum of four high molecular weight proteins released into the biomass for the formation of NPs. One of these was strain particular NADH-subordinate reductase, further, the reduction of metal ions and surface binding of the proteins to the NPs were caused by the tertiary structure of the proteins. Ahmad et al. (2003) and Bhainsa and D'Souza (2006) detailed the extracellular combination of silver NPs using *Fusarium oxysporum* and *Aspergillus fumigatus* individually. Extracellular synthesis of both live and dead fungal biomass has been shown by numerous scientists. Silver NPs were integrated extracellularly by cell-free filtrate of the marine organism *Penicillium fellutanum* by Moteshafi et al. (2012). In this work, a single prominent protein band with a molecular weight of 70 kDa, was detected in the culture filtrate secreted from the fungal biomass. However, in case of intracellular synthesis, reduction of metal ions by fungal mycelium to its nanoform has been one of the survival strategies to detoxify the toxic metal ions. For example, the gold NPs were synthesized intracellularly by *Verticillium* sp. after exposing to chloroauric acid ($HAuCl_4$) solution. In a similar process, the Ag^+ ions are reduced intracellularly by the enzymes secreted due to metal toxicity in vivo and the formation of silver NPs resulted by the bio capping of these proteins (Mohanpuria et al. 2008).

To address this research gap, the biogenesis of nanoparticles was initiated. Although cleanup is necessary to prevent any further discharge of contaminated wastes into the environment, a cost-effective technology needs to be developed for industry to use. The fundamental reason for the treatment of wastewater is to circumvent the effect of pollution of water sources and protect public health through safeguarding of water sources against the spread of diseases. This is carried out through a variety of treatment systems, which could be onsite treatment systems or offsite treatment systems. The trafficking of extracellular membrane vesicles (MVs) and their biological roles are well-studied processes in eukaryotes and an increasing number of new studies are being carried out in diverse bacteria.

In archaea, the production of MVs has been mainly studied in species of the genus *Sulfolobus* and *Thermococcus.* In eukaryotes and bacteria, several studies have shown that MVs can play a role in detoxification. This phenomenon was first observed in eukaryotic marine organisms such as mollusks and crustaceans which accumulate cadmium. Notably, numerous bacteria produce vesicles containing sulfur. Sulfur is an important element for microbial life present in deep-sea environments and is metabolized by a wide variety of microorganisms, which transiently store sulfur in intracellular vesicles. The cellular structure of a microorganism can trap heavy metal ions and subsequently sorb them onto the binding sites of the cell wall. This process is called biosorption or passive uptake, and is independent of the metabolic cycle. The amount of metal sorbed depends on the kinetic equilibrium and composition of the metal at the cellular surface. The mechanism involves several processes, including electrostatic interaction, ion exchange, precipitation, the redox process, and surface complexation. The process is fast and can reach equilibrium within a few minutes. Biosorption can be carried out by fragments of cells and tissues, or by dead biomass or living cells as passive uptake via surface complexation onto the cell wall and other outer layers. The other method is a process in which the heavy metal ions pass across the cell membrane into the cytoplasm, through the cell metabolic cycle. This is referred to as bioaccumulation or active uptake. Metal uptake mechanisms by various biosorbents depend on the cellular surface of the microbes, as well as the exchange of metal ions and complex formations with the metal ions on the reactive chemical sites of the cell surface. The rigid cell wall of fungi is made up of chitin, inorganic ions, lipids, nitrogen-containing polysaccharide, polyphosphates, and proteins. They can tolerate and detoxify metal ions by active uptake, extracellular and intracellular precipitation, and valence transformation, with many absorbing heavy metals into their mycelium and spores. The surface of their cell wall acts as a ligand for binding metal ions, resulting in the removal of metals. The first barrier includes excreted substances like organic acids or/and proteins with an ability to immobilize heavy metals. The second barrier includes the (unspecific) binding of heavy metals by the cell wall and melanins located in the cell wall. Toxic heavy metals that could not be detained outside the cell must be detoxified inside the cell.

2.6. ZnS NPs for Photocatalysis

Exploitation of the renewable sources such as solar energy for the alternate energy source led to the utilization of solar energy for photocatalysis. It is considered as an effective and rapid technique to removal/degrade pollutants from water. ZnS NPs could be utilized as photocatalysts because of their rapid generation of the electron-hole pairs by photo excitation

and profoundly negative reduction potentials of the energized electrons; as conduction band position of ZnS in aqueous solution is higher than that of other semiconductors, such as TiO_2 and ZnO. Semiconducting NPs engaged in photo conversion systems present a temperately wide energy gap between the conduction band (CB) and the valence band (VB) and this separation is known as the band-gap energy (E_{gap}). The absorption of energy by a semiconductor results in electron transfer from the valence band to the conduction band and leave vacancies in the valence band termed as holes. The photo generated electron-hole pair encourages the reduction and oxidation of species adsorbed at the surface of the semiconducting NPs and encourages oxidative degradation of species in solution through radical reactions.

2.7. Cationic dye degradation

Numerous industries create enormous amounts of profoundly shaded wastewaters which are normally poisonous and impervious to regular treatment systems. The utilization of engineered colours in the textile and food industries constitutes serious dangers to general wellbeing. About 60-70 % of colours utilized as a part of the materials enterprises contained azo colours with at least one azo bond. The extreme utilization of azo colours is identified with their high solubility, stability, colour variety and simple dyeing procedure. A portion of these colours are dangerous, mutagenic and cancer-causing compounds, as well as are resistant to oxygen consuming biodegradation and their half-lives under daylight are more prominent than 2000 h (Soltani and Entezari 2013). Discolouration of colour containing effluents is consequently vital and has received expanding consideration amid the most recent decade. Persistent introduction of inappropriately or halfway treated or untreated colouring dyes cause different health hazards to mankind, for example, harm to organs, dangerous to amphibian life, skin malignancy, cell lysis and so forth (Jeyasubramanian et al. 2015; Li et al. 2015). MV is one of the high shading extreme cationic colours, which can grab the attention of the public and the experts. MV absorbs and reflects sunlight into water resulting obstruction on the photosynthesis of oceanic plants (Jafari et al. 2012; Singh et al. 2011; Shamsipur and Rajabi 2014). It was important to degrade MV as it is considered as a potential cancer-causing agent, mutagen and miotic toxic substance and thusly, concerns exist in regards to the biological effect of the presence of MV on to the earth. Therefore, photo degradation is one of the essential techniques for the expulsion of MV from wastewater (Sinha et al. 2014).

Subsequently, the textile industries are an imperative source of contamination of the aquatic framework. Of late, there has been substantial consideration for the expulsion of

colours by various strategies. They are frequently degraded/removed by adsorption which is a physical technique, chlorination, ozonation as synthetic strategies and biodegradation. These evacuation strategies are not successful for an entire degradation and at times just give detachment of the colours with no degradation and creating a secondary waste problem. From the handy perspective, photodegradation of toxins utilizing semiconductor and solar light is an economical process. Since, the solar energy vitality is an abundant energy source, which can be utilized rather than counterfeit light sources that is expensive and hazardous (Akpan and Hameed 2009; Chauhan et al. 2013). Table 2.3 gives a summary of the NPs used for the dye degradation.

Table 2.3: Summary of the use of NPs for degradation of dyes

NPs	Method of Preparation	Dye	Light Illumination	Degradation Efficiency	Reference
ZnS and cadmium doped ZnS NPs	Co-precipitation method	Alizarin red S	Solar light (300 W/m^2)	Degradation efficiency of 50 % and 96.7 % were achieved for ZnS and Cd-ZnS (Cd 0.5 M) NPs respectively within a span of 120 min for a dye concentration of 5 $*10^{-5}$ M.	(Jabeen et al. 2017)
ZnO NPs synthesis in the presence of polyacrylamide grafted guar gum polymer (pAAm-g-GG)	Precipitation method	Acridine orange	UV light (4.0 $* 10^3$ μW/cm^2)	Maximum of 98 % dye degradation was obtained for catalyst dosage of 0.2 g/L, AO dye concentration of 10 mg/L and contact time of 210 min.	(Dhiman et al. 2017)
Biological zinc oxide NPs	*Lagerstroemia speciosa* leaf extract	Methyl orange	Solar light (1250-1300 W/m^2)	93.5 % degradation of 10 mL of dye is achieved with in 2 h and a significant decrease in the COD values is observed from 5600 mg/L to 374 mg/L.	(Saraswathi et al. 2017)
ZnO NPs	Co-precipitation method	Rhodamine B	Visible light (λ> 420 nm)	Efficiency achieved for degrading 5*10^{-6} M dye concentration is 84 %, 78 % and 75 % for spherical NPs, nanosheets, hexagonal NPs respectively in 2 h.	(Akir et al. 2016)

NPs	Method of Preparation	Dye	Light Illumination	Degradation Efficiency	Reference
Se-ZnS NPs	wet impregnation method	Methyl orange dye	UV irradiation	Degradation efficiency of 95 % is achieved for methyl orange using Se-ZnS NPs under UV light irradiation in 160 min.	(Ahluwalia et al. 2016)
ZnO NPs	*Carissa edulis* extract	Congo red	UV-Vis light (365 nm)	97 % of photocatalytic degradation is recorded for 1mM Congo red.	(Fowsiya et al. 2016)
ZnO NPs	Chemical precipitation	Methyl violet	Solar	1.25 mg of methyl violet was sonicated by ZnO NPs, when exposed to solar light it showed 100 % degradation in 80 min.	(Jeyasubramanian et al. 2015)
ZnS/chitosan NPs	Green colloidal chemical method	Methylene blue and Methyl orange	UV light (6 W, $\lambda = 254$ nm)	ZnS–CHI nano-conjugates showed degradation potential of 87 % for MB and 68 % for MO in 120 min.	(Mansur et al. 2014)
Fe^{3+} doped ZnS quantum dots	Co-precipitation method	Methyl violet	UV light (40 W)	95 % degradation of MV is achieved in 90 min for 80 mg/L of quantum dot particles	(Shamsipur and Rajabi 2014)
Core CuS/ZnS core/shell nanocrystals	Hydrothermal method	Rhodamine B	Visible light (20 mW/cm^2)	50 % degradation of Rhodamine B (1×10^{-5} M) is reported in 2 h.	(Thi et al. 2014)

2.8. Phenolic compounds degradation

Persistent organic contaminants such as phenolic compounds, pose serious risks to the environment which show low biodegradability once discharged into natural waters. Probably the most dangerous compounds of this class are those chlorinated and nitro-substituted phenolic compounds (Du et al. 2006). Many of the water pollutants are from industrial and municipal wastes and are toxic, persistent and not readily biodegradable. In most of the industries, phenol and phenolic compounds are widely used and have become common pollutants in wastewater bodies. Phenol finds itself in many applications such as disinfectant, chemical reagent, manufacture of organic compounds and also present as a threat in wastes released from oil refineries, steel industries, pharmaceuticals, plastics, textiles, coal conversion plants. In water bodies, phenolic compounds are considered as priority organic pollutants by USEPA considered due to their toxic, carcinogenic and mutagenic nature, further, it contains endocrine disrupting chemicals.

2.8.1. 2,4-D Herbicide

The herbicide 2,4-D is globally used since 1968 and it is reported as one of the main ingredients among 1500 pesticides. Further, it is considered a toxic and persistent matter and it causes various health impacts on human and animals. Moreover, due to its relatively high solubility in water, 2,4-D was detected in river and drainage water. Several methods including adsorption of hydrogen peroxide/UV irradiation, electrochemical oxidation, a combination of ozonation and photocatalysis have been employed to remove 2,4-D from water (Maltseva et al. 1996; Alfano et al. 2001; Akpan and Hameed 2011; Tang et al. 2013; Schenone et al. 2015). According to previous reports, various microbes such as *Pseudomonas cepacia* AC110, *Pseudomonas putida* UWC3, *Alcaligenes eutrophus* JMP134 (Sandmann 1984; Ogram et al. 1985; Haugland et al. 1990, Greert and Shelton 1992; Dejonghe et al. 2000) were utilized for degradation of 2,4-D. Sun and Pignatello (1993) reported the ability of eubacteria *Halomonadaceae* isolated from Lake site in Southwestern Oregon has a degradation capability of 3000 mg 2,4-D L^{-1} in 3 days due to the presence of *tfd A* gene. Table 2.4 focuses on the herbicide degradation by NPs.

Table 2.4: Summary of the use of NPs for degradation of the herbicide

NPs	Method of Preparation	Herbicide	Light Illumination	Degradation Efficiency	Reference
Magnetic copper ferrite nano-particles (MCFNs)	Co-precipitation method	2,4-D	Ozone / peroxymono-sulfate (PMS) system was used for degradation	MCFNs were used for the complete degradation of 20.0 mg/L 2,4-D at pH = 6.0 for a reaction time of 40 min.	(Jaafarzadeh et al. 2017)
Pt/TiO$_2$ NPs	Sol–gel method	2,4-D and 2,4-DP	Mercury-lamp of illumination 400 W λ=365 nm	The reactor was loaded with 20 mg/L concentration of 2,4-D and 120 mg of the Pt/TiO$_2$ photocatalyst.	(Abdennouri et al. 2015)
FeS NPs	Precipitation method	2,4-D	UV light	10 mg/L of 2,4-D and FeS NPs dose of 0.5 g/L showed 100 % degradation within 300 min.	(Chen et al. 2015)
TiO$_2$ photocatalyst films	Chemical Vapour Deposition method	2,4-D	UV light	The deterioration rate of 2,4-D expanded with increasing microwave intensity, UV intensity and the auxiliary oxidant dosage was considered.	(Lee et al. 2015)

NPs	Method of Preparation	Herbicide	Light Illumination	Degradation Efficiency	Reference
ZnO–Fe_2O_3 coupled oxide NPs	Sol gel method	Dicamba and 2,4-D	Solar light	Complete degradation was achieved at an initial pollutant concentration of 10 mg/L using 0.5 g/L of catalyst loading after 300 min	(Maya-treviño et al. 2014)
Soil, Biochar plus from maize straw and Fe^0 NPs	Laser induced CVD	2,4-D	-	Fe^0 NPs in addition to biochar degraded 2,4-D completely with loading rates of 0.33 and 0.17 g/L within 72 h.	(Bo et al. 2015)

2.8.2.   *PARA Drug*

In view of huge production and quantitative use of PARA, it has been frequently found in the environment, particularly in the aquatic environment with 0.01-0.03 mg/L leading to hazardous effect proving that it is not an absolutely safe drug. PARA or para-acetylaminophenol-acetaminophen is a broadly utilized pain relieving/antipyretic pharmaceutical and set among the main 200 prescriptions in the USA. Regardless of its safety at therapeutic dosages, the medicine might be lethal at higher measurements through an oxidative change of the parent compound to N-acetyl p- benzoquinone-imine (NAB), which is a dangerous compound driving to hepatic necrosis (Ziylan-Yavas et al. 2015).

Several methods for paracetamol degradation were noted such as ozonation, H_2O_2 photolysis, solar photoelectro-Fenton (SPEF) method, β-cyclodextrin/TiO_2 suspension under visible irradiation, sonolysis, photocatalysis and sonophotocatalysis, heterogeneous (TiO_2) photocatalysts (Andreozz et al. 2003; Almeida et al. 2010; Jagannathan et al. 2013; Zhang et al. 2015). The degradation of PARA was reported using *Corynebacterium pseudodiphtheriticum*, *Penicillium* species, *Pseudomonas* sp. strain ST-4, *Stenotrophomonas* sp*., Pseudomonas* sp*., Delftia tsuruhatensis, Penicillium* sp*., Cupriavidus necator* and *Burkholderia* sp. *Delftia tsuruhatensis*, *Pseudomonas aeruginosa* (Grant et al.,1970; Hart and Orr 1974; Gusseme et al. 2011; Wu et al. 2012; Li et al. 2012; Zhang et al. 2013; Khan et al. 2014) were utilized for paracetamol degradation. Table 2.5 focuses on the summary of NPs used for drug degradation.

Table 2.5: Summary of the use of NPs for degradation of the drug

NPs	Method of Preparation	Drug	Light Illumination	Degradation Efficiency	Reference
Lanthanum (La) doped ZnO NPs	Precipitation method	Paracetamol	Visible light	La-doped ZnO photocatalysts were utilized to treat 100 mg/L paracetamol in aqueous solution under visible light illumination after 3 h. 1.0 wt% La doped ZnO photocatalyst demonstrated the most elevated photocatalytic action for the degradation of paracetamol with a degradation proficiency of 99 % and 85 % TOC removal.	(Viet and Lee 2017)
ZnO NPs	Hydro thermal method	Metronidazole	Ultrasound irradiation	Complete degradation of pharmaceuticals waste, metronidazole under ultrasound light was achieved using ZnO NPs of quasi-cylindrical sizes 20–50 nm as a catalyst for the degradation.	(Bhuyan et al. 2016)
n-platinum-loaded TiO_2	Ultra sonication	Paracetamol	Ultrasound, UV and both	Paracetamol showed 100 % degradation using sonolytic oxidation of PCT during catalysis with $Pd–TiO_2$ and $Pd/Au–TiO_2$	(Ziylan-Yavas and Ince 2016)

NPs	Method of Preparation	Drug	Light Illumination	Degradation Efficiency	Reference
NaX nanozeolites and cobalt ferrite NPs	Microwave heating method	Phenol and paracetamol	UV light	The exploratory outline exhibited that the pH of 3.5, H_2O_2 concentration of 50 mmol/L and cobalt nanoferrite estimations of 0.2 g/L enlarge the adequacy of phenol and paracetamol degradation rates at the time in photo-Fenton process. The most extraordinary preliminary phenol and paracetamol degradation efficiencies for initial concentration of 20 mg/L of phenol and paracetamol were seen to be 95 % and 85 %, independently.	(Rad et al. 2015)
ZnO NPs	Mechano-chemical method	Acet aminophen and Chloramphe nicol	UV-light	The ZnO powders annealed at 100 ^{o}C demonstrate most astounding photocatalytic effectiveness and rate constant of dye degradation, which is because of the smaller size of nanocrystallites and their better created surface. The degradation rate of acetaminophen and chloramphenicol increments with a time of mechanical initiation up to 30 min.	(Kaneva et al. 2015)

2.9.   Synthesis of NPs in Bioreactor

The accessibility of a substantial large-scale production technique is essential for the acquaintance of any product with the market. Recently, industrial demands for NPs have increased as the number of potential applications for the material has grown. Because of the expanded request of quantum dots for different applications, researchers have started to investigate the large-scale synthesis of nanocrystal quantum dots by different means. Table 2.6 gives an overview of NPs production in various types of reactors.

Table 2.6: NPs production in various types of reactors

Method	Type of NPs	Production rate	Reference
Bioreactor (*Geobacter sulfurreducens)*	Magnetite NPs 10 and 15 nm	120 g from 50 L bioreactor	(Byrne et al. 2015)
Membrane bioreactor (*Citrobacter braakii*)	Palladium NPs	-	(Hennebel et al. 2011)
Fermentation (*Thermoanaerobacter sp.* TOR-39)	Zn-substituted Magnetite 5–90 nm	1 kg (wet weight) recovered from 30 L fermentations	(Moon et al. 2010)
Microchannel reactor	Barium sulphate NPs 30 to 150 nm	9 L/min	(Wang et al. 2010)
Fixed-bed flow reactor by CVD	Multiwalled carbon nanotubes	100 g/day	(Couteau et al. 2003)
Aerosol flame reactors	Titania NPs 5 nm	150 g/h	(Stark et al. 2002)
Fluidized-bed reactor produced by catalytic CVD	Carbon nanotubes	50 kg/day	(Wang et al. 2002)
Fluidized bed reactor via chemical reaction	Tungsten disulfide hollow onion-like NPs100 nm 0.5 µm	0.4 g per batch	(Feldman et al. 2000)

The state of the art reveals the constraints involved in the chemical synthesis as this process requires high temperature, pressure and produce toxic byproducts. Therefore, biological sources such as bacteria, fungi, yeast and plant extract are exploited. According to the state of the art, it is evident that the use of endophytic fungi is limited to metallic NPs synthesis such as gold and silver. Recent years have evinced the integration of nanomaterials of biological origin in nano-engineered devices where ZnS NPs are proven to be the potential candidates for various advanced applications such as biosensors, catalyst, microbial studies etc., Endophytic fungi have the capability to secrete enzymes which are efficient in degrading of xenobiotics, wood and phenanthrene, owing to these advantages, NPs synthesized from endophytes have been explored. The present research aims for the degradation of organic pollutants from the aqueous phase using biological NPs synthesized from the endophytic fungus *Aspergillus flavus* isolated from a medicinal plant *Nothapodytes foetida* and their large-scale production of ZnS NPs.

CHAPTER 3

3.   EXPERIMENTAL DETAILS

3.1 Collection of samples, isolation, screening and identification of metal tolerant fungal species from endophytic fungi

Healthy and fresh leaves of a medicinal plant, *Nothapodytes foetida,* were collected from Agumbe forest, Western Ghats, Daksina Karnataka, India located at 13º 30 N and 75º 2 E. *Nothapodytes foetida* is a renowned for its pharmacological properties and belongs to the *Icacinaceae* family. The explants (leaves) were cut into small pieces with a sterile scalpel and stored in a sterile polythene bag (Musavi and Balakrishnan, 2013).

Figure 3.1: (a) Location of sampling sites; (b) Leaves of the medicinal plant
Nothapodytes foetida

Firstly, the leaf segments were subjected to surface sterilization using ethanol (75 %) and sodium hypochlorite (2.5 %) followed by water rinsing. Small pieces of the leaves were placed on the Potato Dextrose Agar (PDA) media containing petri plates such that the internal tissues are in contact. These plates were periodically checked to observe fungal growth. The completely grown cultures were taken and sub cultured periodically. After the incubation period, the isolates were streaked on to the plates. Further, the identification of these isolates was carried out at Agharkar Research Institute, Pune, India (Singh et al. 2013; Devi and Joshi 2015).

The isolated fungal strain's growth and tolerance studies were conducted by adding 2 x 5 mm mycelia discs in shake flasks containing Potato Dextrose Broth (PDB). These flasks were kept in a shaker at 115 rpm at 28 °C. At different time intervals the flasks containing the broth were withdrawn at different time intervals and the biomasses were separated by filtering with Whatman filter No.42. paper. These biomasses were rinsed with distilled water for more than three times to remove the media. The biomasses are collected in petri plate and kept in a hot air oven at 70 °C for drying and their dry weights were used for evaluating growth curve. For screening the most tolerant fungal isolate, along with mycelial discs 1mM zinc heptahydrate solution was added to the broth and the biomass was collected periodically. Further, their biomass dry weights were measured and compared with the biomass without adding precursor solution which is the control. Based on the screening, the most tolerant fungal isolate was subjected to precursor zinc hepta hydrate solutions of various concentration range 0.5-3 mM to find the optimal concentration for the synthesis of NPs (Mary et al. 2014).

3.2. Synthesis and optimization of ZnS NPs protocol

3.2.1. *ZnS NPs extracellular biosynthesis*

Fungal mycelial discs of *Aspergillus flavus* (dia 2 mm × 5 mm) were added to 250 ml PDB and kept in an orbital shaker at 28 °C, 115 rpm. After two days of fungal growth, the biomass was separated from the media and added to 3 mM zinc sulfate heptahydrate to facilitate the synthesis process (Mirzadeh et al. 2013).

3.2.2. *Optimization of ZnS biosynthesis process*

The synthesis of NPs was investigated by different process parameters using central composite design (CCD) of response surface methodology (RSM). In order to evaluate the influence of operating parameters on the synthesis of NPs, three main factors were chosen: biomass dry weight (g/L) (β_1), precursor concentration (mM) (β_2) and reaction time (days) (β_3), containing 20 runs with eight factorial points, six axial points and six replicates at the center point (Table 3.1) and the experimental data were fitted to a second-order polynomial model as follows:

$$y = \beta_0 + \beta_1 A + \beta_2 B + \beta_3 C + \beta_{11} A^2 + \beta_{22} B^2 + \beta_{33} C^2 + \beta_{12} AB + \beta_{23} BC + \beta_{31} CA \ldots \ldots (3.1)$$

where, y represents the response variable, β_0 the intercept, β_1, β_2, β_3 coefficients of the independent variables, β_{11}, β_{22}, β_{33} quadratic coefficients, β_{12}, β_{23}, β_{31} interaction

coefficients and A, B, C are the independent variables studied. Design Expert software version 7 was used for multi variate regression analysis and optimization process (Musavi and Balakrishnan 2014).

Table 3.1: Experimental range and levels of the independent variables

Variables	Ranges and levels				
	-1.68	-1	0	1	1.68
Biomass dry weight (g/L)	10.23	9.7	7.5	6.3	6
Precursor concentration (mM)	1	2	3	4	5
Reaction time (days)	3	4	5	6	7

The statistical software package Design Expert (Version 8.0.7.1, Stat-Ease Inc., Minneapolis, USA) statistical package was used to analyze the experimental data. The optimal values of the critical variables were obtained by analyzing the contour plots and the statistical analysis in the form of variance (ANOVA). The effect of a particular component on the response was considered significant only if p value ≤ 0.05 was obtained.

3.3. Studies on the mechanism of ZnS NPs

In order to investigate the mechanism involved in the synthesis process, the biomass and supernatant were characterized by Scanning Electron Microscope (SEM) (JSM-6380, Tokyo), Atomic Force Microscope (AFM) (WITec GmbH, Ulm, Germany). Moreover, protein estimation is carried out by Lowry's assay and identified through total ion chromatogram/ mass spectrum.

3.3.1. Protein precipitation

Cool the required volume of acetone to -20 °C, add four times the sample volume of cold acetone to the tube. Further, incubate for 60 min at -20 °C and centrifuge for 10 min at 12000 rpm. Decant the supernatant and collect the pellet. Allow the acetone to evaporate from the tube at room temperature for 30 min. The protein was lyophilized at -80 °C and incubated overnight at 37 °C.

In order to investigate the role of proteins in NPs formation, Lowry's method was adopted to estimate the extracellular crude protein concentration from the fungal supernatant. A calibration curve was plotted using standard protein Bovine Serum Albumin (BSA) ranging from 0.1 to 1 mg/ml (Figure 3.2). The total protein concentration is exhibited by a colour change of the sample solution in proportion to protein concentration, which is then measured using colorimetric techniques. Absorbance of the test samples were recorded at 660 nm using Ultraviolet-visible (UV-Vis) spectrophotometer (UV-2450, Shimadzu, Japan) and the total protein content was analysed using the linear fit equation of the calibration plot (Waterborg and Matthews 1984).
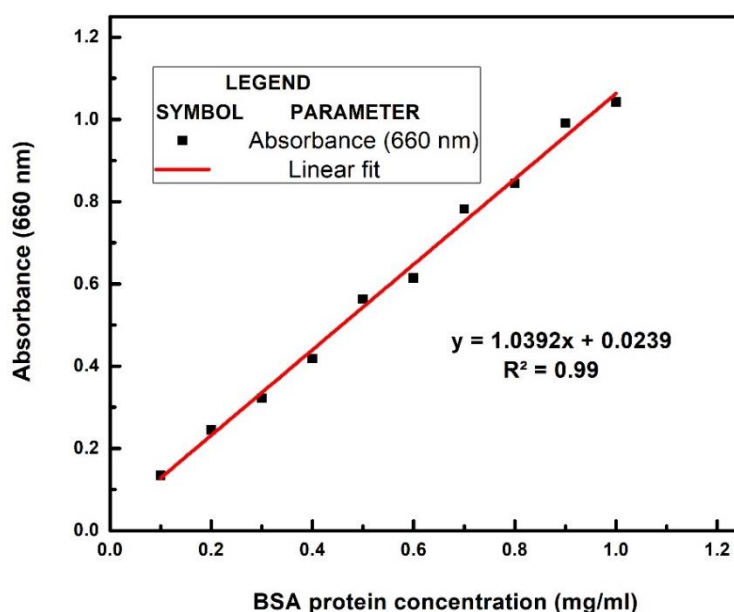
Figure 3.2: Calibration plot of the BSA protein

3.3.2. HPLC and LC-MS

The retention time of the proteins present in the NPs were estimated by High-performance liquid chromatography (HPLC) (Shimadzu LC-10, HPLC system, USA) and Liquid chromatography-Mass spectrometry (LC-MS) method (Shimadzu LC-MS model, LCMS-8040, USA). The system consisted of C-18 guard column (4.6×250 mm, 5 µm size) and the system was operated using acetonitrile/water in binary mode with isopropanol and water in the ratio of 60:40. These components were filtered through 0.2 µ membrane filter before use and were pumped from the solvent reservoir at a flow rate of 1 ml/min at an ambient temperature (25–28 °C). The sample injection volume was 20 µl and the wavelength

of the UV–Vis detector was set at 254 nm. The conditions involve an oven temperature of 26 $^{\circ}$C, carrier gas N_2 and pump pressure of 100 bar.

3.3.3. *Morphological characterization*

During the biosynthesis process, both the biomass and supernatant were characterized using SEM and AFM in order to investigate the distribution of the NPs in both the regime. The fungal biomass before and after the addition of the precursor was oven dried at 70 $^{\circ}$C for 4 h and further characterized using SEM. The pretreated samples were sputtered with gold particles using a sputter coater under vacuum at an accelerating voltage of 12 kV to capture images and observed under SEM (JEM-2100, JOEL, Tokyo). The NPs were immobilized on a glass slide for 6 h at room temperature and allowed to be dried. The samples were studied using contact mode with a cantilever tip at 150 Hz and 70 mW. Scan rates were set in the 0.5–1 Hz range depending on the size of the scanned area; it consists of Diode-pumped solid-state (DPSS) laser (Alpha300RA AFM, WITec GmbH, Ulm, Germany).

3.4.   Characterization of synthesized NPs

3.4.1. *Morphological characterization*

The biosynthesized product was characterized based on Transmission Electron Microscopy (TEM) (JEM-2100, JOEL, Tokyo) operating at 200 kV, a drop of lyophilized (FD5-series Freeze Dryer) cell-free filtrate-containing ZnS NPs was placed on the carbon-coated copper grids and kept under vacuum desiccation overnight before loading them onto a specimen holder. For the analysis, the NPs sample of the desired concentration was flushed through a folded capillary cell and the measurement was carried out; a sufficient sample volume was used to completely cover the electrodes of the cell. To avoid air bubbles in the cell, the samples were injected slowly and analysis was only carried out if there were no visible air bubble inclusions present. Then the cell was placed in the sample holder and the corresponding Dynamic light scattering (DLS) (Horiba, nanopartica SZ-100, Japan) measurements were taken. Preliminary characterization for the formation of ZnS NPs was checked by analysis under SEM (JSM-6380, JOEL, Tokyo) and the composition is given by Energy Dispersive Analyses of X-rays (EDAX). X-ray diffraction (XRD) (JOEL, DX GE-2P vertical goniometer, Japan) patterns were recorded on a Riga KuC/max-2500 diffractometer using graphite filtered Cu Kα radiation at 30 kV and 20 mA with a scanning rate of 4° min^{-1} from 2θ = 20° to 70° angles. The diffraction angles obtained for the samples were compared

using 'X'pert high score software with search and match facility and compared with the data by the International Center for Diffraction Data (ICDD).

3.4.2. Optical characterization

Samples were withdrawn from the 5-day-old fungal cultures, for measuring the absorbance it is taken in a cuvette and measured using UV-Vis spectroscopy (UV-2450, Shimadzu, Japan). The band gap was determined by Tauc plot and the crystallite size was calculated based on Scherrer equation as follows:

$$D = k\,\lambda\,/\,\beta\,\cos\theta \ldots\ldots\ldots\ldots\ldots (3.2)$$

where, D, λ, θ, β and k size of the crystalline, wavelength and Bragg angle line broadening at half the maximum intensity (FWHM) dimensionless factor close to unity.

For diffuse reflectance spectroscopy (DRS) experiments were taken using a UV-Vis spectroscopy Varian, Cary 5000 in a diffuse reflectance mode within a spectral range of 175 – 3300 nm. The optical band gap energy (E_g) is calculated by the Kubelka and Munk method (Reddy et al. 2014, Poornaprakash et al. 2013).

$$(\alpha h\upsilon)\,\alpha\,(h\upsilon - E_g)^{n/2}\ldots\ldots\ldots\ldots..(3.3)$$

where, A is the absorbance (a.u), $h\upsilon$ is the energy of the photon and E_g is the band gap energy of the material, $n = 1$ for direct band gap material.

$$F(R) = (1 - R^2)/2R$$

$$[F(R)h\upsilon]^2 = A(h\upsilon - E_g] \ldots\ldots\ldots (3.4)$$

where, R is the absolute reflectance of the material, $h\upsilon$ is the photon energy and E_g is the optical band gap.

Photoluminescence spectra were achieved through fluorescence measurement (Fluorolog 3 TCSPC, Horiba, Japan), xenon lamp as an excitation source and at an excitation wavelength of 315 nm and grating 1200 g/mm. All measurements were performed at room temperature.

$$\frac{\phi_S}{\phi_R} = I_S A_R n_S^2 / I_R A_S n_R^2 \quad \ldots\ldots\ldots\ldots\ldots (3.5)$$

where, ϕ is the quantum yield (%), A is the absorbance in (a.u), I is the intensity of the fluorescence peak in (a.u) at the excitation wavelength, n is the refractive index of the solvent used for dissolving the NPs, S and R refers to sample and reference (Rhodamine-6G) respectively

In order to investigate the crystallization, structural disorder and defects of the ZnS NPs, Raman measurements were performed at room temperature. The instrument used for this

spectroscopy was a Confocal RAMAN Imaging System (WITec GmbH, Ulm, Germany) alpha 300RA. A fiber coupled DPSS laser 532 nm with maximum output power after single mode fiber coupling of 70 mW, grating 600 g/mm, an integration time of 10 sec.

$$\Delta\omega = -38\omega_o \Delta a/a_o \quad ………………. (3.6)$$

where ω_o is Raman frequency of bulk ZnS, a_o is the bulk ZnS lattice constant, Δa is the change in lattice constant, and 8 is the Gruneisen constant with a value of 1.28 for ZnS.

For, Fourier Transfer Infra-Red (FTIR) Spectrometer (JASCO spectrometer 4100, Perkin–Elmer, USA) for the spectral range of 4000 – 600 cm^{-1} with resolution of 4 cm^{-1} attenuated total reflection (ATR) mode.

3.4.3. Thermal characterization

The thermal stability of the samples was studied using the thermal analysis technique, for the recording of Thermo-Gravimetry (TG), Derivative Thermo gravimetric Analyzer (DTG) (Model: Perkin Elmer, Diamond) and Differential Scanning Calorimeter (DSC) (Mettler Toledo DSC 822e) analyses under airflow. 35 mg of samples were heated at the heating rate of 10 °C/min in the temperature range of 35–800 °C in TGA-DTG and heating rate at room temperature to 700 °C in 7 min in case of DSC. The specimens were heated from room temperature to 900 °C with an increment of 10 °C/min in air. Samples analyzed were contained within alumina crucibles and heated at a rate of 10 °C min^{-1} under flowing air flow (Darezereshki et al. 2011; Mirzadeh et al. 2013).

3.4.4. Stability studies

To study the stability of NPs, initially spectrum was recorded based on UV measurements and it is noted that stability is decreased with time. The results were analyzed at λ_{max} of 315 nm for ZnS NPs for 30 days (Sadeghi et al. 2014; Ray et al. 2015) and these values determine the stability for NPs based on the absorbance values.

For this zeta potential analyzer, the temperature is set at 25 °C and at scattering angle equal to 90° (Horiba, nanopartica SZ-100). For the analysis, the NPs sample of the desired concentration was flushed through a folded capillary cell and the measurement was carried out; a sufficient sample volume was used to completely cover the electrodes of the cell. To avoid air bubbles in the cell, the sample was injected slowly and analysis was only carried out if there were no visible air bubble inclusions present. Then the cell was placed in the sample holder and the corresponding zeta-potential measurements were taken (Tantra et al. 2010).

The Electrochemical workstation was employed for the electrochemical characterization of the ZnS NPs samples (VERTEX Ivium I.A.E.I.S, Netherlands). It consists of three electrodes namely the working electrode (Pt electrode), the reference electrode (calomel electrode) and the counter electrode (Pt wire). The cyclic voltammetry curve was obtained by sweeping the potential at a rate of 25 mV/s between -2.5 V and 2.5 V (Murugadoss et al. 2016).

3.5. Degradation of organic pollutants using ZnS NPs

3.5.1. Degradation studies

To study the catalytic activity of ZnS NPs for the degradation process, three model pollutants MV ($C_{24}H_{28}N_3Cl$, 393.9g/mol), 2,4-D ($C_8H_6Cl_2O_3$, 221g/mol), PARA ($C_8H_9NO_2$, 151g/mol) was used for the study. The experiments were carried out using natural sunlight from 11 A.M. to 4 P.M. with the average solar intensity of 1.4 x 10^5 lx using lux meter (KM-LUX-100K, India).

The experimental system was loaded with MV/2,4-D/ PARA along with the catalyst and it was placed on a magnetic stirrer to ensure homogeneous agitation. Aliquots of samples were taken for the analysis at regular intervals of time and centrifuged at 8000 rpm for 10 min. The progress of the photocatalytic reaction was observed by recording optical density (OD) at 570 nm wavelength for dye using UV-Vis spectrophotometer (UV-2450, Shimadzu, Japan). The same protocol was followed for 2,4-D and PARA samples and OD was recorded at 280 nm and 248 nm respectively. Effect of pH was studied by varying the pH of NPs solution from 3-13 at pollutant concentration of 100 mg/L at constant time (Bokare et al. 2008; Soltani et al. 2013; El-Gamal et al. 2015).

Prior to irradiation, the mixture was maintained in dark for 30 min under stirring conditions to reach adsorption equilibrium. The percentage degradation efficiency (η) at a reaction time *t* (min) is calculated as follows:

$$\eta = (C_0 - C_t)/C_0 * 100 \dots\dots(3.7)$$

where, C_0 is the initial concentration (mg/L) and C_t is the final concentration (mg /L) at a reaction time *t*.

3.5.2. Kinetics of degradation

The kinetics of degradation was studied based on the pseudo first-order kinetic equation and the rate constants (k_1) were determined from the slope. The equation for pseudo first-order kinetic model given as follows:

$$\ln A_o/A_t = k_1 t \ldots\ldots\ldots\ldots\ldots\ldots(3.8)$$

where A_o and A_t are the initial and final absorbance (a.u) at time t (min); k = pseudo first-order rate constant respectively (El-Zomrawy 2013; Tiya-Djowe et al. 2015).

3.5.3. Thermodynamic studies

The Gibbs free energy (ΔG_0) equation of chemical reactions is suitable to analyse the closed systems that exchange energy, with the outside, therefore it can be used to describe photocatalytic reactions. The ΔG_0 after light excitation forms the thermodynamic cause of photocatalysis. Generally, the ΔG_0 of interfacial transfer of electrons in photocatalysis is smaller than the change of internal energy. Batch experiments were conducted both in dark and in the presence of light at 306 K and 312 K respectively, to evaluate thermodynamics of the photocatalysis process. A negative Gibbs free energy change indicates that the adsorption is favourable. The ΔG value is determined using equations (3.9) and (3.10) as follows:

$$\Delta G = G_{dark} - G_{light} \ldots\ldots\ldots\ldots\ldots \text{ (3.9)}$$

$$\Delta G^0 = -RT\, ln\ (k_c) \ldots\ldots\ldots\ldots\ldots \text{ (3.10)}$$

where, G_{dark} and G_{light}, G change of a semiconductor in the dark and under light excitation, K_c = C_{Ae}/C_e is the equilibrium constant, C_{Ae} and C_e are the concentration (mg/L) of pollutant on NPs and in solution, respectively, R is the universal gas constant (8.314 J/mol/K) and T is the temperature in Kelvin.

Based on the UV-Vis spectroscopy /DRS results, the band edge positions of the valence band and the conduction band of ZnS can be found out using the following equation:

$$E_{VB} = \chi - E_e + 0.5\ E_{bg} \ldots\ldots\ldots\ldots\ldots(3.11)$$

$$E_{CB} = E_{VB} - E_{bg} \ldots\ldots\ldots\ldots\ldots \text{ (3.12)}$$

where E_{VB} and E_{CB} are the valence band and conduction band edge potentials of the ZnS, χ isthe electronegativity of ZnS, which can be calculated as the geometric mean of the absolute electro negativities of the sulfur and zinc and found out to be 5.26 eV. E_e is the energy of the

free electrons on the free scale, i.e. 4.5 eV and E_{bg} is the calculated band gap of the ZnS, i.e. 3.75 eV.

3.6. Analysis to study the interaction of pollutant and NPs

3.6.1. AFM and FT-IR analysis

To confirm the interaction of ZnS NPs and pollutants, AFM analysis was carried out. Samples were immobilized on a glass slide for 6 h at room temperature for adherence on to the slide. The instrument was operated at contact mode with a cantilever tip at 150 Hz and 70 mW, scan rates were set in the range of 0.5–1 Hz depending on the size of the scan area, DPSS laser (Alpha300RA AFM, WITec GmbH, Ulm, Germany). The samples before and after degradation were recorded to analyze the functional groups and the structural changes. FTIR spectral analysis was carried out at ATR mode in the range of 4000–400 cm^{-1} in order to find the presence of functional groups before and after degradation of organic pollutants (JASCO spectrometer 4100, Perkin–Elmer, USA).

3.6.2. Fluorescence analysis

To test the quenching/enhancement efficiency of organic pollutants on ZnS NPs with respect to time at a given excitation wavelength of 315 nm. At periodic intervals of time, aliquots of the sample were withdrawn and the intensity of the emission spectra were recorded by fluorescence spectrometer (Fluorolog 3 TCSPC, Horiba, USA). The fluorescence emission and absorption spectra determine the interaction of organic pollutants with nanoparticle fluorophores. In order to understand energy transfer the distance between NPs and organic pollutants molecules was calculated using Forster mechanism of non-radiative energy transfer (Kavitha et al. 2014; Bhavani and Sivasamy 2016). According to Forster theory, the energy transfer effect is related not only to the distance (r_o) between the acceptor and donor but also to the critical energy transfer distance (R_o), i.e.

$$E = 1 - \frac{F}{F_o} = \frac{R_o^6}{R_o^6 + r_o^6} \ldots\ldots\ldots\ldots (3.13)$$

where, F is the fluorescence intensity of the donor in the presence of the acceptor, F_o is the fluorescence intensity of the donor in the absence of the acceptor and R_o is the critical distance at which the efficiency of energy transfer is 50 %, given as:

$$R_o^6 = 8.8 \, X10^{-25} k^2 n^{-4} \emptyset J(\lambda) \ldots\ldots\ldots\ldots (3.14)$$

$$r_o^6 = (1 - \frac{1}{\emptyset}) R_o^6 \ldots\ldots\ldots\ldots\ldots (3.15)$$

where, k^2 is the spatial orientation factor of the dipole, n is the refractive index of the medium, φ is the fluorescence quantum yield of the donor and J is the overlap integral of the fluorescence emission spectrum of the donor and absorption spectra of the acceptor, given by the equation:

$$J(\lambda) = \frac{\int_0^\infty F(\lambda)\, \varepsilon(\lambda)\, \lambda^4\, d\lambda}{\int_0^\infty F(\lambda)\, d\lambda} \quad\text{...............(3.16)}$$

where, $F(\lambda)$ is the fluorescence intensity of the fluorescence donor at wavelength λ and $\varepsilon(\lambda)$ is the molar absorptivity of the acceptor at wavelength λ.

3.7.   Mineralization studies

The total organic carbon (TOC) is one of the most important composite parameters in the assessment of the organic pollution of water. It employs the catalytic oxidation method via combustion by oxidizing the organic molecules in an aliquot of sample water to CO_2, measuring the resultant CO_2 concentration and expressing this response as carbon concentration. These measurements were carried out by TOC analyzer (Shimadzu TOC analyzer, Japan). The chemical oxygen demand (COD) was also determined in the supernatant samples using the standard open reflux method. The COD determines the amount of oxygen required for chemical oxidation of organic matter using a strong chemical oxidant, such as potassium dichromate ($K_2Cr_2O_7$) under reflux conditions. The organic matter present in sample gets oxidized completely by $K_2Cr_2O_7$ in the presence of sulphuric acid, silver sulphate and mercury sulphate to produce CO_2 and H_2O. The sample was refluxed with a known amount of $K_2Cr_2O_7$ in the sulphuric acid medium and the excess $K_2Cr_2O_7$ was determined by titration against ferrous ammonium sulphate, using ferroin as an indicator. The dichromate consumed by the sample is equivalent to the amount of O_2 required to oxidize the organic matter. The inorganics such as nitrates, nitrite and chloride ions concentration were measured by the standard spectroscopic, colorimetric method and an argentometric method respectively. The C(org) in mol CxHyOz m^{-3} and COD/TOC (mol O_2 m^{-3}) is calculated using the equation below for MV, 2,4-D and PARA.

$$C(org) = (4/(4x + y - 2z))TOC/COD\ldots\ldots\ldots\ldots\ldots(3.17)$$

3.8.   Degradation pathway analysis

The intermediates formed during the process of degradation were analysed by liquid chromatography-mass spectrometry (LC-MS) method (Shimadzu LC-MS model, LCMS-8040, USA). Samples were collected and stored in clean sample bottles. The LC-MS consisted of a C-18 guard column (4.6×250 mm, $5\ \mu$m size) and the system was operated using

acetonitrile/water in binary mode using isopropanol and water in the ratio of 60:40. The sample injection volume was 1 mL. The column was flushed with acetonitrile at the equilibration stage, and operated at a flow rate of 1 mL/min and washing and elution were carried out using isopropanol and acetonitrile, respectively. These components were filtered through 0.2 μm membrane filter before use and were pumped from the solvent reservoir at a flow rate of 0.5 mL/min, at ambient temperature (25-28 °C). The sample injection volume was 20 μL and the wavelength of the UV-Vis detector was set at 570 nm, 280 nm and 248 nm for MV, 2,4-D and PARA, respectively (Chen et al., 2010; Gan et al., 2014). The oven temperature was set at 26 °C, pump pressure at 100 bar and N_2 was used as the carrier gas. In order to determine the lowest detectable concentration all the organic pollutants, quality control stock solutions were prepared and calibration standards and serial dilutions were made at different ranges and tested individually. The LC-MS system was operated in full scan mode (m/z 50-500). From the electropherograms, the limits of detection were calculated using the peak height (i.e. the signal) and the standard deviation of the baseline (i.e. noise) (S/N=1). All the control and experimental samples were analyzed in duplicates. (Chen et al. 2010; Gan et al. 2014).

3.9. Production of NPs in a stirred tank reactor

3.9.1. Reactor specifications

The stirred tank reactor is one of the most important types of bioreactor for industrial production processes. There are various advantages of stirred tank reactor such as low capital/ operating costs, efficient oxygen transfer to growing cells and flexible operating conditions. The reactor used in this study is made up of a double jacketed borosilicate glass vessel with the top driven magnetic coupled motor having variable rpm for microbial fermentation mode. The bioreactor consists of four baffles and aeration is provided through an external air pump connected via glass metered needle valve rotameter with ring type air sparger. Various ports for pH, dissolved oxygen (DO) and temperature probe had been setup. Inoculation/sample ports for sampling are available. Polytetrafluoroethylene (PTFE) (0.22 micron) filter is fitted on the top of the condenser with inlet and outlet nozzles (Figure 3.3).
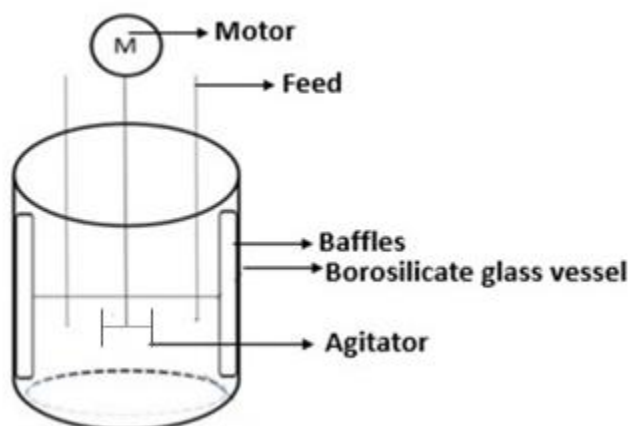
Figure 3.3: Schematic representation of the stirred tank reactor

3.9.2. Culture conditions

To set the seed culture, *Aspergillus flavus* was inoculated into the PDB medium and incubated at 30 ℃. After cultivation, 48 h spore suspension was obtained by rinsing the biomass with distilled water (Lu et al. 2015). The stock spore suspension was prepared and was added to the PDB media along with tween 80 (0.1 % v/v). Based on the growth curve, 100 mL of 48 h culture was taken as seed culture and transferred into the reactor (Byrne et al. 2016).

After preliminary studies, the culture conditions such as size of the inoculum (2 % - 20 % (w/v)), working volume (1- 2 L), agitation speed (70-120 rpm), precursor solution (10-50 mM) and reaction time (1-3 days) were optimized for 3 L bioreactor. The agitation rate was calculated using the equation (3.18) and (3.19),

$$V = \frac{\pi}{4} D_t^2 H \quad \text{...............} \quad (3.18)$$

$$N \propto \left(\frac{1}{D}\right)^{2/3} \quad \text{................} \quad (3.19)$$

where, V is the volume of the tank; D_t is the diameter of the tank; H is the height of the reactor, N is the agitation speed and D diameter of the tank.

There was no pH control after inoculation and temperature are maintained at 30 ℃. DO and flow rate was maintained at 6.8 mg/L and 1.5 LPM respectively.

To estimate the dry biomass weight, the homogeneous broth was filtered using Whatman filter paper (Whatman filter No.42) and the cells were weighed after being washed with distilled water and dried in a hot air oven at 40 ℃ overnight (Mantzouridou and Naziri, 2017).

3.9.3. Characterization of synthesized NPs

To evaluate the formation of NPs, aliquots of samples from the bioreactor were withdrawn and the absorbance were noted at 315 nm by UV-Vis spectrometer (UV-2450, Shimadzu, Japan). ZnS NPs synthesis under optimum conditions were confirmed using XRD (JOEL, DX GE-2P vertical goniometer, Japan) and TEM (JEM-2100, JOEL, Tokyo) (Moon et al. 2010) measurements.

CHAPTER 4

4. RESULTS AND DISCUSSION

The current section deals with the outcomes of the methodologies for synthesis, mechanism, characterization and degradation studies of ZnS NPs with appropriate justification from the literature. Initially, the results related to isolation of tolerant fungal strains from endophytic fungi by the growth, optimization of the ZnS tolerant fungus and the mechanism involved in the biosynthesis of ZnS NPs are briefed. Subsequently the structural, morphological, optical, thermal and stability are detailed. The degradation studies of MV, 2,4-D and PARA are discussed based on the degradation efficiency by optimizing the parameters further the interaction between ZnS NPs and pollutants, mineralization studies and the degradation mechanism are reported. Finally, their large-scale production and process variables responsible for the NPs formation are assessed in the reactor.

4.1. Isolation of fungus from collected samples and their tolerance studies

Medicinal plants provide a unique environment for endophytes where it receives nutrition and protection from the host plant, in turn, the endophytes protect the host plant from various biotic and abiotic stresses. In the present study, three endophytic fungi were isolated from the leaves of medicinal plant *Nothapodytes foetida* and were identified as *Aspergillus flavus*, *Aspergillus ficuum* and *Trichoderma parcermosum* based on the report given by Agharkar Research Institute, Pune, India (Figure 4.1). The growth studies reveal that *Aspergillus flavus*, *Aspergillus ficuum* and *Trichoderma parcermosum* attained maximum biomass on the 5th day of their growth cycle and remained at the stationary phase later. Figure 4.2 (a) reveals that the biomass dry weight was 20 g/L, 8.6 g/L and 2.5 g/L respectively based on their growth cycle. The acclimatization studies with 1 mM zinc heptahydrate solution, all three fungi found to be tolerant and their biomass yields were 19.6 g/L, 9.8 g/L, 1.6 g/L for *Aspergillus flavus*, *Aspergillus ficuum* and *Trichoderma parcermosum* respectively. As shown in Figure 4.2 (b), *Aspergillus flavus* was found to have the highest tolerance level, therefore it was considered for the synthesis of ZnS NPs.
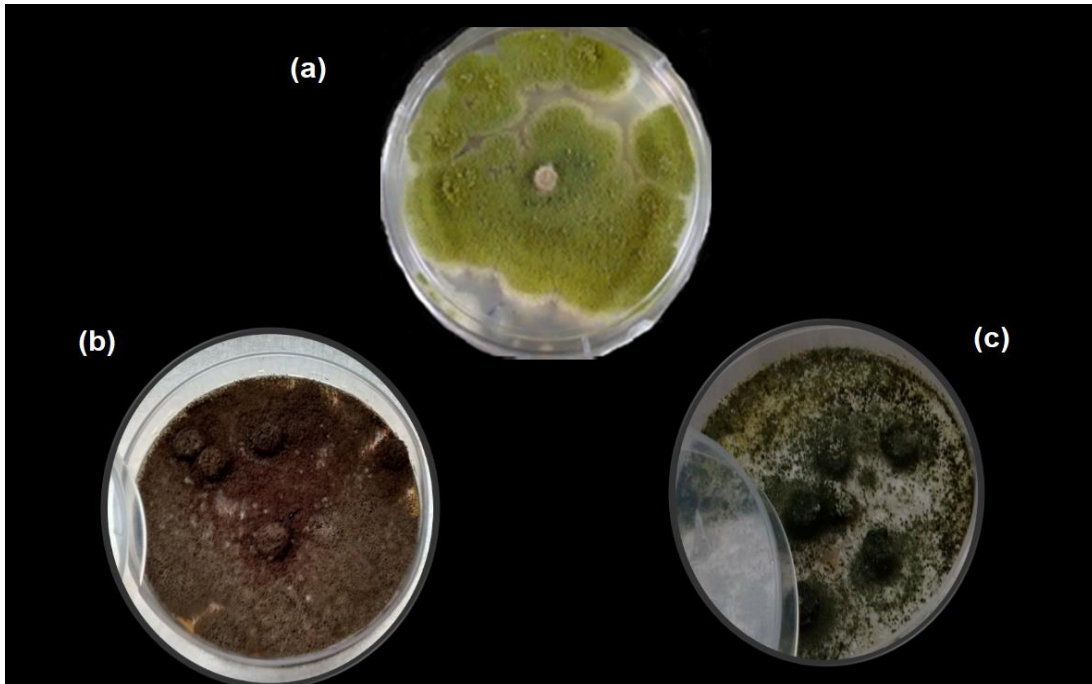
Figure 4.1: Isolated endophytic fungal species on PDA plates (a) *Aspergillus flavus*, **(b)** *Aspergillus ficuum* **and (c)** *Trichoderma parcermosum*
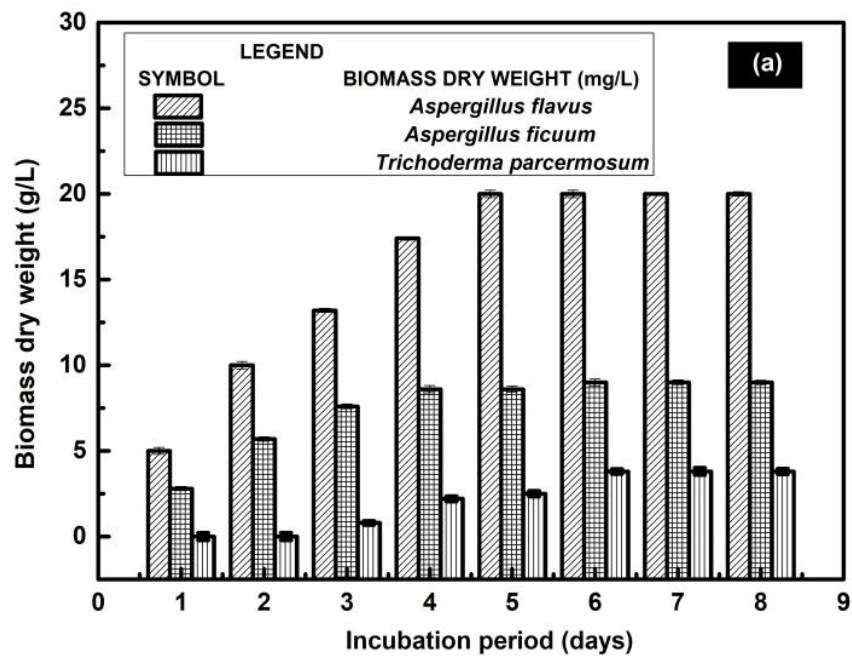
Figure 4.2 (a): Biomass yield of endophytic fungi *Aspergillus flavus*, *Aspergillus ficuum* **and** *Trichoderma parcermosum* **with respect to incubation time**
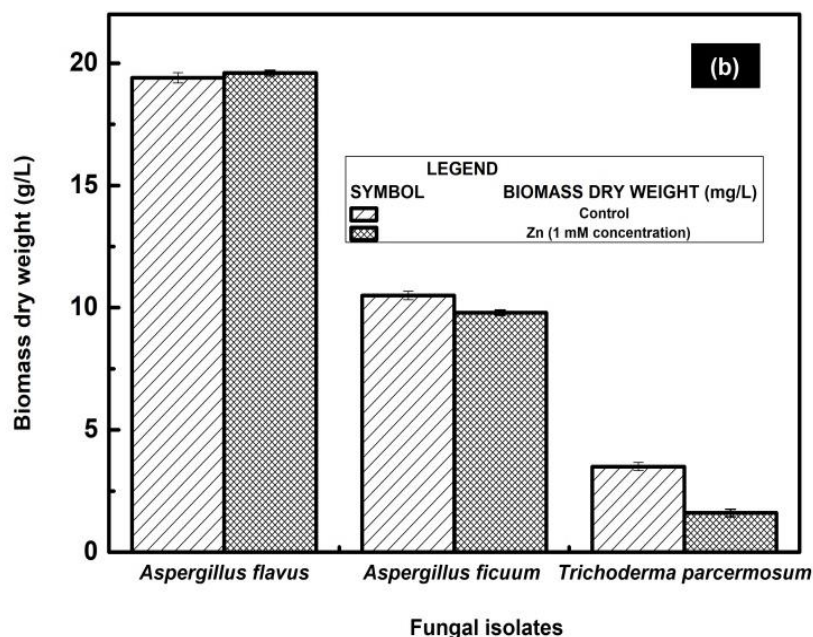
**Figure 4.2 (b) : Biomass yield of endophytic fungi *Aspergillus flavus*, *Aspergillus ficuum*
and *Trichoderma parcermosum* in presence of 1mM zinc heptahydrate solution
precursor solution**

4.2. Optimization of ZnS NPs synthesis process

The adequacy of the model was checked using analysis of variance (ANOVA) which was tested using Fisher's statistical analysis (Table 4.1). The model F value of 6.90 implied that the model was significant and also showed that there was 0.29 % chance that the model F value could occur due to noise. We obtained the number 7.1 of adeq precision (greater than 4 is desirable) indicates that the experiments performed were highly reliable. The results obtained from the CCD were fitted to a second-order polynomial equation below to explain the dependence of *Aspergillus flavus* growth and biomass production on the medium components.

$$y = 1.20 - 0.020\,A + 0.035\,B + 0.061\,C + 0.014\,AB + 0.014\,BC + 0.024\,AC - 0.091\,A^2 - 0.10\,B^2 - 0.074\,C^2 \ldots\ldots\ldots.(4.1)$$

where, y represents the response variable and A, B, C are the independent variables
The maximum predicted absorbance was found to be 1.19 (a.u) which is comparable to the experimental value of 1.2 (a.u) (Table 4.2) at biomass dry weight (g/L), precursor concentration (mM) and reaction time (days) concentrations of 7.5 (g/L), 3 mM and 5th day respectively for 20 runs (Figure 4.3: (a), (b) and (c)). Based on these results, growth curve and the effect of

different salt concentrations of zinc precursor on *Aspergillus flavus* growth is depicted in Figure 4.4 (a) and Figure 4.4 (b).

Table 4.1: ANOVA for Response Surface Quadratic model

Source	Sum of Squares	Mean Square	F Value	p-value Prob> F	
Model	0.374	0.041	6.895	0.002	Significant
A-A	0.005	0.005	0.912	0.361	
B-B	0.016	0.016	2.815	0.124	
C-C	0.051	0.051	8.545	0.015	
AB	0.001	0.001	0.250	0.627	
AC	0.001	0.001	0.250	0.627	
BC	0.004	0.004	0.748	0.407	
A^2	0.120	0.120	19.976	0.001	
B^2	0.149	0.149	24.881	0.0005	
C^2	0.078	0.078	12.996	0.004	

Table 4.2: Central Composite Design matrix for in dependent variables in uncoded units along with experimental and predicted values of biomass

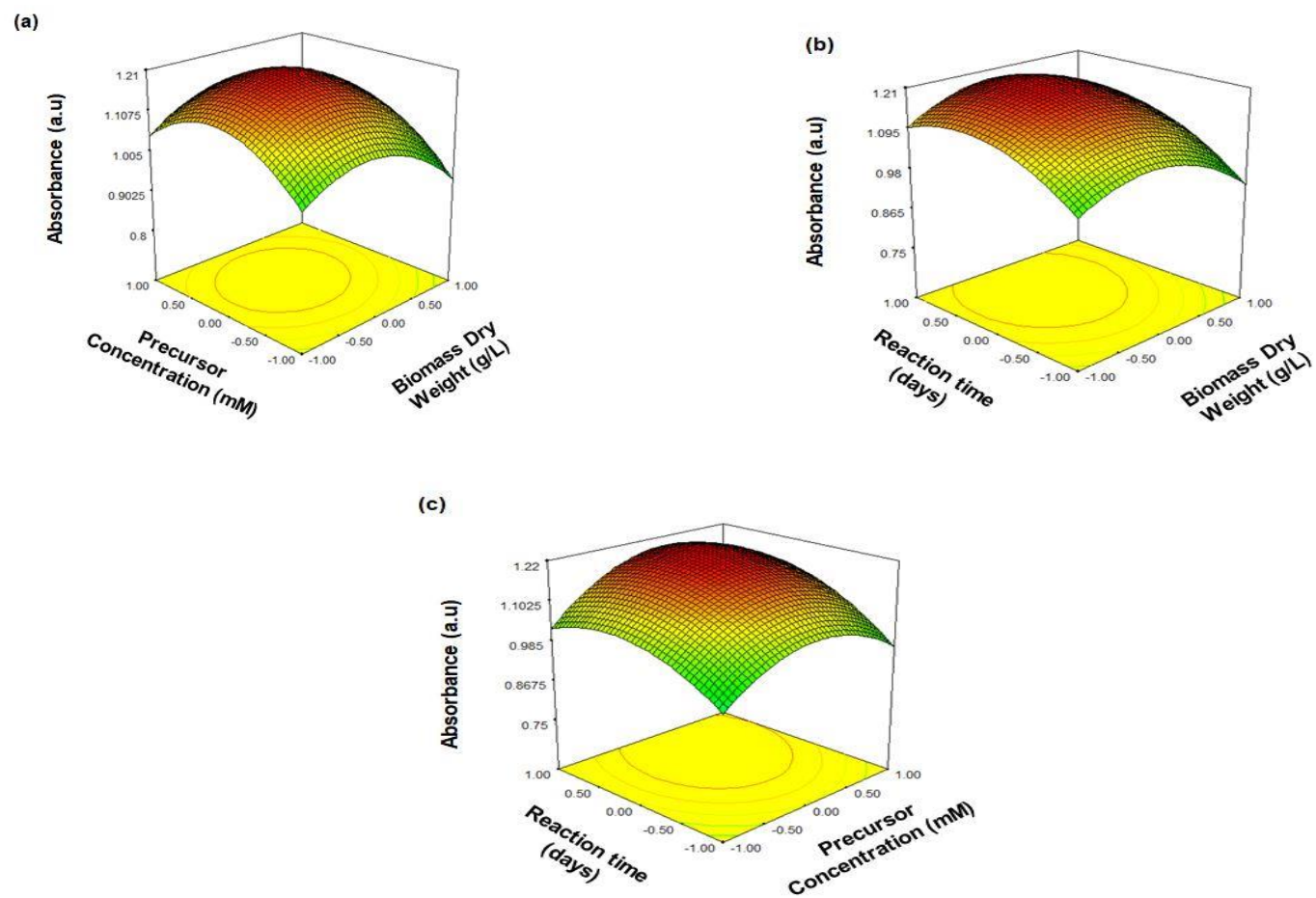| Runs	Biomass dry weight (g/L)	Precursor concentration (mM)	Reaction time (days)	Experimental value Absorbance (a.u)	Predicted value Absorbance (a.u)
1	0	0	1.681	1.1	1.091
2	1.681	0	0	0.85	0.904
3	-1	-1	-1	0.96	0.903
4	-1	1	-1	1	0.899
5	0	-1.681	0	0.8	0.848
6	0	1.681	0	0.89	0.967
7	0	0	0	1.2	1.196
8	0	0	0	1.2	1.196
9	0	0	0	1.2	1.196
10	-1	1	1	1.05	1.042
11	0	0	-1.681	0.75	0.884
12	1	1	1	1.09	1.057
13	1	-1	-1	0.89	0.967
14	0	0	0	1.2	1.196
15	0	0	0	1.2	1.196
16	-1	-1	1	0.98	0.951
17	0	0	0	1.2	1.196
18	1	-1	1	0.9	0.911
19	1	1	-1	0.92	0.859
20	-1.681	0	0	0.9	0.911

Figure 4.3: **Surface and Contour plot of absorbance (a.u) vs (a) precursor concentration (mM); (b) biomass dry weight (g/L); (c) reaction time (days)**
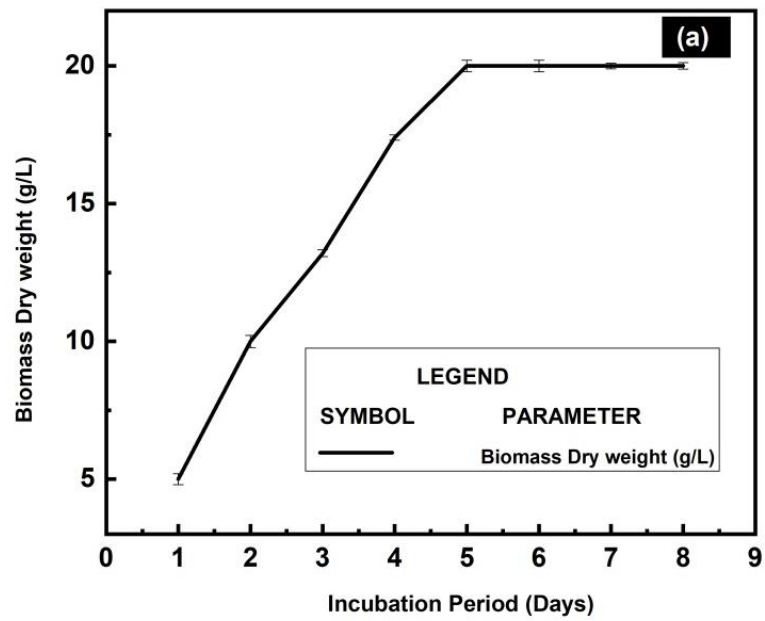
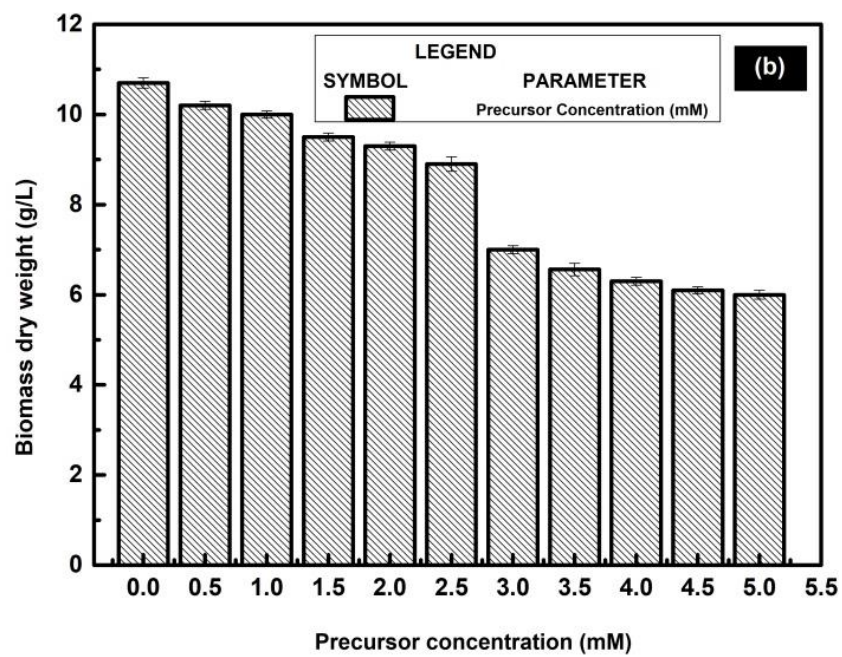**Figure 4.4 (a): Growth curve of endophytic fungi *Aspergillus flavus***

Figure 4.4 (b): Effect of zinc precursor concentrations on *Aspergillus flavus* growth

4.3. Biosynthesis and mechanism of ZnS NPs using endophytic fungi *Aspergillus flavus*

Fungal spores in basal PDB medium at the onset of the exponential phase, i.e, after 48 h of growth, were utilized for initiating biosynthesis of ZnS NPs. After the addition of precursor solution to the biomass, the reaction mixture was incubated at 72 h for the NPs formation; later the biomass was separated and further subjected to characterization to confirm the biosynthesis of ZnS NPs.

4.3.1. *Morphological analysis based on SEM and AFM*

The understanding of a plausible mechanism involved in the biosynthesis of NPs is the key step to scale-up the process for mass level production. It is evident that there is a significant change in the cross-section of fungal mycelium in presence of precursor solution (Figure 4.5: (b)-(d)), compared to the cells cultured in the control PDB medium (Figure 4.5: (a)) as demonstrated by SEM results. A characteristic change in the morphology-curling and formation of hyphal coils in response to metal stress is observed. Moreover, dense growth and thickening of the hyphae are also observed in response to the metal precursor solution. Such modifications on the surface of fungi indicate the production of intracellular compounds due to heavy metals stress and result in the increase in pressure within the mycelia leading to the outward growth of the cell wall structures (Paraszkiewicz et al. 2010). The cell wall protrusions increased the formation of intracellular vacuoles that serve as storage compartments for thiol-containing compounds. These compounds might be responsible for the binding of metal ions into the intracellular regions and accumulate them in the vacuoles. The extent of these changes reflected the metal stress further causing the rupture of mycelium.

The AFM analysis further confirmed the extracellular formation of ZnS NPs. From, Figures 4.6: (a)-(c) and 4.7 (a)-(c) it can be observed that the surface of the slide changed with respect to time in case of the supernatant which indicates that the formation and growth of the NPs in the media. Whereas, the AFM analysis of biomass revealed that the surface of the biomass remained unchanged with respect to time further confirming that the proteins are responsible for NPs synthesis with the involvement of the cytoplasmic material from the mycelia (Cao and Wang 2004; Georgiev et al. 2013; Nomura et al. 2015; Salvadori et al. 2014).
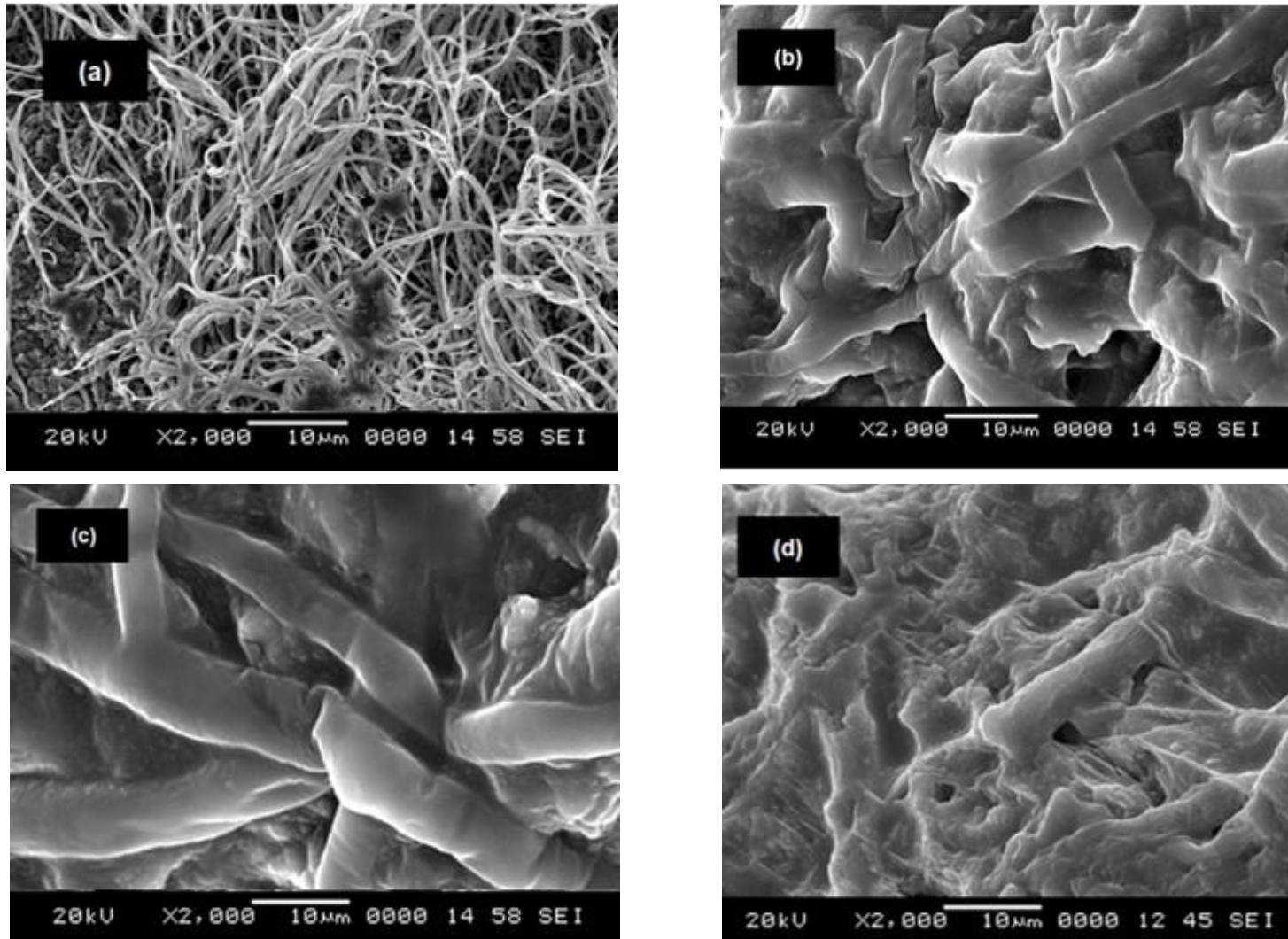
Figure 4.5: SEM images of the surface of *Aspergillus flavus* biomass (a) before the addition of precursor solution; (b) 15 min (c) 30 min and (d) 1 hr after the addition of precursor solution
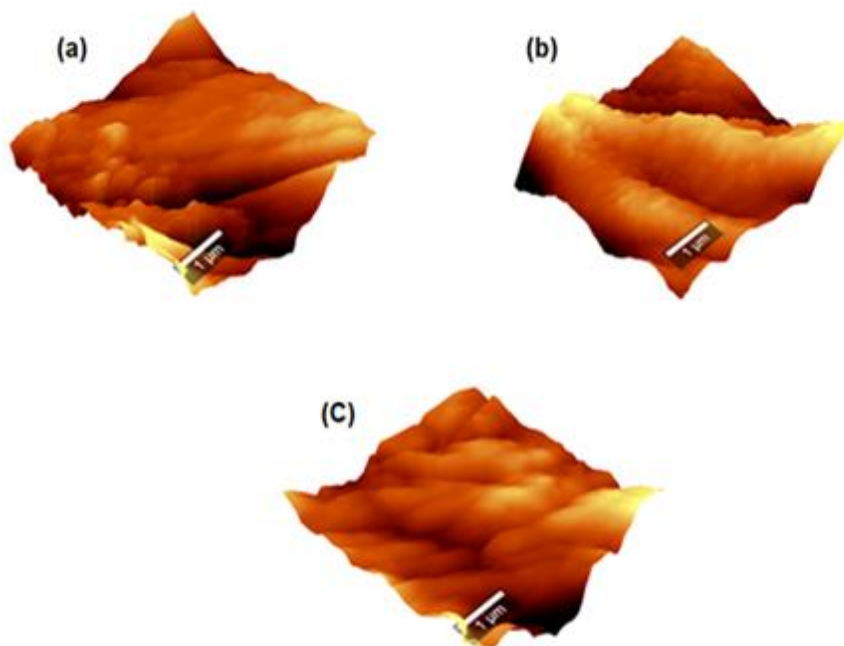
Figure 4.6: AFM 3D micrographs of fungal biomass (a) day 1 (b) day 2 and (c) day 3
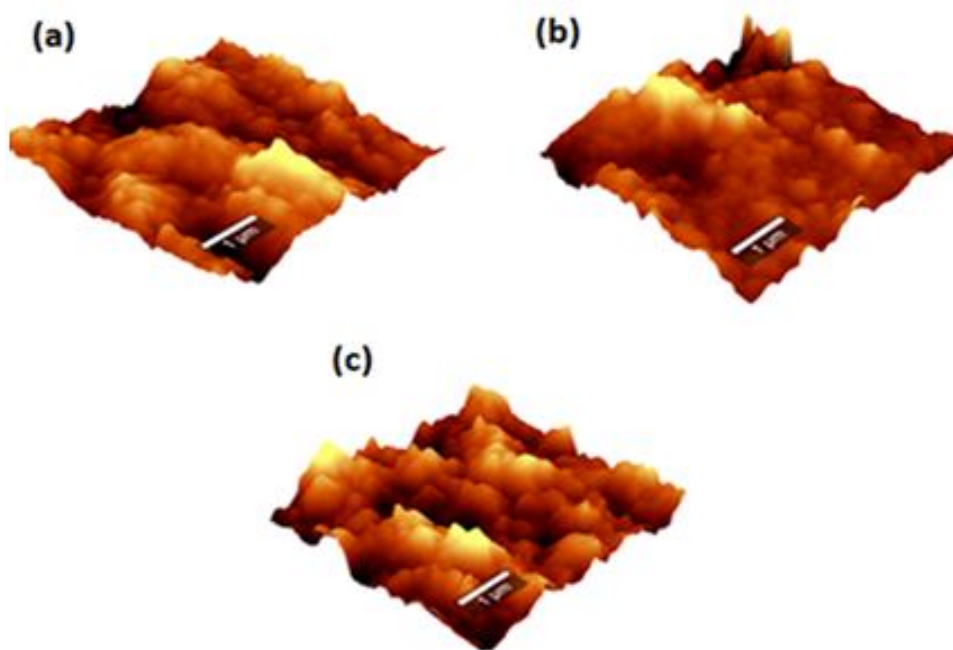
Figure 4.7: AFM 3D micrographs of supernatant (a) day 1 (b) day 2 and (c) day 3

4.3.2. Quantification of the total protein and LC–MS analysis

The total protein concentration was estimated as 0.11 (mg/ml) from the standard curve obtained from Lowry protein assay (Figure 3.2). It is evident that the proteins released help in stabilization of the NPs that act as capping material on the surface of NPs. The values of various retention times attained by HPLC are 6.33, 6.42, 6.55, 6.93, 7.29, 7.42 and 7.70 min (Figure: 4.8) and these values between 6-10 min corresponds to residues of glutathione. The LC–MS chromatogram of the major residue for the retention time 6.93 is depicted in Figure: 4.9. m/z peaks of the samples at 149, 301 and 579 are correlated to the m/z peaks of residual glutathione units (GSH) and phytochelatins. The phytochelatins which are the linear polymers of the γ-glutamylcysteine (γ−Glu− Cys)$_n$ a portion of glutathione, could be enzymatically produced by stepwise condensation of γ-Glu-Cys moieties to growing phytochelatin chain (PC). The PCs are the principal heavy metal detoxifying components in both plants and fungal kingdom. The PC plays a key role in maintaining cell homeostasis under heavy metal stress by binding to heavy metals and trafficking them to vacuoles or periplasmic space for storage (Damodaran et al. 2013; Mary et al. 2015).
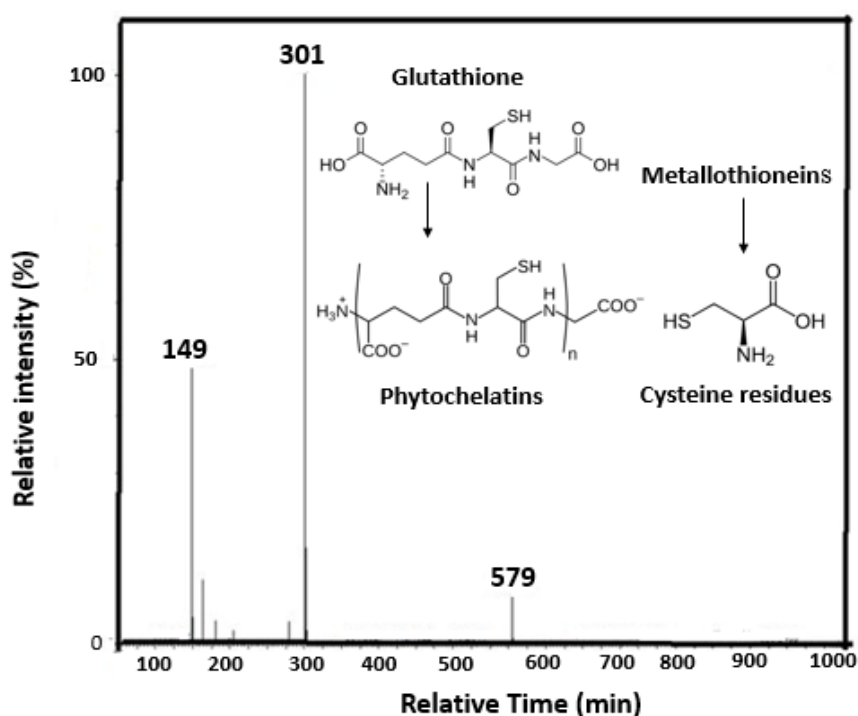
Figure 4.8: HPLC profile of acetone precipitated crude protein extract
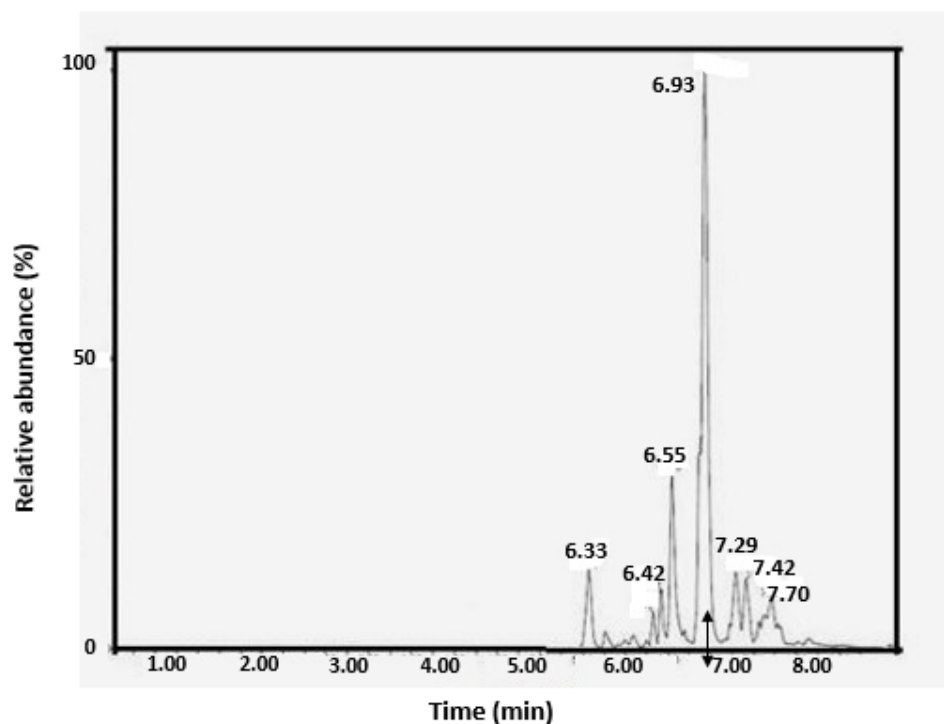
Figure 4.9: LC-MS mass spectrum at retention time 6.9 (min) depicting m/z ratio

4.3.3. Possible mechanism governing the biosynthesis

Biologically NPs are synthesized by exploiting the detoxification mechanisms involved in fungi (Figure 4.10). The detoxification systems allow the fungus to counteract the accumulation of ROS directly or indirectly, as a part of the detoxification response (Colpaert et al. 2011). Metal or its compound, after coming in contact with the microbe, is generally dealt with at the nanoscale because it is a scale natural to biological systems. Once the metal ions enter the cytosol, the metal might also have triggered the family of oxygenases held in the endoplasmic reticulum, chiefly intended for cellular level detoxification through the process of oxidation/oxygenation (Ballottin et al. 2016; Jha and Prasad 2012). During the ZnS NPs synthesis, initially the sulphate ions are taken in (SO_4^{2-}) from the extracellular environment and get reduced to sulphide ions (S^{2-}) with the help of sulphite reductase which later gets coupled with zinc metal ions in the solution which resulted in the formation of ZnS NPs.

The fungal cells exposed to metal ions clearly revealed phytochelatin induction (Gekeler et al. 1988; Mehra and Winge 1991; Perales-Vela et al. 2006; Singh et al. 2016; Singh and Bishnoi 2015). Phytochelatins are produced in cells and tissues after exposure to a range of heavy metal

ions (Durán et al. 2005; Hulkoti and Taranath 2014; Jain et al. 2011; Kitching et al. 2015; Mittal et al. 2013; Mohanpuria et al. 2008; Salvadori et al. 2014; Sandana and Rose 2014; Thakkar et al. 2010). The major molecules that contribute to the detoxification mechanisms in fungal cells are glutathione (γ-Glu-Cys-Gly) and two groups of metal binding ligands: metallothioneins and phytochelatins. When the fungal mycelium is challenged with metal ions, it triggers its membrane bound as well as cytosolic metabolites in order to circumvent the oxidative stress manifested in the form of ROS generation. Quinones at the membrane level of the detoxification system of fungi which readily undergo tautomerization; cytoplasmic metabolite weaponry such as phytochelatin, heavy metal tolerance factor 1 (HMT-I), glutathione and membrane bound mono- oxygenases, etc., which tend to detoxify such changes.
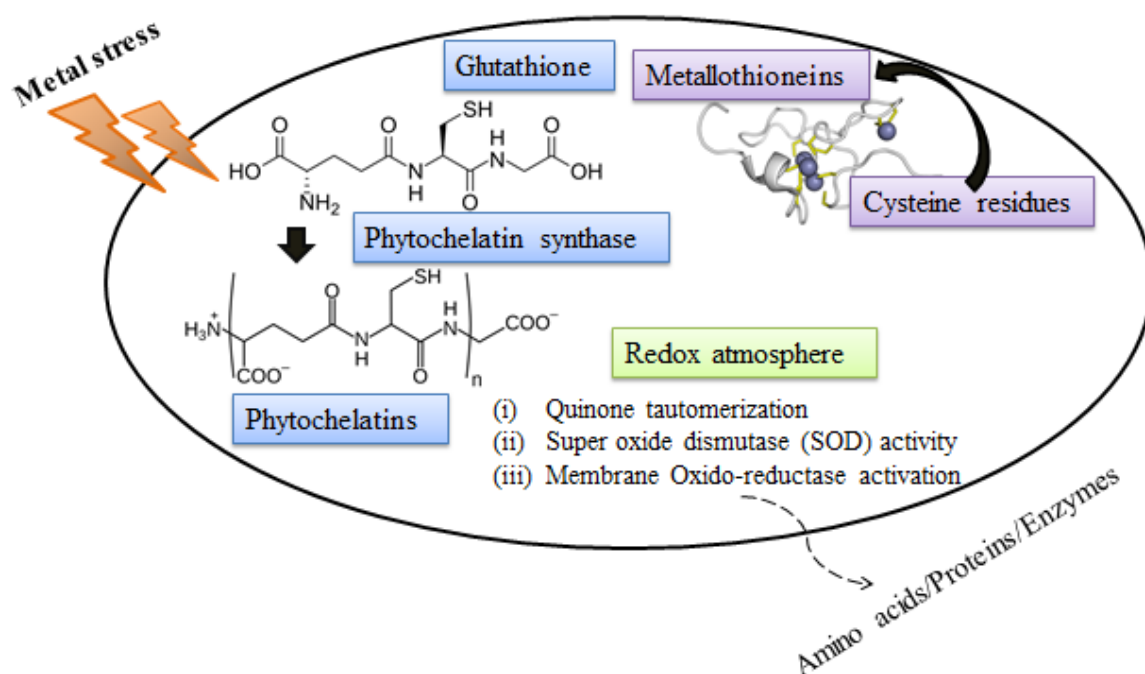
Figure 4.10: Schematic of the probable mechanism involved in the biosynthesis of NPs

4.4. Morphological characterization

The morphology and particle diameter of the synthesized ZnS NPs were examined using TEM. Figure 4.11: (a, b) reveals that the ZnS NPs were of size range 12–24 nm (Sandana and Rose 2014) and the prominent lattice fringes in the TEM image at magnification 5 nm reveal that the NPs are crystalline in nature (Onwudiwe and Strydom 2015) (Figure 4.11: (c)). The attained crystallite size of 0.5 nm was estimated using Scherrer formula (equation: 3.2),

this difference in the particle size diameter and the crystallite size indicate that the NPs are polycrystalline in nature. Further, the selected area electron diffraction (SAED) patterns by the ZnS NPs showed concentric rings confirming the polycrystallinity of the material (Hudlikar et al. 2012) (Figure 4.11: (d)).
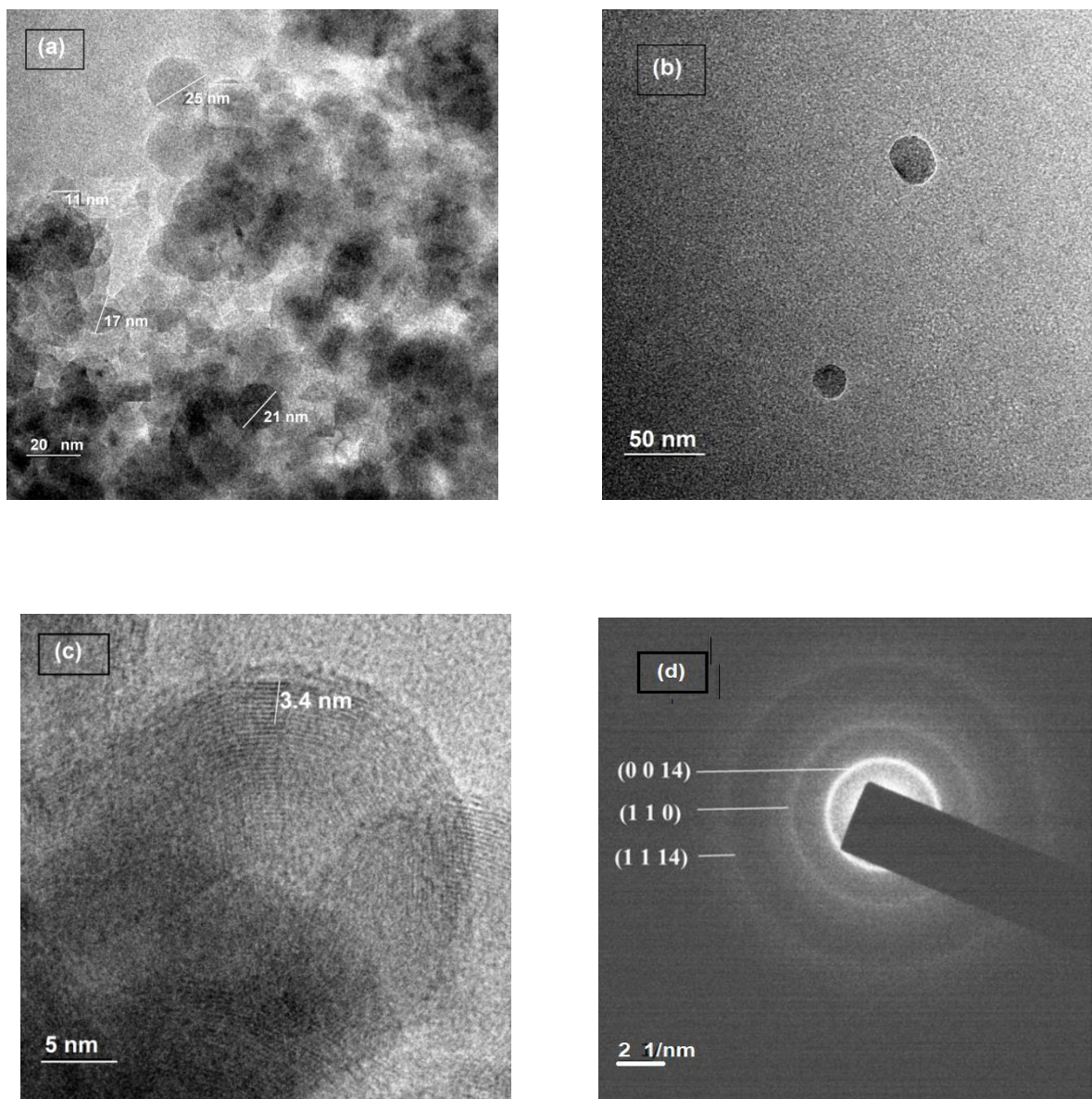
Figure 4.11: (a, b) TEM micrographs (c) Lattice -fringe finger print image and (d) SAED pattern with concentric rings

Particle size histogram of ZnS NPs affirms that the average particle diameter as 18 nm (Figure 4.12) and the mean diameter via DLS as 58.9 nm with a particle size distribution of D20 (Figure 4.13). Due to the presence of the ionic layer around the NPs, the mean diameter

in DLS is observed to be larger than TEM. As far as DLS is concerned, the theory states that when a dispersed NPs moves through a liquid medium, a thin electric dipole layer of the solvent adheres to its surface. This layer influences the movement of the particle in the medium, thus the hydrodynamic diameter gives the information of the inorganic core along with any coating material and the solvent layer attached to the particle as it moves under the influence of Brownian motion. While estimating size by TEM, this hydration layer is not present, hence, the information reveal that inorganic core is known and the coating layer is not present. Therefore, the hydrodynamic diameter is always greater than the size estimated by TEM (Vicentini et al. 2014; Nikitin et al. 2015). Further, the elemental analysis of the samples by EDAX (Figure 4.14) revealed that the atomic ratio of Zn:S is 0.98:1.00, a very close value to the theoretical expectation (Bai et al. 2006).

The d-spacing (Å) and percentage intensities of the NPs were determined by XRD which recorded from 20° to 60° angles. The XRD data indicates that the diffraction peaks centered at 28.45^o, 38.9^o, 47.54^o, 57° (2θ) can be well-indexed to the hexagonal phase of ZnS which are in good agreement with standard ICDD data (ICDD card No. 01-089-2195) with maximum intensity (Chen et al. 2014) (Figure 4.15).
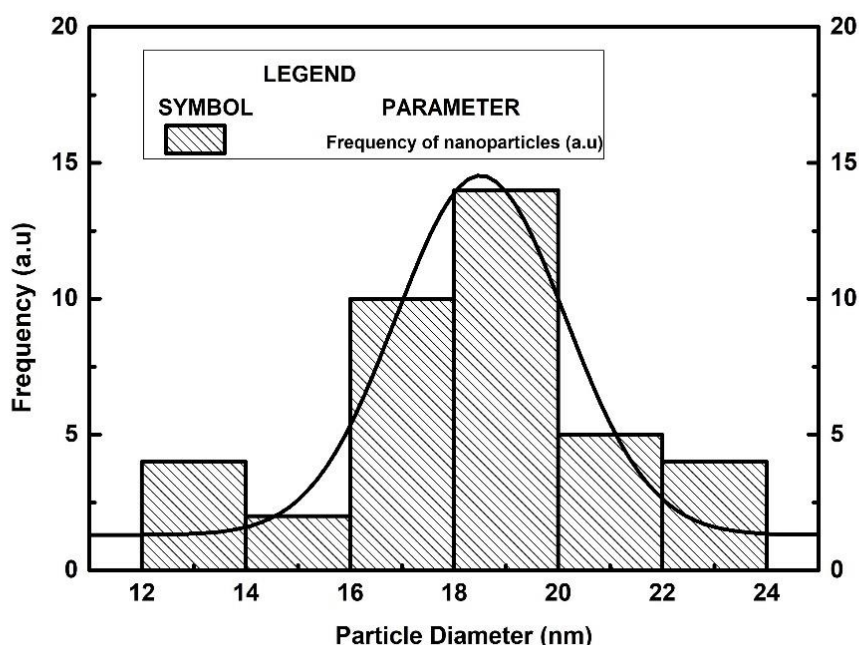
Figure 4.12: Particle size histograms evaluated by TEM image
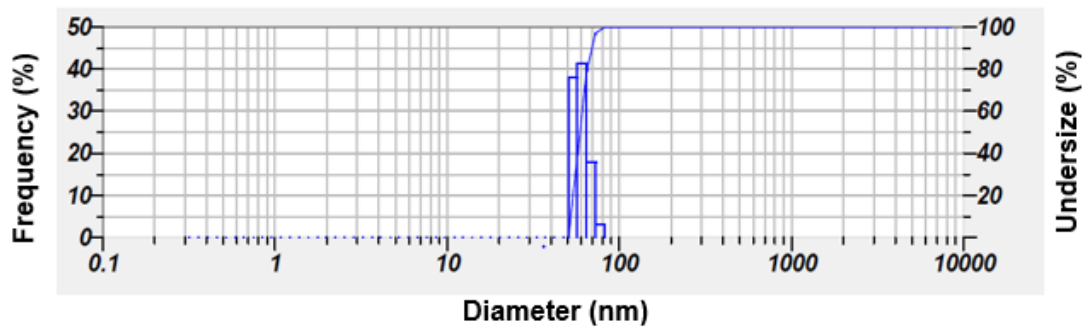
Figure 4.13: Size distribution measured by the DLS technique
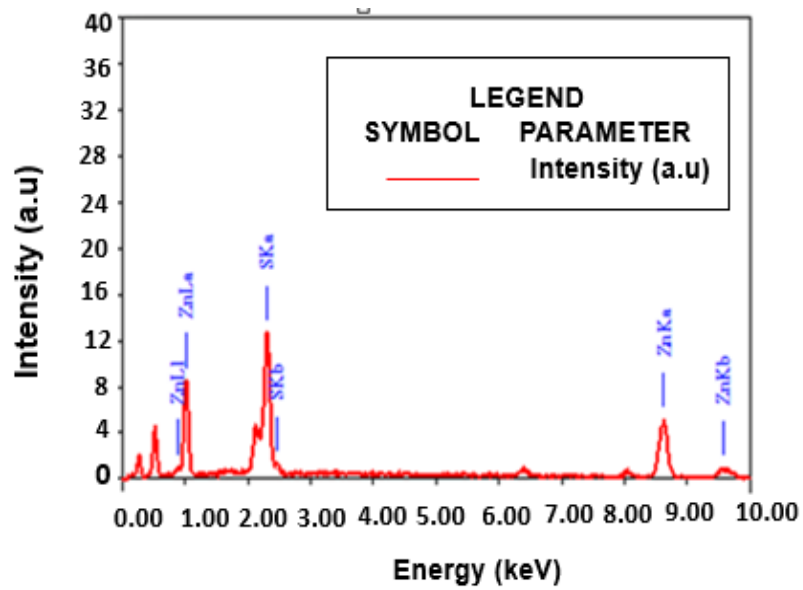
Figure 4.14: Elemental analysis of ZnS NPs by EDAX graph
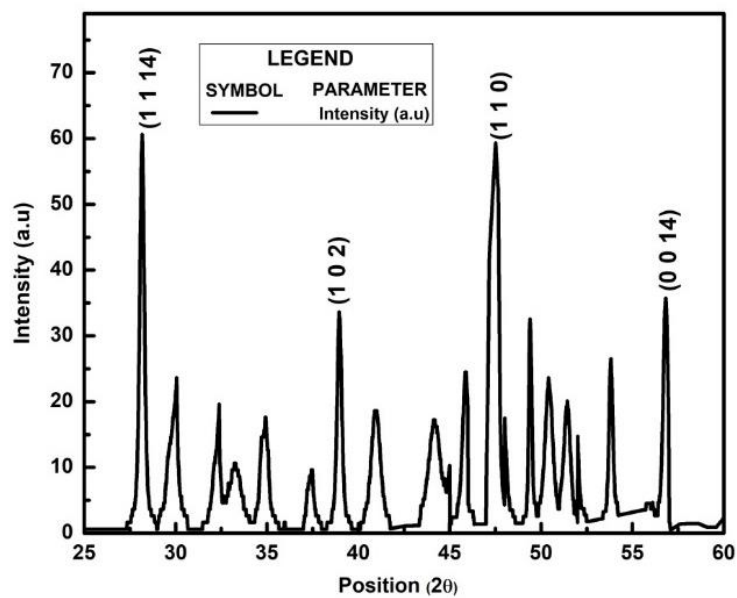
Figure 4.15: XRD pattern of the ZnS NPs

4.5. Optical properties

UV–Vis and DRS spectrum exhibited a strong surface plasmon resonance, due to their quantum size effect. UV–Vis spectrum recorded from the biosynthesized ZnS NPs exhibit the appearance of the absorption peak at 315 nm and a blue shift is observed compared to the bulk values of ZnS (345 nm) as shown Figure 4.16: (a). In the case of the DRS, the wavelength range of 200–2000 nm is recorded at room temperature. A similar phenomenon is observed in the case of DRS spectrum, where the absorption edge of the samples slightly shifted to lower wavelength compared to the bulk (Figure 4.17: (a)). Band gap value of ZnS NPs is estimated to be 3.75 eV (3.6 eV for bulk ZnS) from the Tauc plot drawn using equation (3.3) from UV-visible spectrum values as shown in the Figure 4.16: (b). The DRS spectrum was analyzed using Kubelka - Munk (Figure 4.17: (b)) method as given in the equation (3.4).
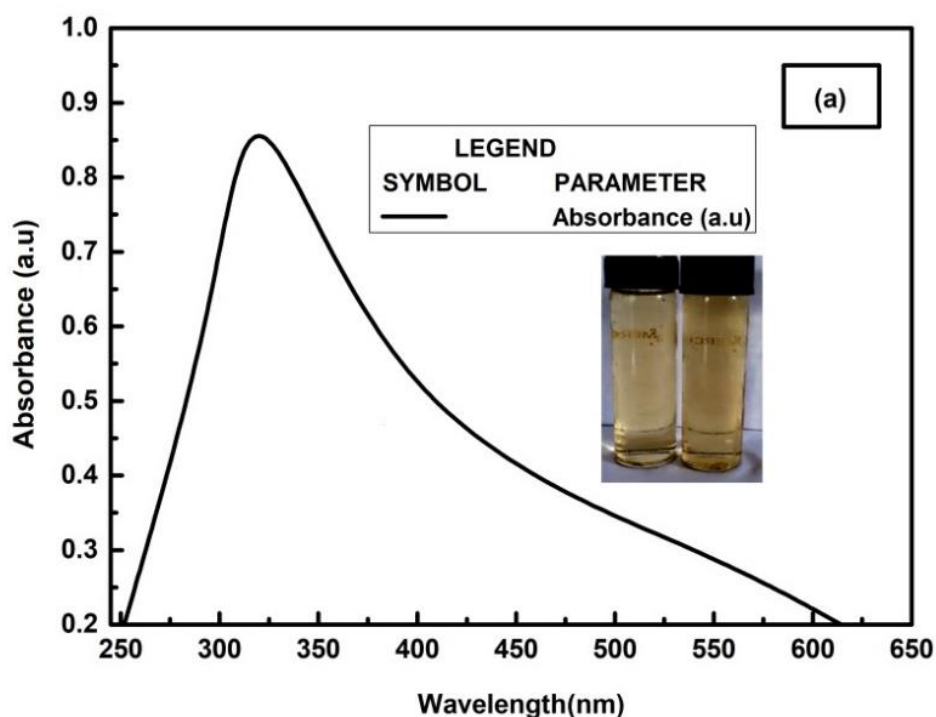
Figure 4.16 (a): UV–visible spectrum of ZnS NPs
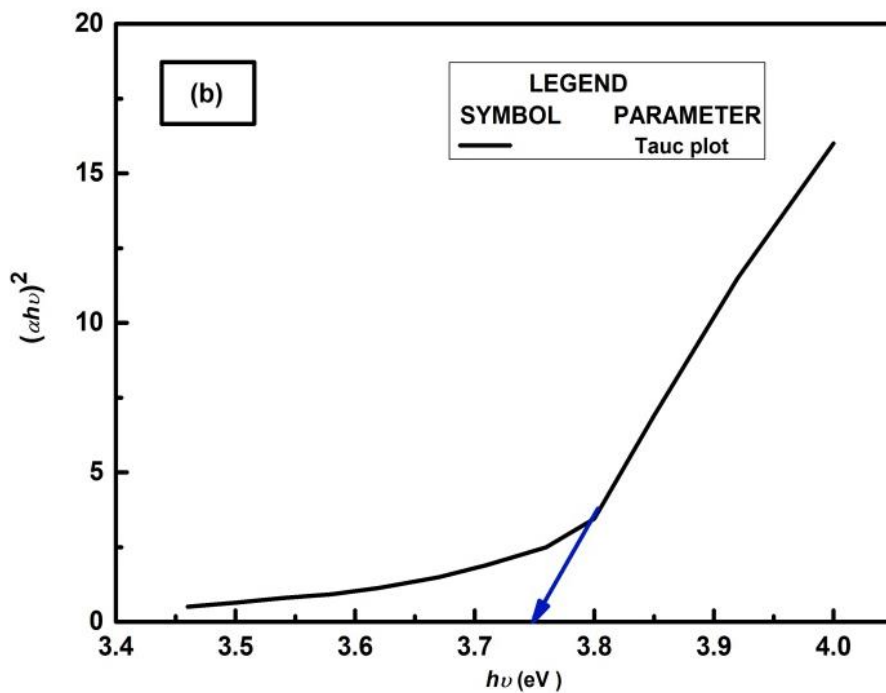
Figure 4.16 (b): Tauc plot for band gap of ZnS NPs
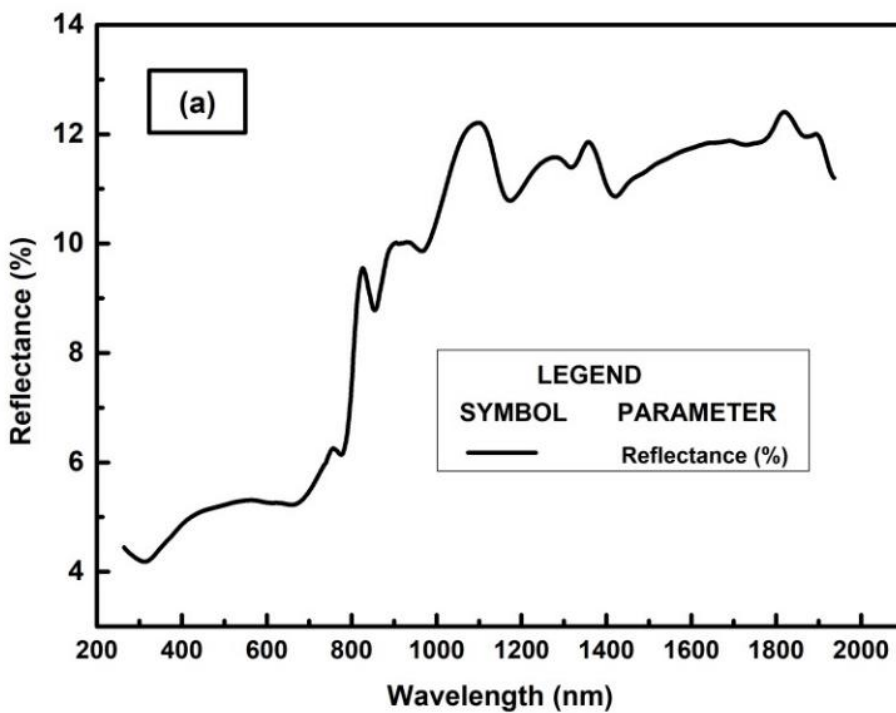
Figure 4.17(a): Diffuse Reflectance Spectrum of ZnS NPs
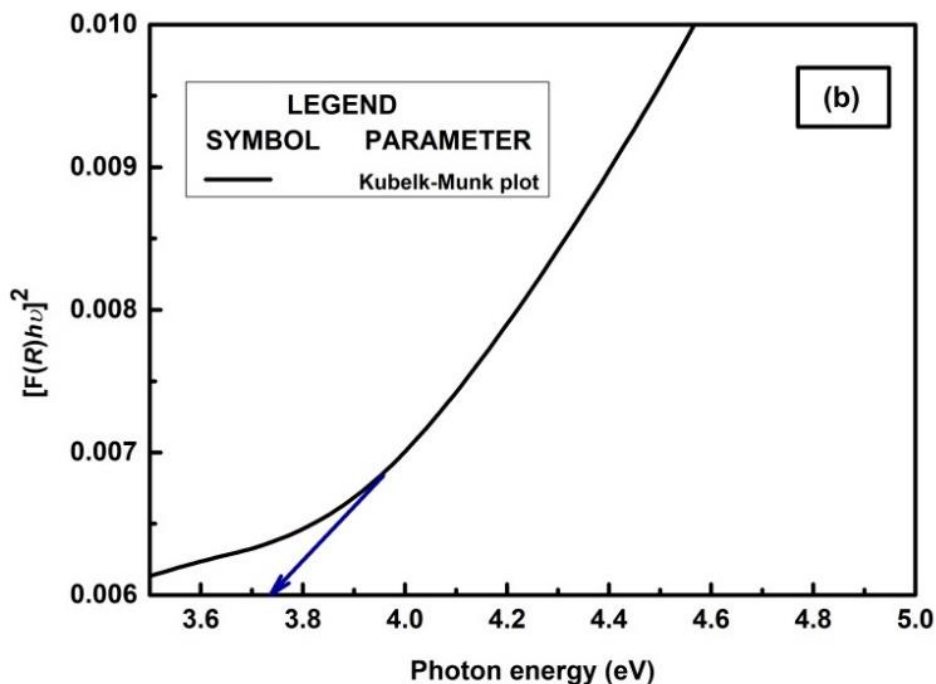
Figure 4.17 (b): Kubelk–Munk plot for band gap estimation of ZnS NPs

The presence of functional groups on the surface of the ZnS NPs is confirmed by FT-IR spectrum as shown in Figure 4.18. The spectral peaks are found to be at 1641, 1507, 1410, 794 cm^{-1} that corresponds to -C-C- stretching, -N-O- asymmetric stretch, -C-C- stretching, -C-H- bending due to the presence of amine groups of proteins, respectively (Onwudiwe et al. 2015). The FTIR peak at 3202 cm^{-1} may be ascribed to -O-H- stretching vibrations of the surface adsorbed moisture (Baker and Satish 2012) and peak at 657 cm^{-1} corresponds to -C-S-stretch. The presence of protein capping on the surface of NPs is confirmed by the thiol groups which are sulfur-bearing proteins' residues such as cysteine and methionine (Sanghi and Verma 2009). These protein molecules act as surface coating molecules which avoid internal agglomeration which in turn increases the stability of the NPs. These FTIR results justify the role of bioactive compounds responsible for mediating and stabilizing the NPs which has been well demonstrated in scientific literature.
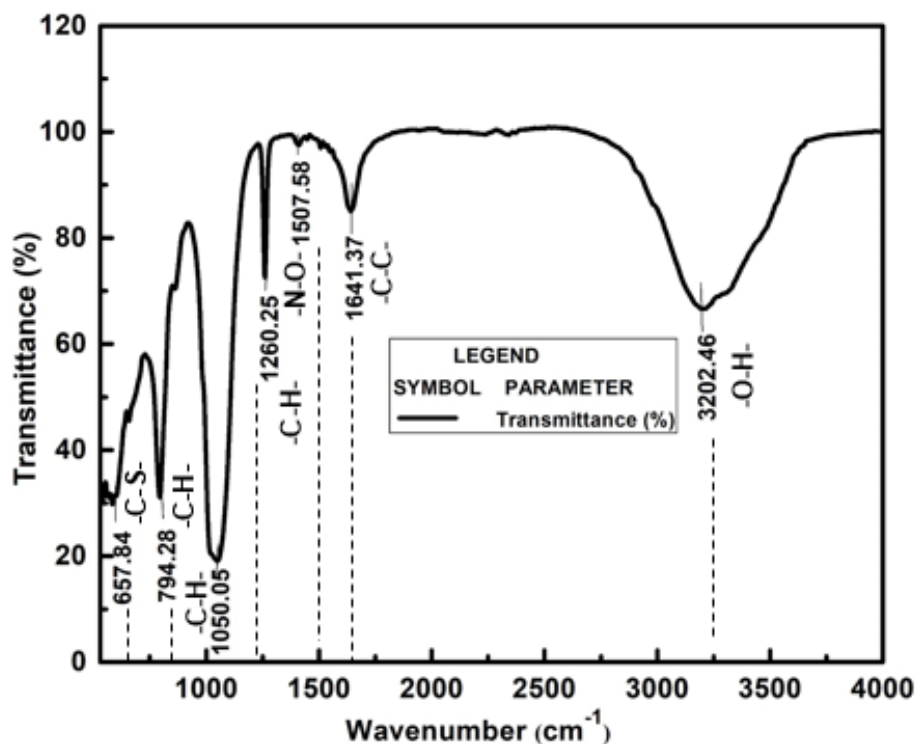
Figure 4.18: FTIR spectrum of ZnS NPs

To vibrational and rotational frequency modes of ZnS NPs using Raman spectrum analysis is given in Figure 4.19. The peak at 219 cm^{-1} corresponded to second order longitudinal acoustic mode (LA phonon mode), in this case, there was a shift in energy from bulk ZnS 224 cm^{-1} (Radhu and Vijayan 2011). The vibrational properties of bulk ZnS were measured at 304 cm^{-1} and 312 cm^{-1} which are second order ZnS Raman peaks, in this case, due to the quantum confinement effect a shift in the peak is observed i.e., at 295 cm^{-1} (Trajić et al. 2015). Emission peak around 432 cm^{-1} in ZnS NPs corresponded to sulfur vacancies (Kumar et al. 2013). The peak at 563 cm^{-1} corresponds to second-order spectrum of wurtzite ZnS and this value corresponds to the high-frequency region (540-600 cm^{-1}) formed by optical overtones and combinations (Anand 2015). These size-induced optical mode softening (red shift) and acoustical mode hardening (blue shift) effects can be related to bond-order length-strength (BOLS) correlation mechanism and these effects are known to occur in several semiconductor nanostructures such as CdS, InP, CeO$_2$ and ZnO, the electron–phonon interaction is different from the bulk due to the reduced symmetry, different surface strains as well as the different number of nearest neighbors (Wesselinowa and Apostolov 1997; Goharshadi et al. 2013). The observed shift is a consequence of the combined effect of

confinement as well as the strain in the lattice due to defects. The relationship between the Raman shift and the change of the lattice parameter can be calculated by equation 3.6. The calculated shifts in the lattice position are $\Delta a_1 = -0.005$ nm and $\Delta a_2 = -0.0042$ nm.
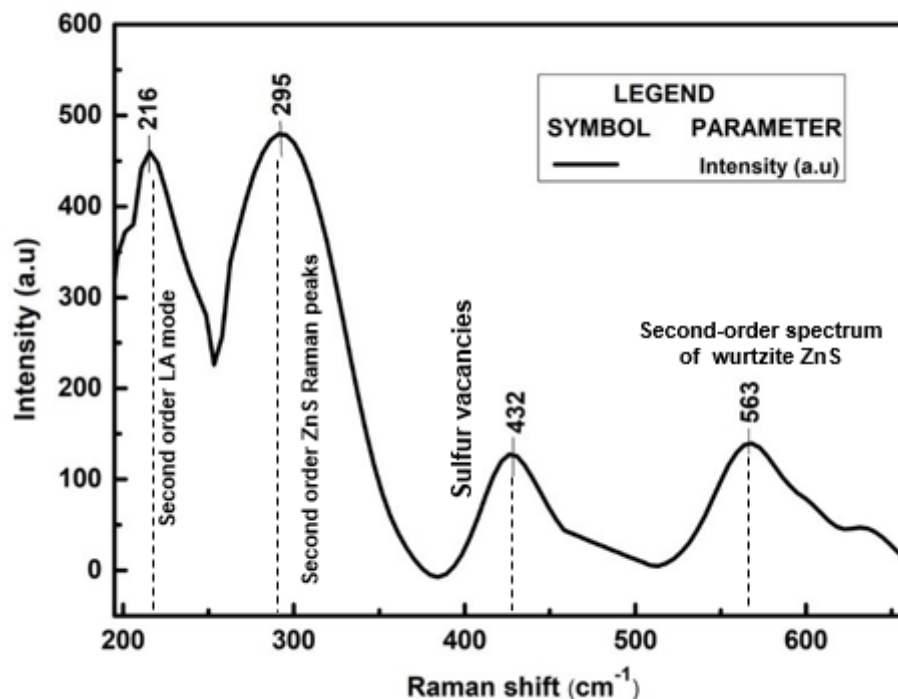
Figure 4.19: Raman spectrum of ZnS NPs

Photoluminescent spectrum is an effective tool to evaluate the defects and optical properties of ZnS NPs as a photonic material. Broadening of the emission peak could be attributed to both size distribution and an increase in the surface states owing to the increase in surface to volume ratio for ZnS NPs (Naeimi and Foroughi 2015). Figure 4.20 shows the photoluminescence spectrum of ZnS NPs at an excitation wavelength of 315 nm and the emission peak is noted at 420 nm. This photoluminescence spectrum exhibits size-dependent quantum confinement effects with a broad peak at 420 nm indicating surface irregularity attributed to the presence of sulphur vacancies in the lattice (Hudlikar et al. 2012; Sandana and Rose 2014; Li et al. 2013). We speculate that the emissions correspond to the electron or holes hollow traps which act as recombination centers for photogenerated charge carriers and this phenomenon may be due to photo-oxidation process which occurs on the surface of ZnS NPs in the presence of UV light (Frasco and Chaniotakis 2009). Based on our findings, the quantum

yield of the biogenic ZnS NPs was calculated as 14 % which is the probability of a photon being emitted after one photon has been absorbed. (Gaunt et al. 2005; Zehentbauer et al. 2014).
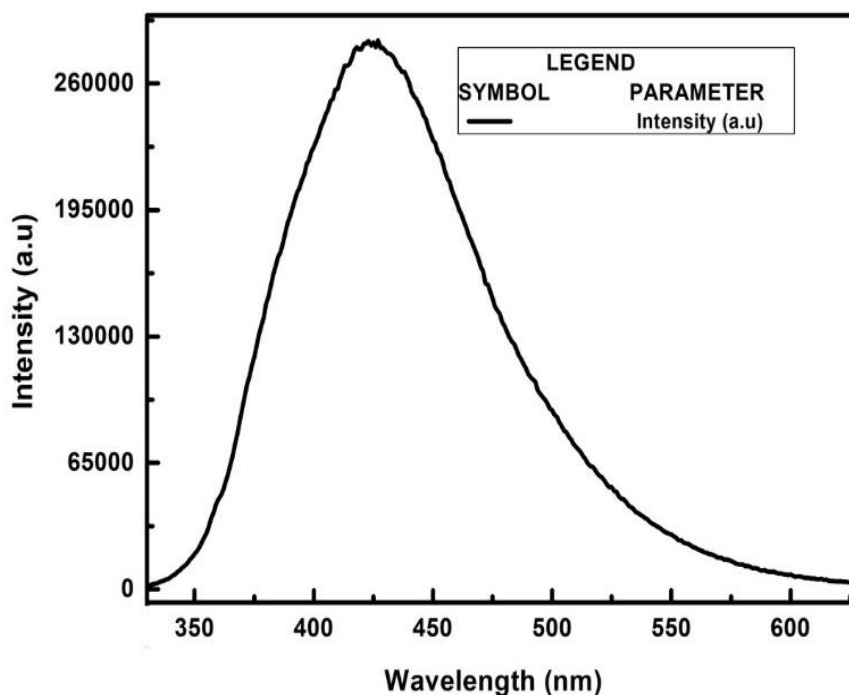
Figure 4.20: Fluorescence spectra of ZnS NPs

4.6.   Thermal stability

To determine the thermal stability of the ZnS NPs, TGA, TGA-DTG and DSC characterization studies were carried out. According to TGA data plots given in figure 4.21 (a), it is evident that the decomposition started around 100 $^{\circ}$C and continued upto 620 $^{\circ}$C. The weight loss was recorded to be approximately 72 % with respect to mass change. In TGA-DTG graph maximum rate of decomposition and change of mass as a function of temperature was recorded at 292 $^{\circ}$C and 53.9 % respectively (Figure 4.21 (b)). DSC curve (Figure 4.21 (c)) exothermic peaks at 80 $^{\circ}$C, 120 $^{\circ}$C, 250 $^{\circ}$C and an endothermic peak at 280 $^{\circ}$C (Mirzadeh et al. 2013). The exothermic peak exhibited at 450 $^{\circ}$C can be attributed to the crystallization of ZnS NPs (Chen et al. 2008)
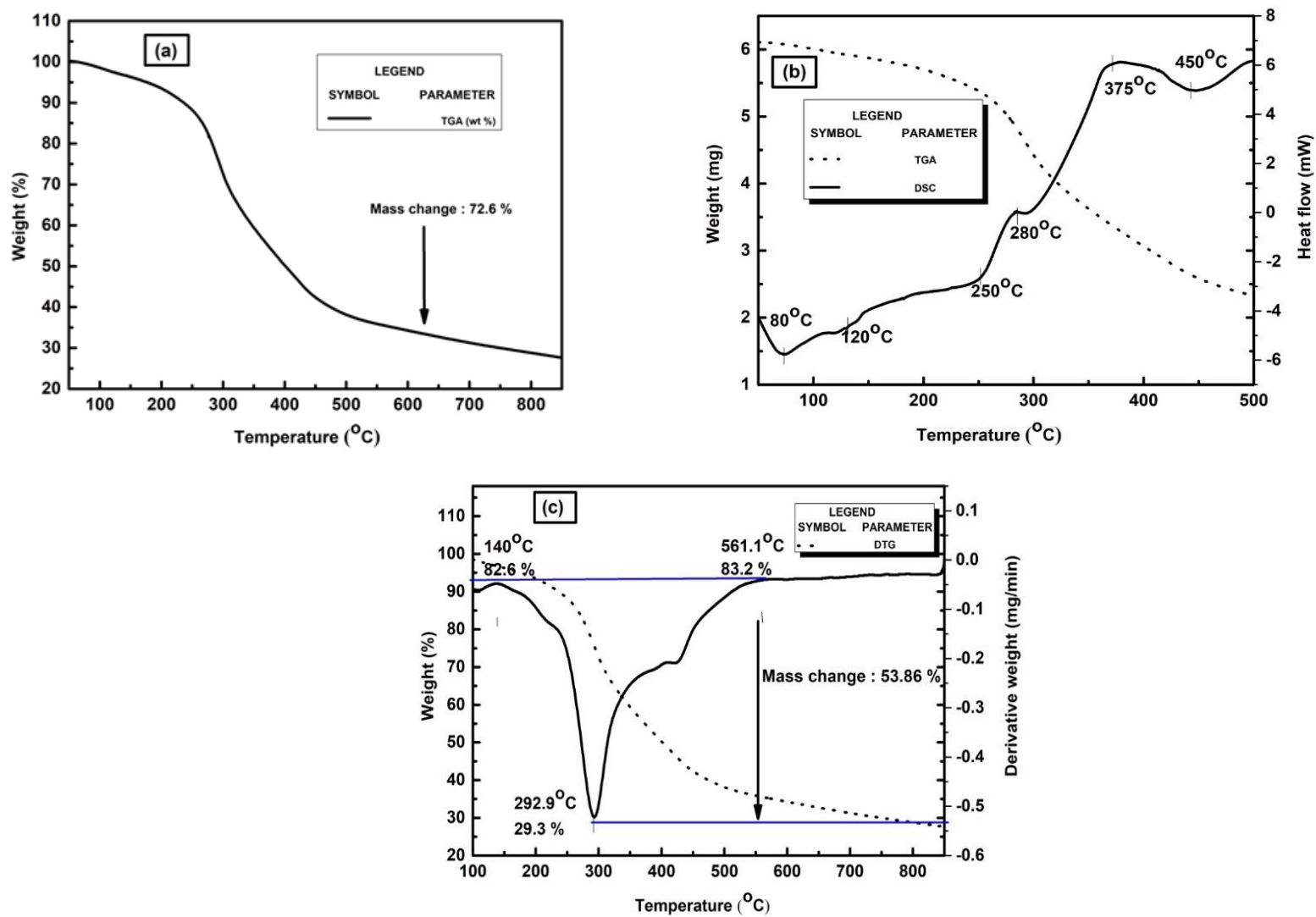
Figure 4.21: (a) TGA; (b) TGA-DTG and (c) TGA-DSC curves of the ZnS NPs

4.7. Stability studies

Cyclic voltammetry (CV) measurements demonstrated the stability of the NPs, where the shift in the oxidation/reduction peak is correlated to the stability of NPs. The analysis is performed at a fixed scan rate of 25 mV/s for 4 cycles and it was observed that the curves overlap with each other indicating that the samples have cyclic stability, this phenomenon may be due to the stability provided by the biocapping by proteins around the NPs (Figure 4.22). In the four cycles, the long-term structural stability was determined by continuous CV cycles from −2.5 V and 2.5 V at room temperature. It is observed that in one of the cycles, the oxidation voltammogram showed open circuit potential from −0.016 V to a potential of 0.031 V, indicating the absence of surface available ZnS^0 or ZnS^1 which can be oxidized into ZnO. The voltammetry curves for the sample showed one anodic peak in the forward scan and one cathodic peak in the reverse scan. The total area of reduction and oxidation peaks are observed to be similar, thus indicating the stability of NPs (Hedberg et al. 2016; Du et al. 2013). Further, based on the intensity of the absorbance curve, it is evident that there is a drastic shift in the absorbance on the 15th day, this may be due to the degeneration of proteins engulfing the NPs (Figure 4.23). The zeta potential of the ZnS NPs for different pH values, viz 3, 5, 7 and 9 are recorded to be −7.4, −12.7, −18.6 and −22.3 mV respectively as shown in Figure 4.24 and a maximum value away from the isoelectric point was found to be -22.3 mV at pH 9 (Suganthi and Rajan 2012; Mehta et al. 2011).
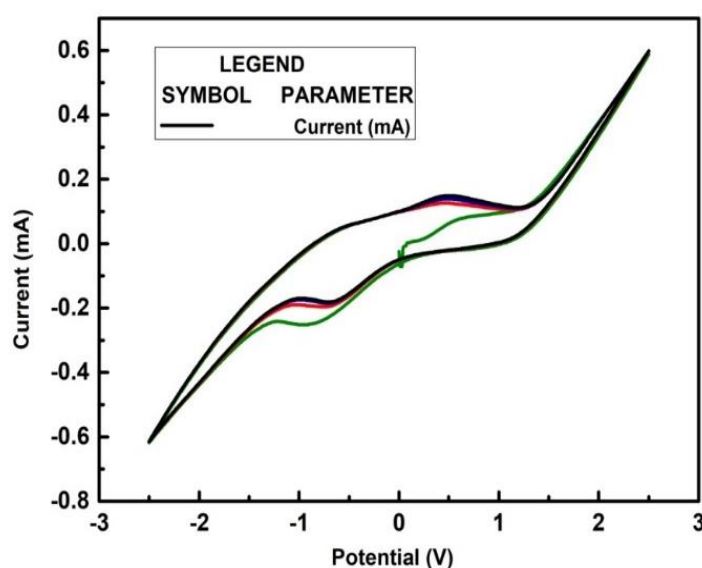
Figure 4.22: Cyclic voltammetry studies of ZnS NPs
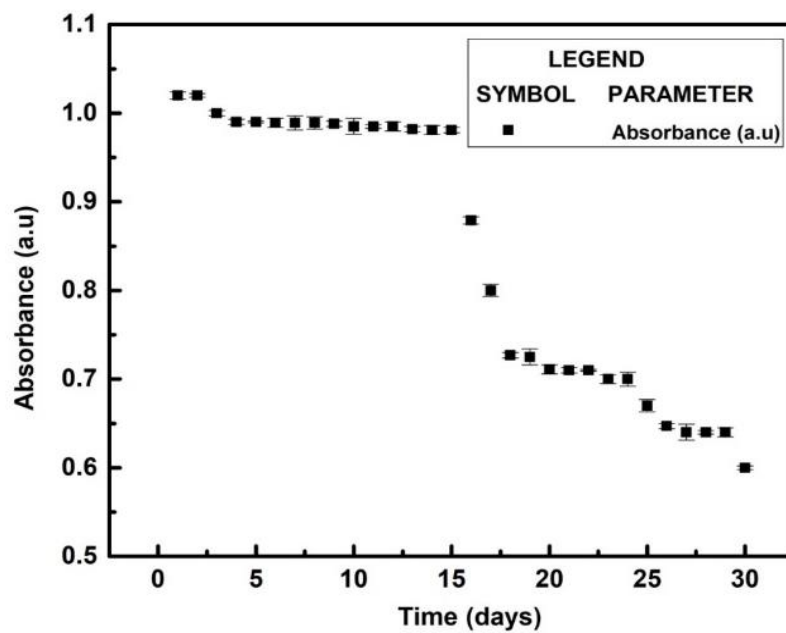
Figure 4.23: Photo stability of the ZnS NPs
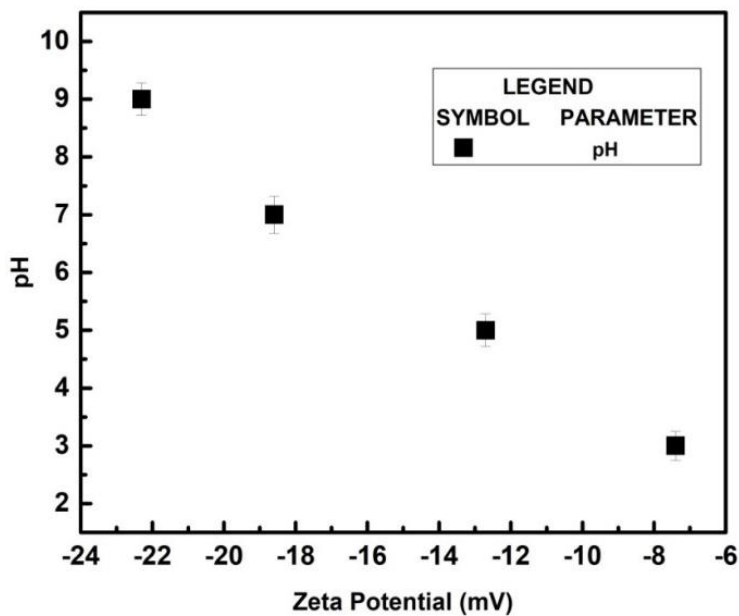
Figure 4.24: Zeta potential values of the ZnS NPs at different pH

4.8. Parameters affecting degradation process

4.8.1. Effect of time and their rate kinetics

Figure 4.25: (a) depicts that the degradation efficiency of MV is calculated based on equation (3.7) and it is observed that it (Soltani and Entezari 2013) is more in presence of solar radiation compared to the absence of solar light. In the presence of light source, the photons excite the surface electrons of the catalyst, whereby these electrons move from the valence band to the conduction band leaving positive holes in the valence band, which further reacts with water to release hydroxyl ions that degrade the chemical structure of the dye. From figure 4.15: (a) it is evident that in the presence of solar irradiation the degradation efficiency of about 87 % is achieved. However in absence of solar irradiation, the degradation efficiency had dropped to 29 % and remained almost constant after 120 min due to the competitiveness of the parent dye molecules with intermediates/short chain aliphatics during the photocatalytic degradation process (Chauhan et al. 2014; Velmurugan et al. 2013). The kinetic rate constant for degradation of the dye (k_{MV}) was estimated to be 0.46 min^{-1} with a R^2 value 0.95 as shown in Figure: 4.26 (a) (Gupta and Bhattacharyya 2008; Kooh et al. 2017). A degradation efficiency of 17 % was also observed under solar irradiation in absence of ZnS NPs.

Figure: 4.25 (b) represents the degradation (%) of ZnS NPs on 2,4-D (pH 11), both in presence and absence of solar irradiation. The efficiencies are found to be 33 % and 25 % respectively and in absence of both ZnS NPs it is found to be 19 % after 270 min of solar radiation. For PARA % degradation it is found to be 51 % and 35 % in presence and absence of solar irradiation respectively after 240 min and in the absence of ZnS NPs it is found to be 23 % under solar irradiation (Figure: 4.25 (c)). However, the degradation efficiencies of ZnS NPs over 2,4-D and PARA is less compared to MV due to their complex phenolic structure. The calculated rate constants ($k_{2,4-D}$ and k_{PARA}) are 0.089 min^{-1} and 0.0023 min^{-1} with R^2 values 0.98 and 0.96 for 2,4-D and PARA respectively (Figure: 4.26 (b) and Figure: 4.26 (c)).
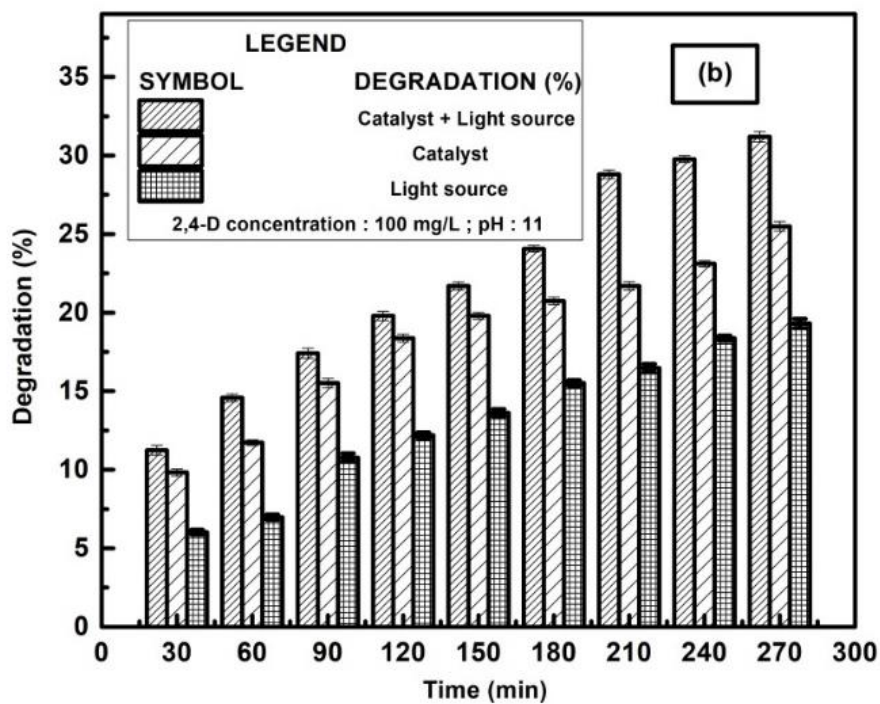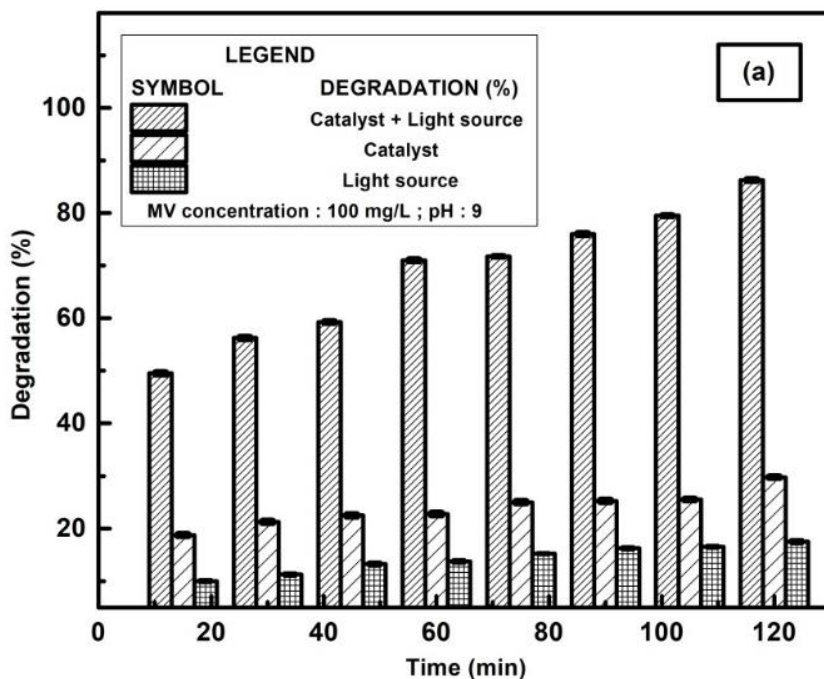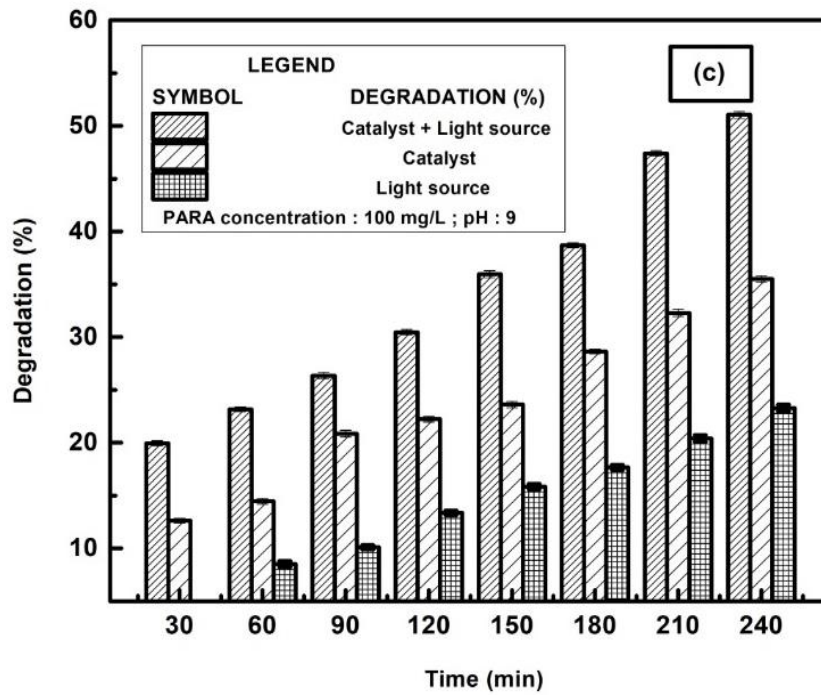
Figure 4.25: Photo degradation of (a) MV (b) 2,4-D and (c) PARA with time comparing the effect of catalyst and the light source
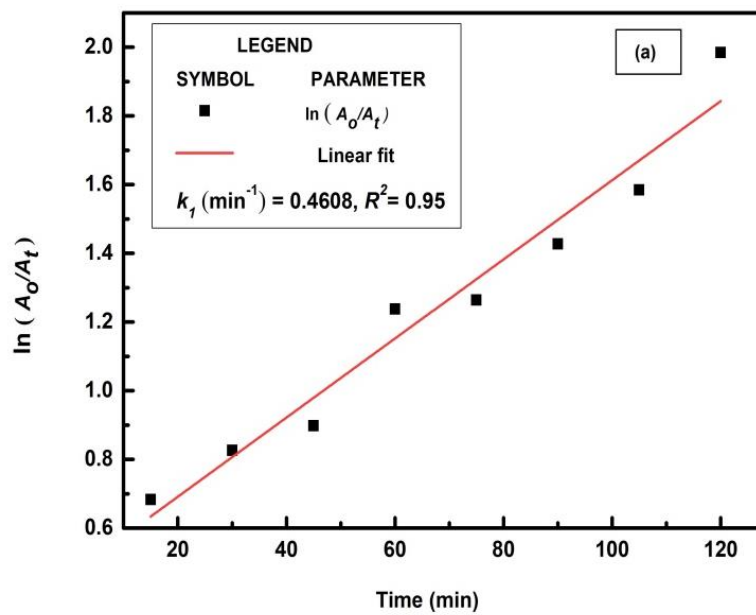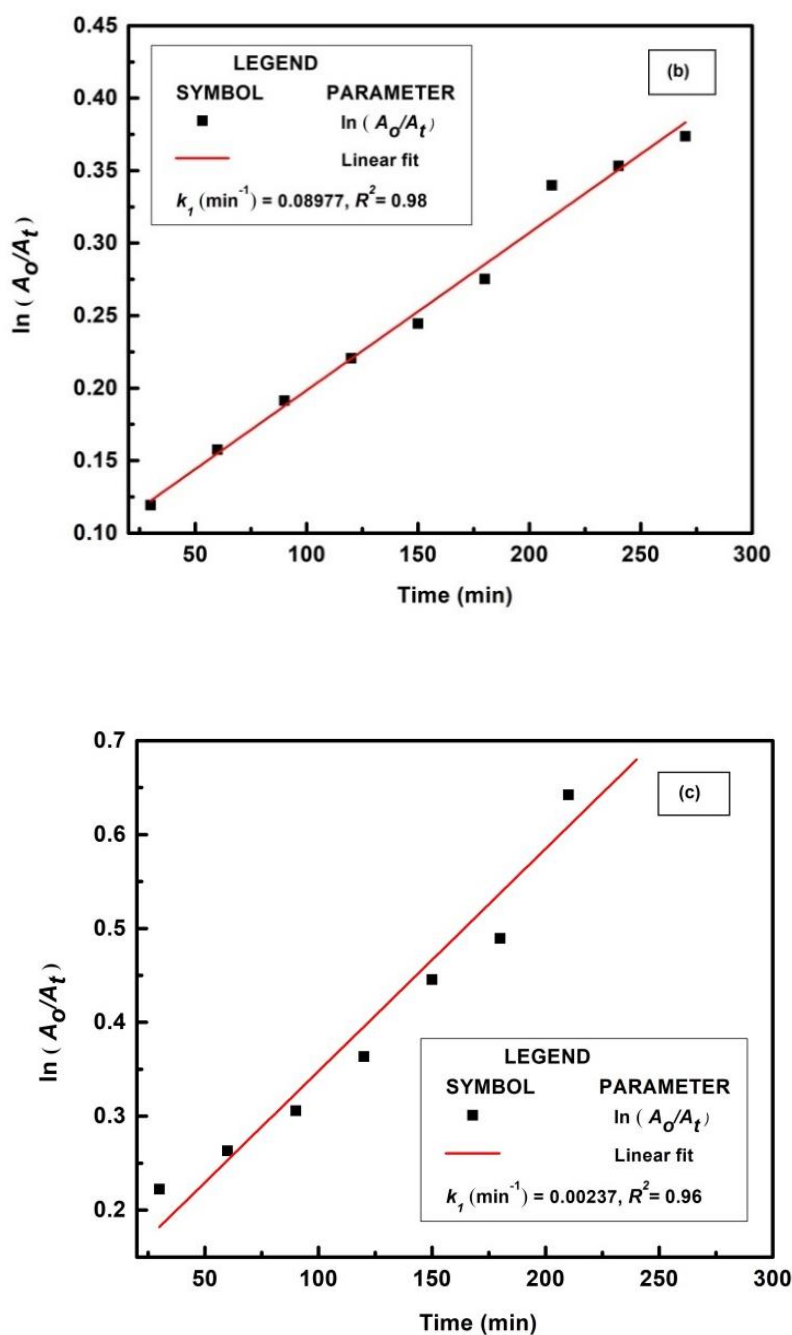
Figure 4.26: Pseudo first-order kinetics plot for (a) MV, (b) 2,4-D and (c) PARA in presence of ZnS NPs

4.8.2. *Effect of pH*

The effect of pH on the photocatalytic degradation is related to surface properties of NPs since most of the semiconductor NPs exhibit amphoteric behaviour. The degradation efficiency of ZnS NPs was found to increase from 43.2 % to 87 % with increase pH from 3 to

9 for 100 mg/L of dye concentration within 120 min as shown in figure 4.27. The maximum efficiency was observed at pH 9 below the isoelectric point of ZnS NPs which is between pH 7.0–7.5 (Ahluwalia et al. 2016).The surface of ZnS photocatalyst NPs is positively charged in acidic solutions and negatively charged in alkaline solutions. At acidic pHs, surplus amount of H^+ ions compete with the cations of the dye molecule showing little/low degradation efficiencies whereas, at alkaline pH values, higher concentrations of hydroxyl ions are produced to form hydroxyl radicals under photo-excitation and helps cleaving the bonds in higher order molecules (Benzene rings). Moreover, MV falls in the category of triphenylmethane dye, adding an OH^- ion in central carbon converts the cation into carbinol base nonresonant. The conjugation between the benzene nuclei is disturbed and the molecule becomes colourless. However, for pHs > 9 there is a decrease in the degradation of MV dye which may be due to increase in the availability of hydroxyl ions and these ions compete among themselves and lead to the decrease in degradation process. Hence, pH 9.0 was selected as the optimum value for further studies (Shamsipur and Rajabi 2014).

The photocatalytic degradation of 2,4-D under acidic conditions, between pH 3 – 4 found to be significant and dropped towards the neutral pH 7. Further increase in degradation efficiency, was observed above pH 8 to 11 and it remained unchanged for the rest. The reason for this trend might be because of the 2,4-D is an anionic compound which can react with the free radicals that are produced in the strong acidic medium, pH 3 to 4 supported by the ZnS photocatalytic activity with the involvement of functional groups carboxy groups -C-C-, -C=C, -C-S- and -O-H- that are active in acidic medium. Whereas similar degradation efficiencies where observed even for pHs above 10 in the alkaline medium where -C-H- and -N-O- functional groups are active. A maximum degradation efficiency of approximately 33 % was observed at both pH 3 and 11 (Akpan and Hameed 2011). At alkaline pH, 2,4-D takes an ionized form which is water-soluble that changes its properties and remains in the water column. Even in the case of PARA, the experiments showed better results under alkaline conditions and a maximum is observed at pH 9 (Fang et al. 2011; Khataee et al. 2015). Under alkaline conditions, degradation is enhanced this is due to improved interaction of the hydroxylated photocatalyst surface and negatively charged PARA. The enhancement of the pH value from 3 to 9 finally leads to an increase of the photocatalytic abatements from 18 % to 51 % (Choina et al. 2015).
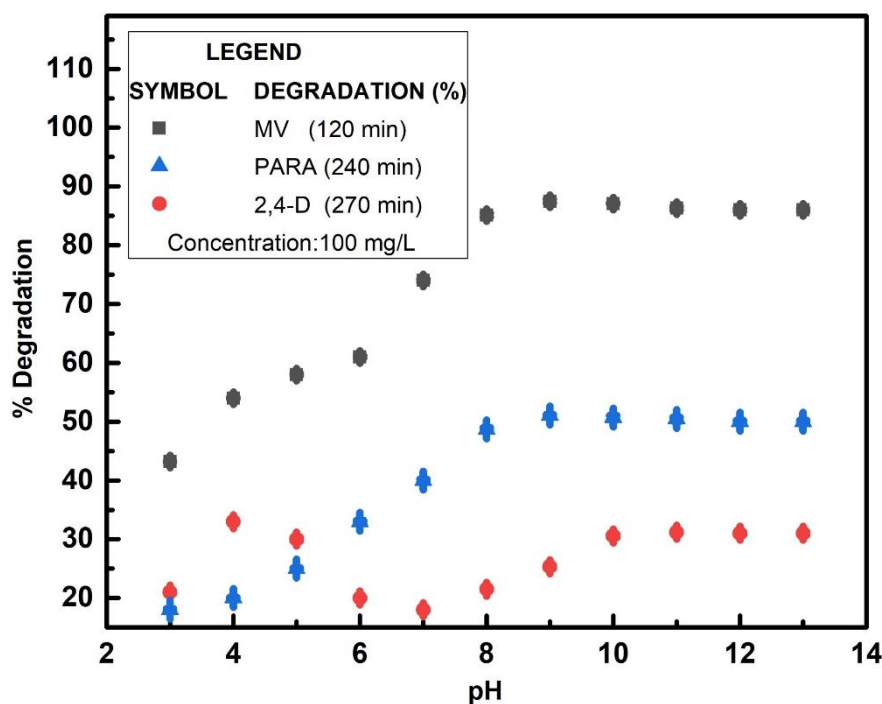
Figure 4.27: Effect of varying pH on degradation (%) of MV, 2,4-D and PARA

4.8.3. AFM studies

The presence of organic pollutants onto NPs was confirmed by AFM characterization. The results indicate that physical interactions during the sorption process of organic pollutants on the surface of NPs (Pal et al. 2015; Bhavani and Sivasamy 2016). Figure. 4.28: (a) reveal that the average roughness (S_a) and root mean square roughness (S_q) to be 50 nm and 65 nm respectively for MV whereas the average roughness for 2,4-D and PARA are 11 nm (S_a), 20 nm (S_q) as and 23 nm (S_a), 42 nm (S_q) respectively as obtained from Figure. 4.28: (b) and (c). Thus, from the above results it is evident that the surface roughness of MV is comparatively greater than the rest indicating that higher amount of organic pollutant molecules attached to the surface of the ZnS NPs.
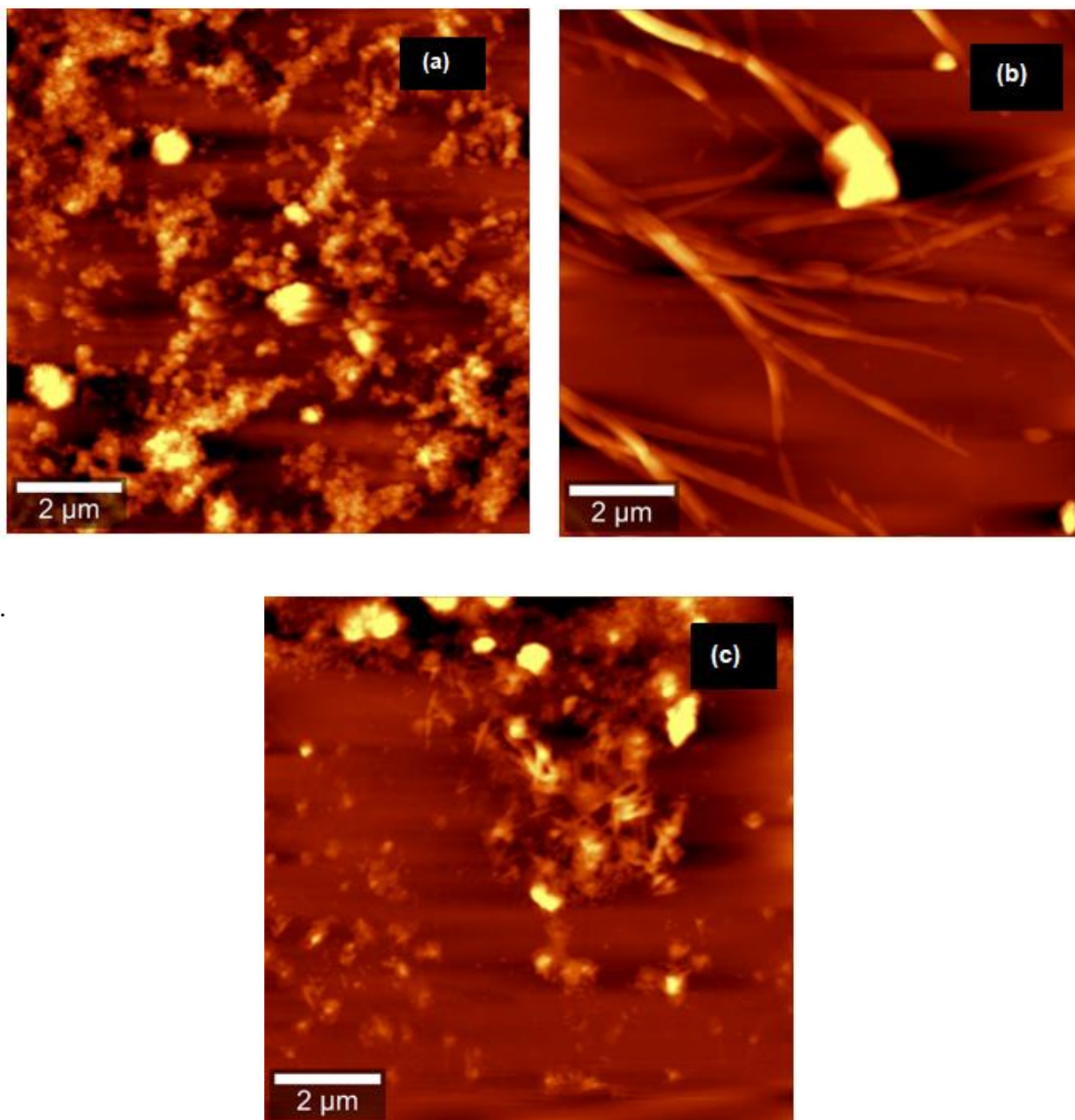
Figure 4.28: Topography showing adsorption of pollutants on ZnS NPs on the surface of pollutants (a) MV; (b) 2,4-D; (c) PARA

4.8.4. Fluorescence characteristics

From the results it is evident that the FRET efficiency decreases with increase in time for MV and PARA (Figure: 4.29 (a) and Figure: 4.29 (c)). The probability of the energy transfer depends on the overlap of the emission band of the fluorophore molecules with the absorption spectra of the organic pollutant molecules. For MV and PARA, ZnS NPs act as a quencher, this fluorescence quenching may be due to photo induced electron transfer process between the excited MV/PARA molecules and the ZnS NPs. Their E values vary from 5 % to 36 %; 65 % to 86 % and its corresponding $J(\lambda)$ values are 0.2 x 10^{-17} to 1.7 x 10^{-17} cm^3 L g^{-1}; 9.6 x 10^{-17} to 4.7 x 10^{-17} cm^3 L g^{-1} for MV and PARA respectively.

For 2,4-D fluorescence increases with a decrease in time (Figure: 4.29 (b)) this enhancement of fluorescence is probably due to (i) the spectral changes which might be because of the formation of ion-pair complex between NPs and 2,4-D (ii) the ROS enhances the radical's formation, which subsequently dissociates/breaks the complex resulting in colour enhancement. The E values varies from 28 % to 98 % and their $J(\lambda)$ values are 9.3 x 10^{-17} to 6.4 x 10^{-17} cm^3 L g^{-1} for 2,4-D (El-Kemary and El-Shamy 2009; Kavitha et al. 2014; Liu et al. 2016; Asif et al. 2016).
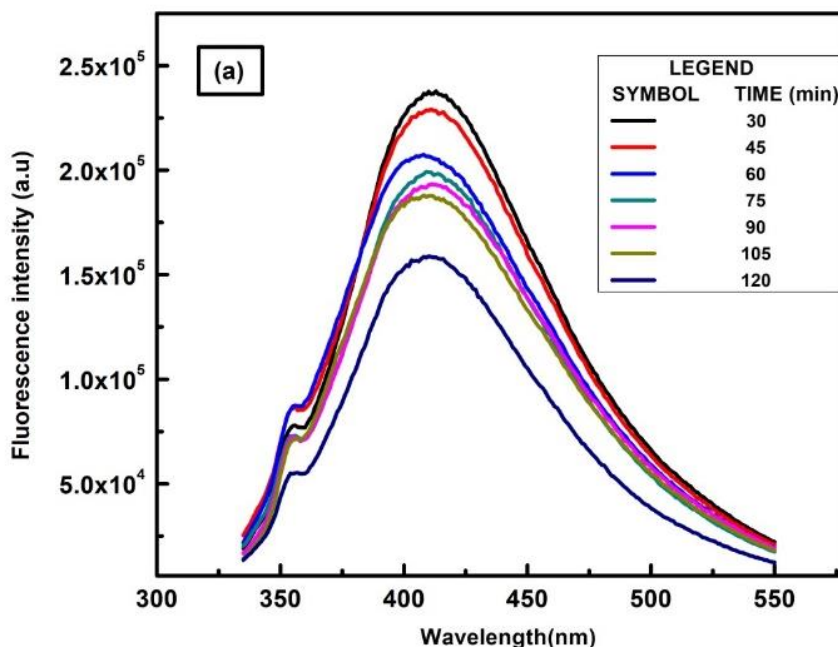
Figure 4.29: Fluorescence quenching effect of (a) MV by ZnS NPs
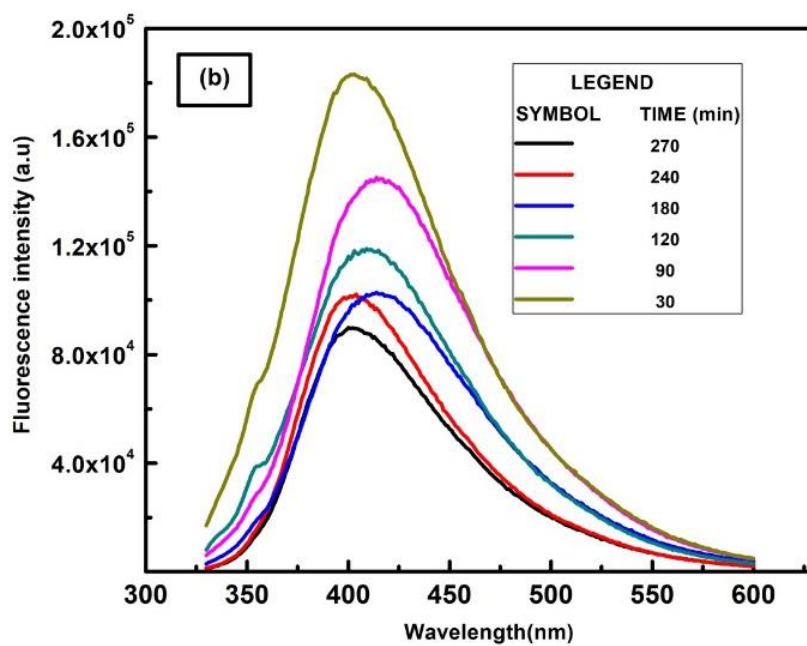
Figure 4.29: Fluorescence enhancement effect of (b) 2,4-D by ZnS NPs
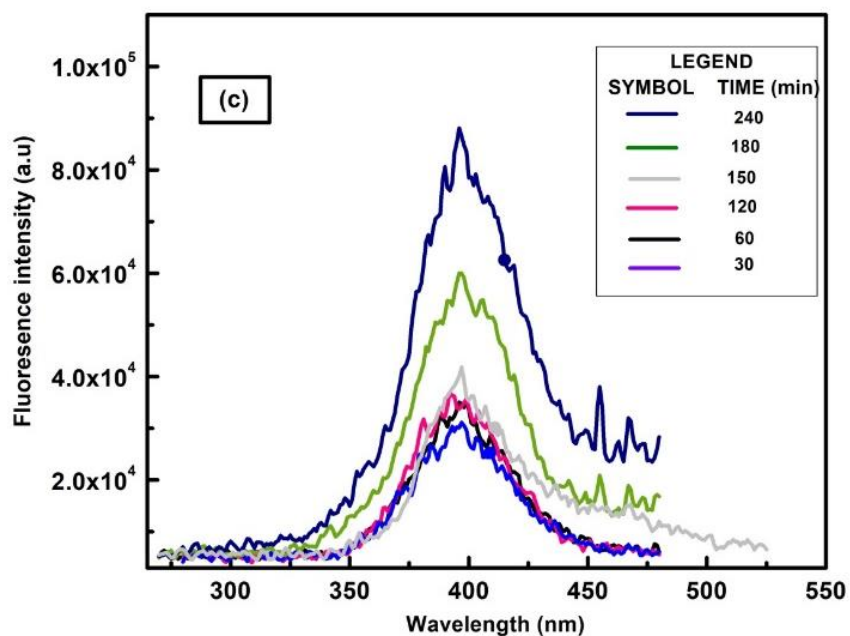
Figure 4.29: Fluorescence quenching effect of (c) PARA by ZnS NPs

4.8.5. COD, TOC and other trace elements measurements

The samples at different time intervals of MV, PARA and 2,4-D undergoing degradation process were analyzed for COD and TOC in order to estimate the organic contents. The MV dye belonging to triarylmethane class of dye undergoes mineralization involving the breakdown of chromogenic group i.e., the azo group, cleaving the triazine moiety of the aromatic ring molecule. The methyl group attached to the aromatic ring under goes oxidization and further de-amination of amino groups so that the dye molecules breakdown into their simpler compounds. The mineralization of N present in the dye may yield to NO^{3-}/ NO^{2-} / N_2, chloride (Cl) to Cl^- ions and carbon, hydrogen, oxygen (C, H, O) to CO_2 / H_2O. A significant decrease of 78 %, 55.5 %, 47.6 % and 74 %, 57.2 %, 44.5 % is observed with respect to COD and TOC for MV, 2,4-D and PARA respectively, thus confirming the mineralization process (Figure: 4.30 (a), (b) and (c)) (Kuo and Chen 2012; Cai et al. 2016). It is notable that even though there is a significant decrease in the TOC values the mineralization process is not complete, indicating the presence of highly recalcitrant small organic molecules which remained in the solution due to intermediates formation (Sakthivel et al. 2003).
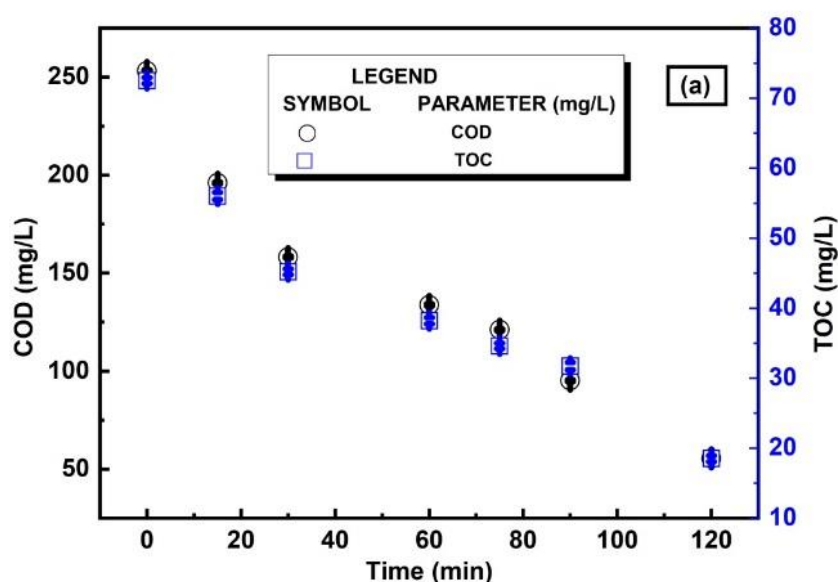
Figure 4.30: Mineralization of pollutants based on COD and TOC for (a) MV
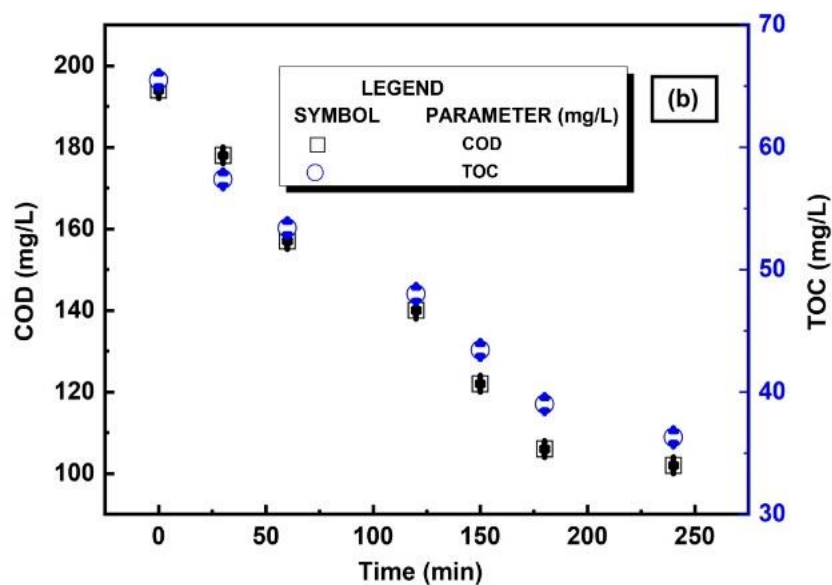
Figure 4.30: Mineralization of pollutants based on COD and TOC for (b) 2,4-D
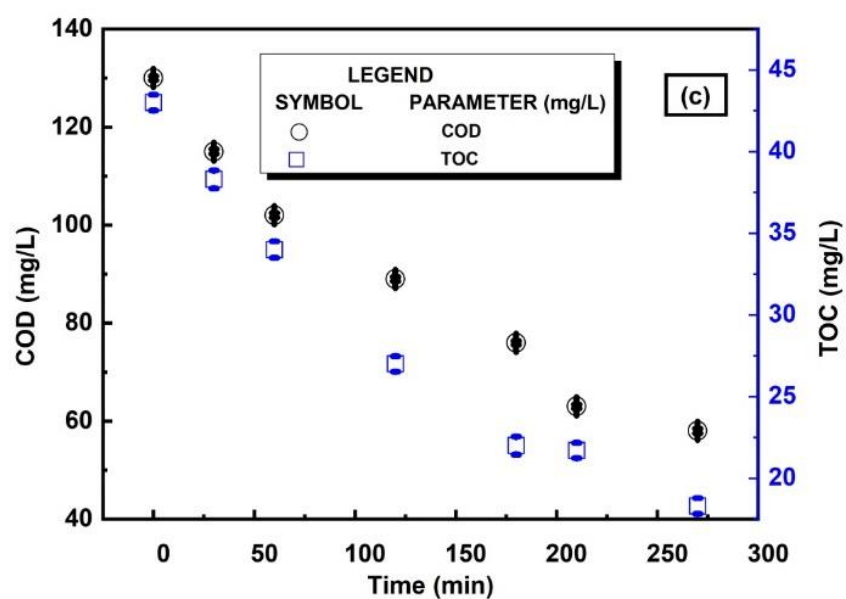
Figure 4.30: Mineralization of pollutants based on COD and TOC for (c) PARA

The photocatalytic degradation mechanism of the pollutants using ZnS NPs under solar irradiation is usually initiated by generation of charge carriers (Kaur et al. 2016). Based on this phenomenon E_{VB} and E_{CB} values were calculated to be 2.63 and -1.12 respectively. The ΔG_0

(kJ/mol) values are -0.7 kJ/mol, -1.153 kJ/mol and -2 kJ/mol for MV, 2,4-D and PARA respectively (El-kamash et al. 2005; Sheela et al. 2012; Liu et al. 2014). The amount of oxygen required is calculated for each of the organic pollutants to complete the reaction by the stoichiometric equations given in equations below. Figure. 4.31: (a), (b) and (c) depicts the C(org) in mol and the amount of oxygen required for the reaction is 276.3 g, 114.36 g and 456 g for MV, 2,4-D and PARA respectively. The stoichiometric equations are written based on the end products generated i.e., CO_2, H_2O are the inorganics. Further, these equations are balanced.

$$C_{24}H_{28}N_3Cl + 34.5\ O_2 + 3e^- \rightarrow 24\ CO_2 + 2\ NO_2^- + NO_3^- + Cl^- + 14\ H_2O \ \text{.......(4.2)}$$

$$C_8H_6Cl_2O_3 + 8\ O_2 + e^- \rightarrow 8\ CO_2 + 2\ Cl^- + 3\ H_2O \ \text{.............(4.3)}$$

$$2\ C_8H_9NO_2 + 20.5\ O_2 + e^- \rightarrow 16\ CO_2 + 2\ NO_2^- + 9\ H_2O \ \text{..........(4.4)}$$
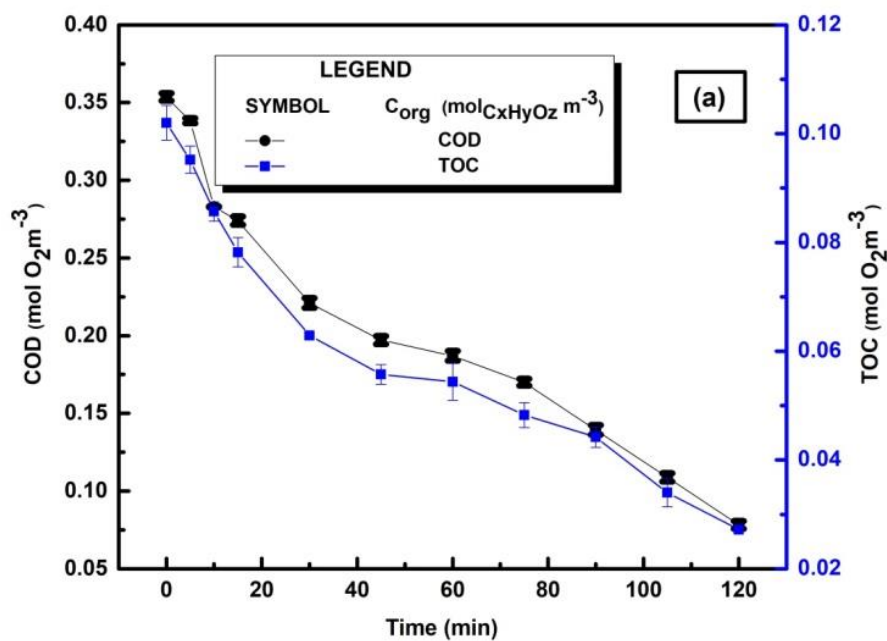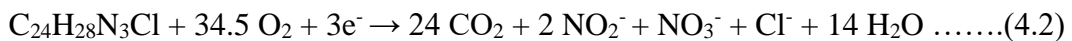
Figure 4.31: C(org) in mol$_{CxHyOz}$ m^{-3} and COD/TOC (mol O$_2$ m^{-3}) for (a) MV
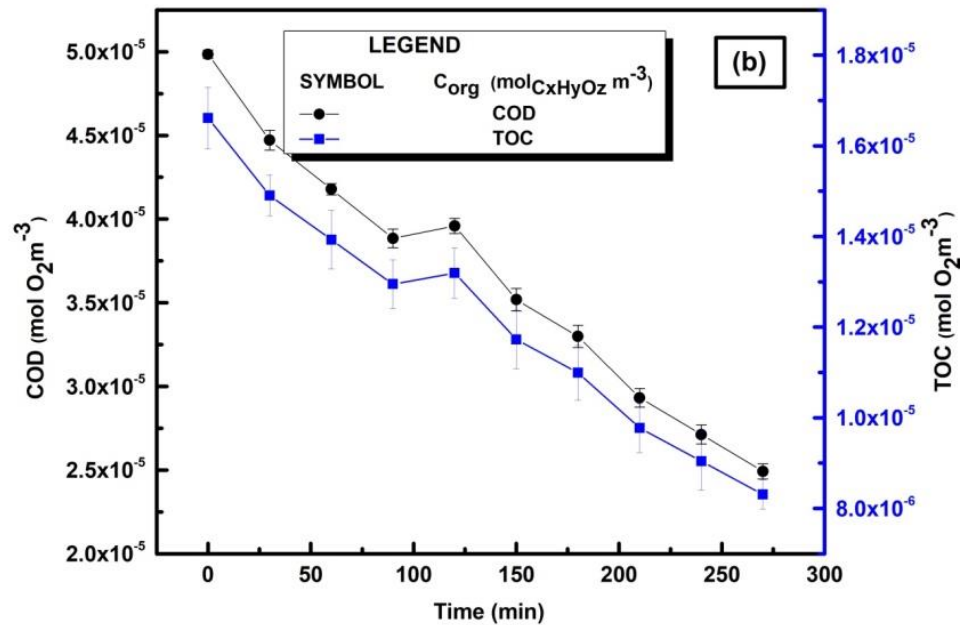
Figure 4.31: C(org) in mol$_{CxHyOz}$ m^{-3} and COD/TOC (mol O$_2$ m^{-3}) for (b) 2,4-D
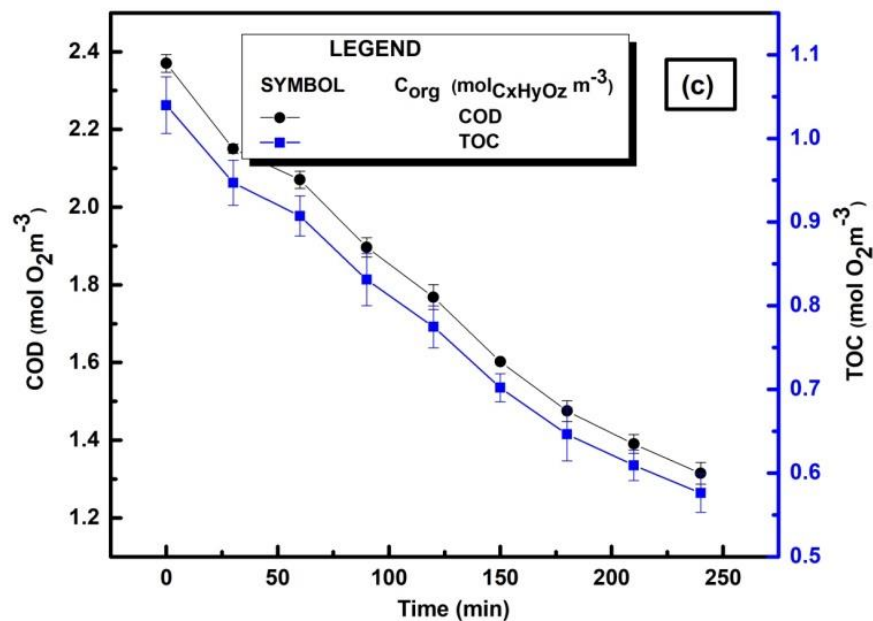
Figure 4.31: C(org) in mol$_{CxHyOz}$ m^{-3} and COD/TOC (mol O$_2$ m^{-3}) for (c) PARA

The inorganics content such as nitrates, nitrites and chlorides present in the samples are estimated and it is found that there is an increase in the nitrates from 0.96 to 1.98 mg/L, nitrites

from 0.24 to 0.32 mg/L and chlorides from 8.87 to 35.5 mg/L for MV as shown in Figure 4.32: (a) and (b). Similarly, for 2,4-D the chlorides ions are present in the range of 0.46 to 0.7 mg/L whereas for PARA nitrites it is from 0.45 to 0.64 mg/L and nitrates concentration is negligible (Tichonovas et al. 2013) (Figure 4.33 and Figure 4.34).
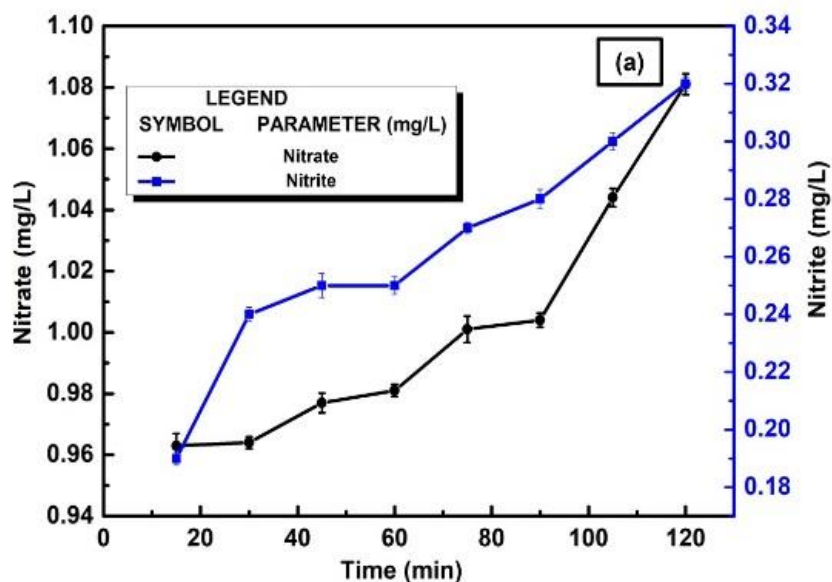
Figure 4.32: Estimation of (a) nitrates/nitrites for MV dye
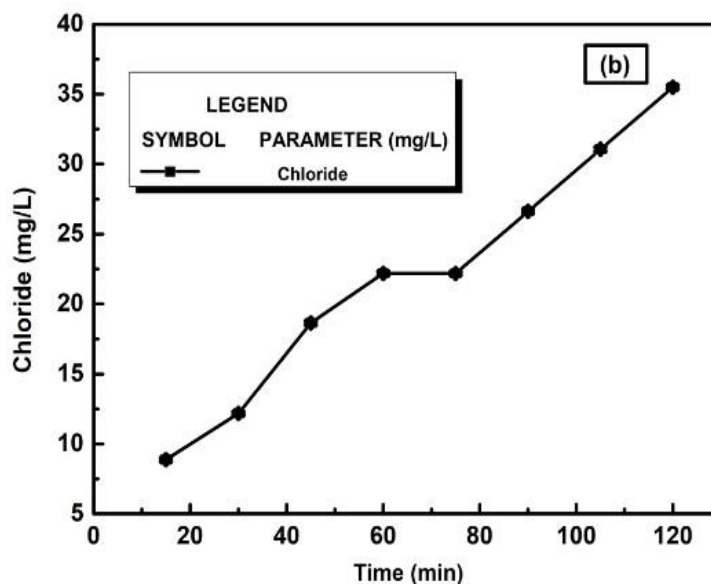
Figure 4.32: Estimation of (b) chlorides for MV dye
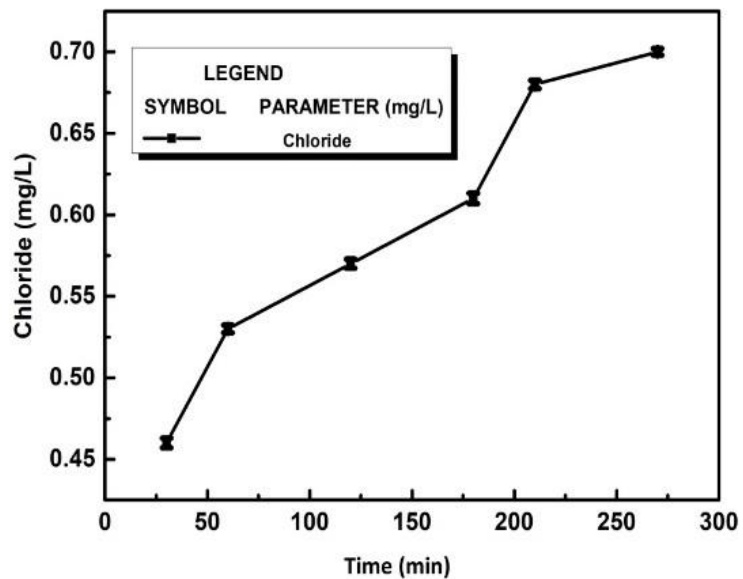
Figure 4.33: Estimation of chlorides from 2,4-D herbicide
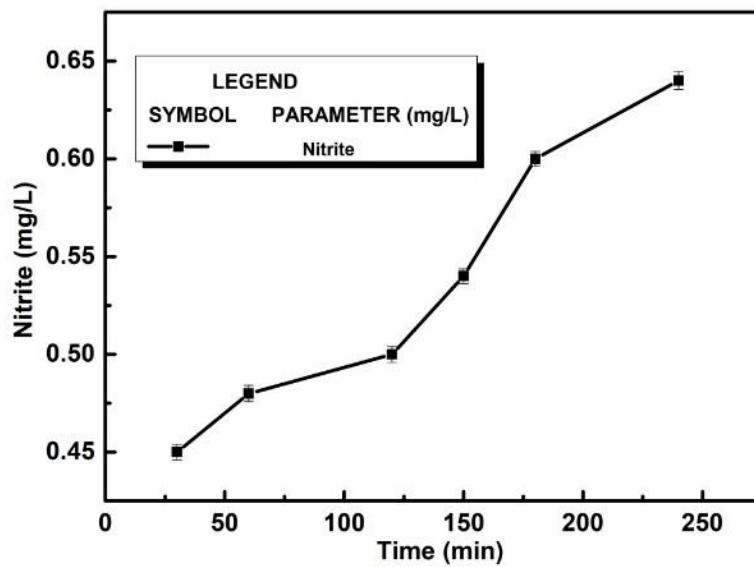
Figure 4.34: Estimation of nitrites from PARA drug

4.9. Degradation mechanism

4.9.1. FTIR analysis

FTIR spectral peaks for MV before degradation is interpreted as 1575 cm^{-1}, 1470 cm^{-1}, 1344 cm^{-1}, 1157 cm^{-1} corresponding to -C=C- stretching, -C-H- bending, -C-C- stretching and –C-N- stretching due to presence of amines and the peaks at 936 cm^{-1}, 908 cm^{-1} and 826 cm^{-1} corresponds to –C-H- out of plane bend as shown in Figure 4.35: (a). However, after the degradation process spectral peaks at 1581 cm^{-1}, 1345 cm^{-1}, 1159 cm^{-1}, 1066 cm^{-1}, 825 cm^{-1} and 699 cm^{-1} are comparable with -C=C- aromatic ring stretch, -C-C- stretching, -C-N- stretching, -C-H- aromatic in plane bending and –C-H- out of plane bend whereas peak at 3249 cm^{-1} is identical to -O-H- stretch of hydroxyl group as given in Figure 4.35: (b). For 2,4-D the spectral peaks at 703 cm^{-1}, 787 cm^{-1}, 835 cm^{-1}, 870 cm^{-1}, 1072 cm^{-1}, 1225 cm^{-1} represents -C-C- bonding, 1306 cm^{-1}, 1484 cm^{-1} and 1700 cm^{-1} corresponds to -C-H-, -N=O- and -C=C- before degradation as per Figure 4.36: (a). On the other hand, Figure 4.36: (b) depicts the spectral peaks at 969 cm^{-1}, 1083 cm^{-1}, 1114 cm^{-1} and 1633 cm^{-1} identical to -C-H- bending and stretching, -C-O- carboxyl group, -C=C- aromatic ring in phenyl group after degradation. In Figure 4.37: (a) the spectral peaks of PARA before degradation are observed at 842 cm^{-1} and 870 cm^{-1} corresponding to -C-H- aromatic ring, 1021 cm^{-1}, 1109 cm^{-1}, 1147 cm^{-1} corresponds to -C-C- bending, 1248 cm^{-1} and 1371 cm^{-1} -C-O- aromatic ring in phenyl group, 1431 cm^{-1} -C-N- stretch of primary, 1516 cm^{-1} and 1548 cm^{-1} -N-H- bend secondary aromatic amine, 1658 cm^{-1} -C=C- aromatic ring in phenyl group. After degradation, the spectral peaks at 680 cm^{-1}, 805 cm^{-1}, 836 cm^{-1} corresponds to -C-H-, 1015 cm^{-1}, 1105 cm^{-1}, 1225 cm^{-1}, 1433 cm^{-1} similar to -C-O- bonding and the peaks at 1323 cm^{-1}, 1368 cm^{-1}, 1506 cm^{-1}, 1557 cm^{-1}, 1608 cm^{-1} and 1649 cm^{-1} is relative to -N=O-, -C=N-, -C=C- as given in Figure 4.37: (b). A shift in peak position and reduction in peak intensity is observed in the degraded product is compared to the pure samples due to the substitution/breaking down of the functional groups (Baker and Satish 2012; Onwudiwe et al. 2014; Shah 2014).
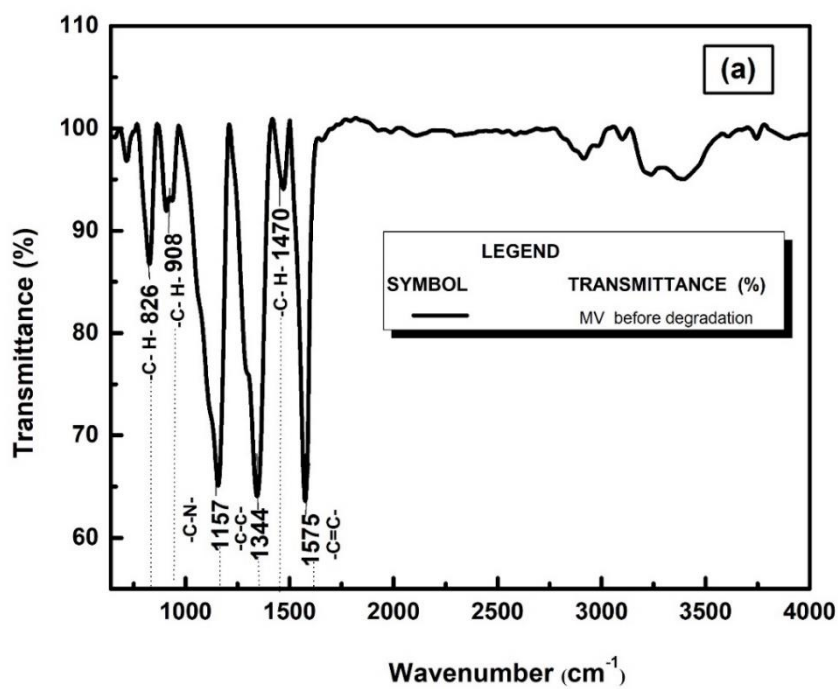
Figure 4.35: FTIR spectra of MV (a) before degradation
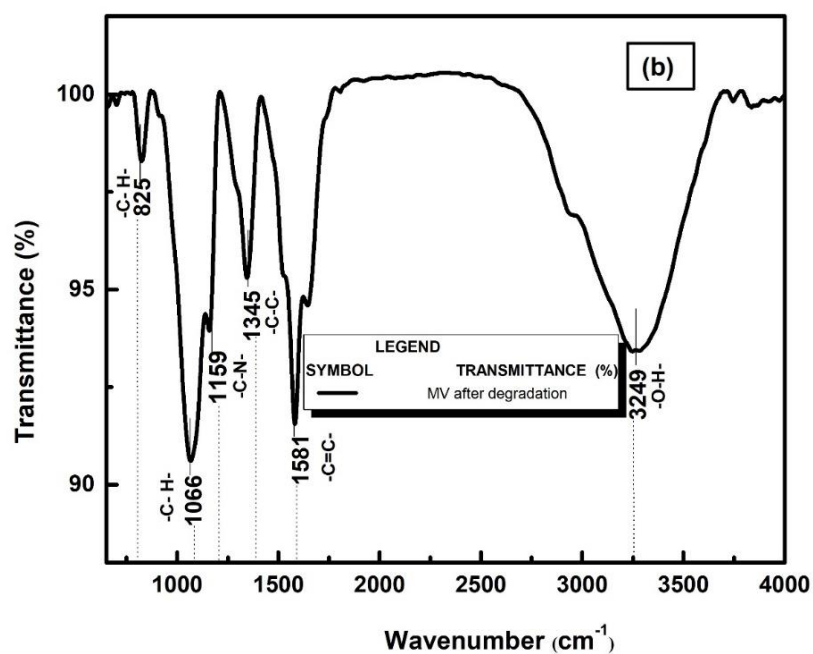
Figure 4.35: FTIR spectra of MV (b) after degradation
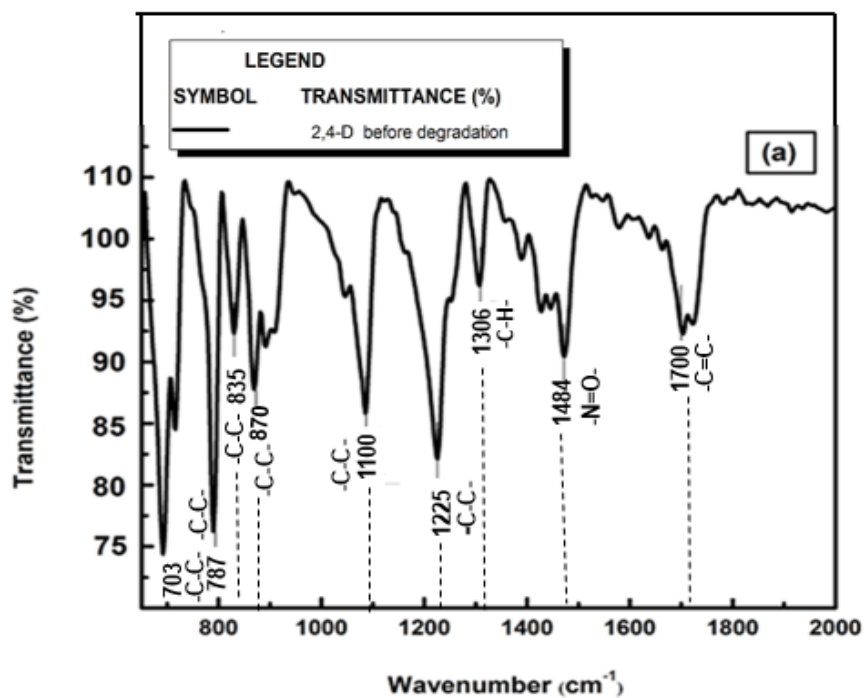
Figure 4.36: FTIR spectra of 2,4-D (a) before degradation
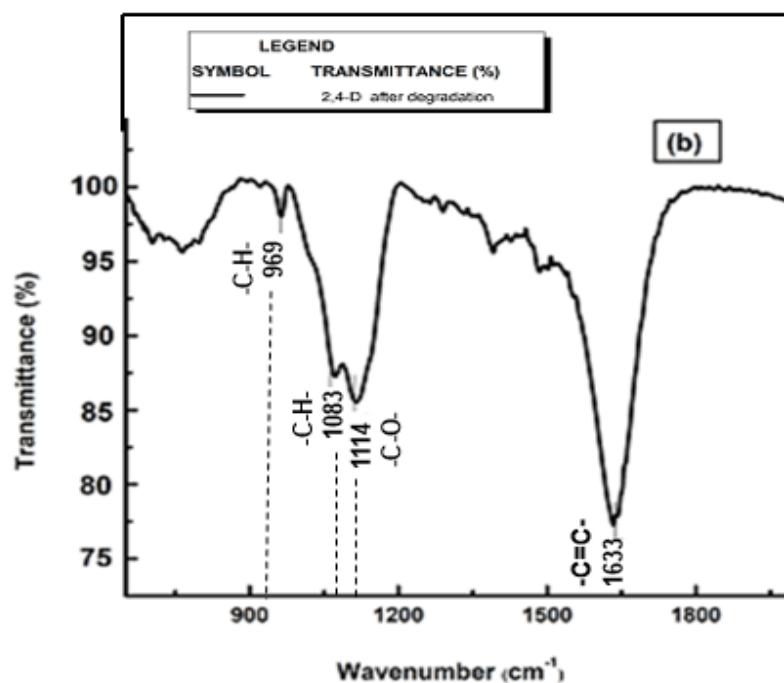
Figure 4.36: FTIR spectra of 2,4-D (b) after degradation
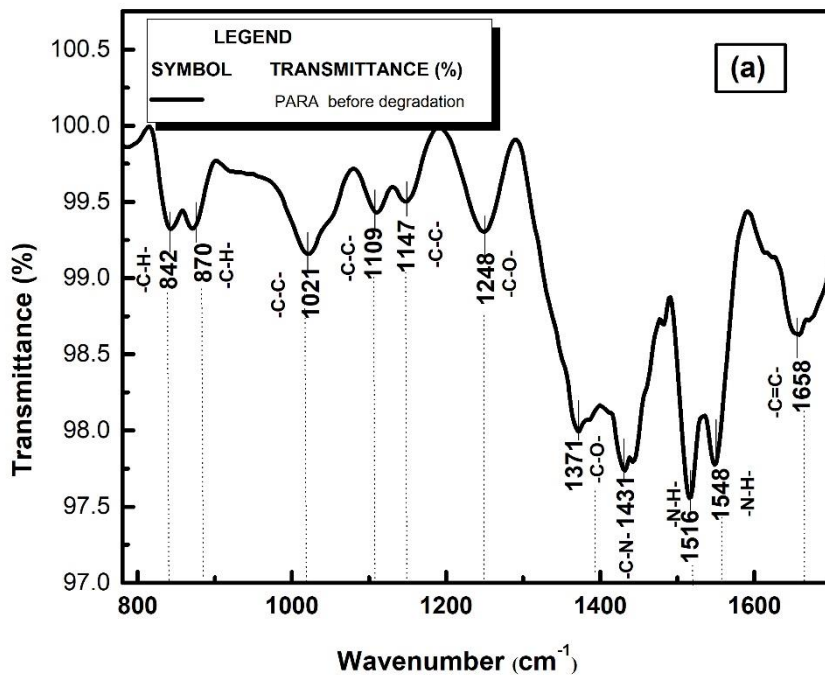
Figure 4.37: FTIR spectra of PARA (a) before degradation
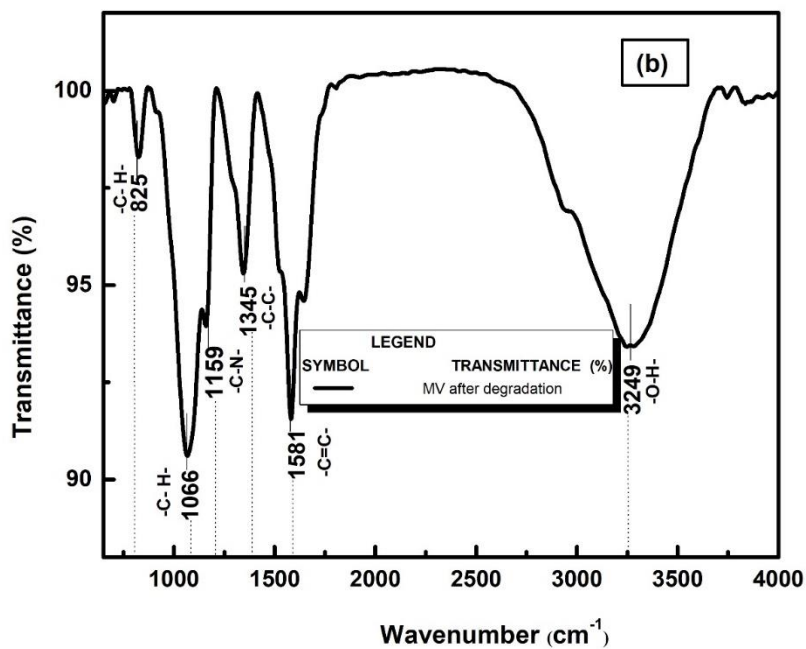
Figure 4.37: FTIR spectra of PARA (b) after degradation

4.9.2. LC-MS analysis

The mechanism involved in the degradation process of the MV dye is initiated by the intermediates formed by *N*-de-methylation process (Figure 4.38 (a)). Initially MV (m/z=379) gives rise to leucomethyl violet (m/z= 373) by removal of hydrogen molecules (Figure 4.38 (a)) further, leucomethyl violet degradation mechanism follows two routes, in the first route leucomethyl violet (m/z= 373) is reduced to pararosaline (m/z=287) and benzo(g)indazole (m/z=167), benzo(g)indazole is formed by removal of a methyl groups from pararosaline and the remaining elements are eluted out of the column. In the second route the intermediates obtained are 2-(4-formylphenyl)-6-methoxy-1-methylimidazo[1,2-a] pyridin-1-ium (m/z=237), 2-phenylquinoline-4-ol(m/z=222), 2-methylamino-phenol (m/z=123), 2,2-dimethyl-2,3-dihydro-1H-pyrrol-1-olate (m/z=112). 2-(4-formylphenyl)-6-methoxy-1-methylimidazo[1,2-a] pyridin-1-ium produced by removal of methyl groups from the leucomethyl violet structure. Later the hydroxyl radicals attack the conjugated structure resulting in other two intermediates containing phenolic groups. Due to the stronger auxochromic moieties cleavage of the central benzene ring is not observed which might be the reason for not obtaining 100% removal even after reaching an equilibrium state. Therefore, the conclusion drawn is that methylation is favoured over cleavage of the MV chromophore ring structure. This phenomenon indicate that the *N*-de-methylation process predominates and that the cleavage of the conjugated structure occurs at a slower rate (Gupta et al. 2006; Fan et al. 2009; Hisaindee et al. 2013; Bhattacharjee et al. 2015).

2,4-Dichlorophenol (m/z = 221) decomposition is favoured by the presence of electron-withdrawing groups located at the ortho, para and meta positions to the chlorine atoms, which facilitate the dehalogenation reaction (Figure 4.39 (b)). In Figure 4.38 (b) the first step in the photocatalytic degradation mechanism of 2,4-D involved the attack of the hydroxyl radicals on the chlorine positions forming 2,4-dichlorocatechol (m/z = 179). The major decay pathway of 2,4-D upon hydroxyl radical attack is via the homolysis of the -C1-O- bond on the aromatic ring to yield 2,4-dichlorophenol (2,4-DCP) (m/z = 162). In a subsequent step, the hydroxyl radical may predominantly replace the chlorine atom of 2,4-DCP to form 2-chloroethyl benzene (m/z = 140). Finally, the oxidation of the aromatic intermediates by oxidation of the aromatic ring leads to the formation of short linear compound succinic acid (m/z = 117) (Maya-Treviño et al. 2014; Jaafarzadeh et al. 2017; Lee et al. 2016).

For PARA, the mechanistic options can be envisaged for hydroxyl radical-dependent ortho hydroxylation. A general mechanism for the reaction of dissociated phenol involving the

initial formation of the phenoxyl radical, leading to the formation of quinone, biphenols and p-benzoquinone are identified as a major product (Figure 4.40 (c)). It involves a direct substitution reaction to give N-acetyl-p-benzoquinone imine (m/z = 149) which would decompose to yield hydroxy benzoquinone (m/z = 123) and hydroquinone (m/z = 110). The other pathway would probably be conversion of the primary radical adduct to 4-acetylaminocatechol (m/z = 167) as reported in Figure 4.38 (c) (Vogna et al. 2002; Graham et al. 2004; Wu et al. 2009; Moctezuma et al. 2012; Jallouli et al. 2017).
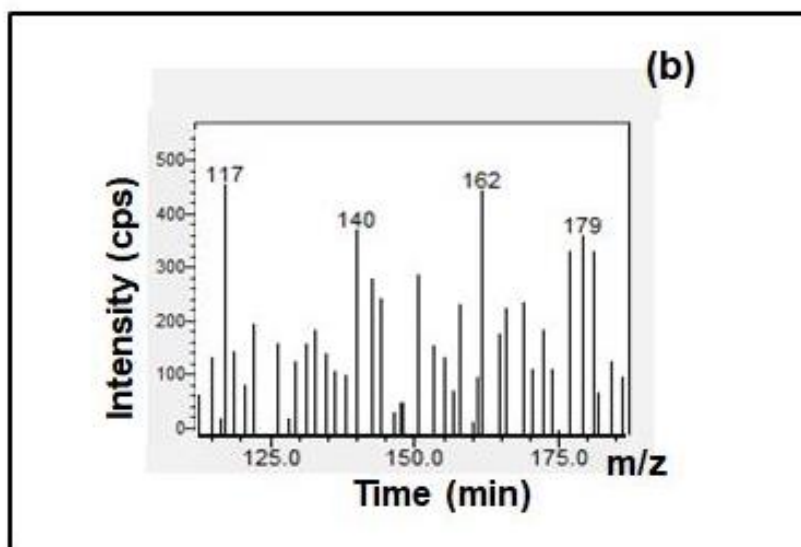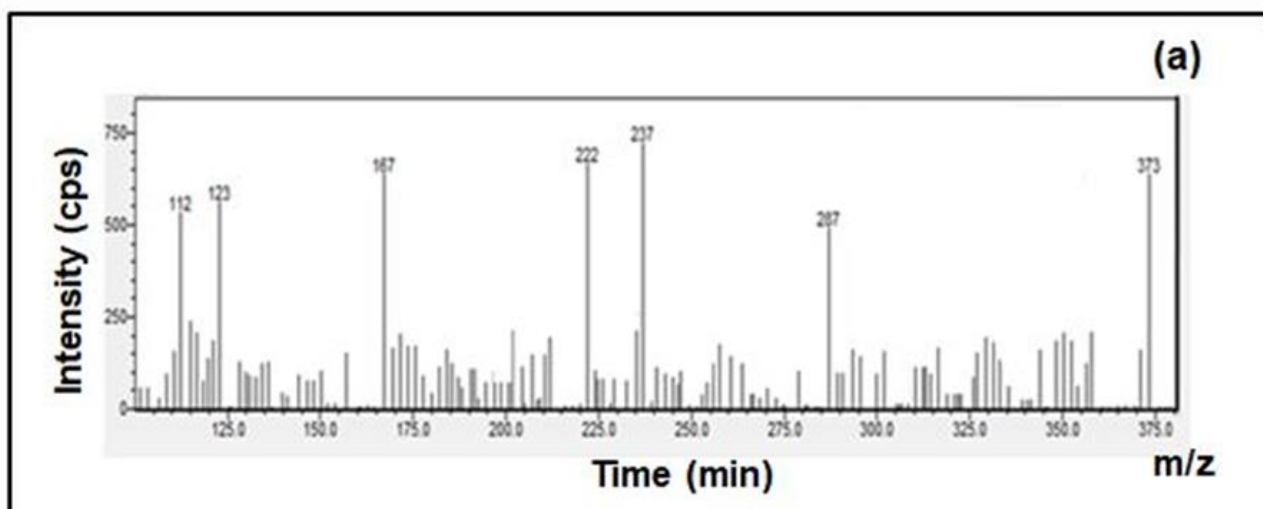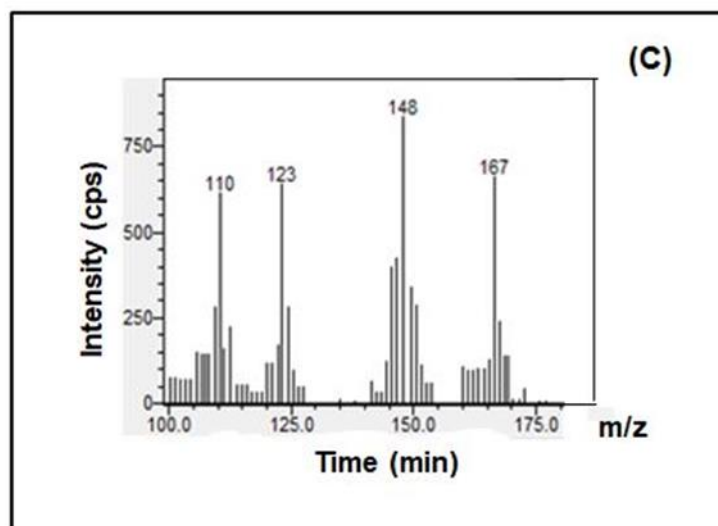
Figure 4.38: LC–MS chromatogram obtained from degraded (a) MV sample after 120 min, (b) 2,4-D sample after 270 min, (c) PARA sample after 240 min
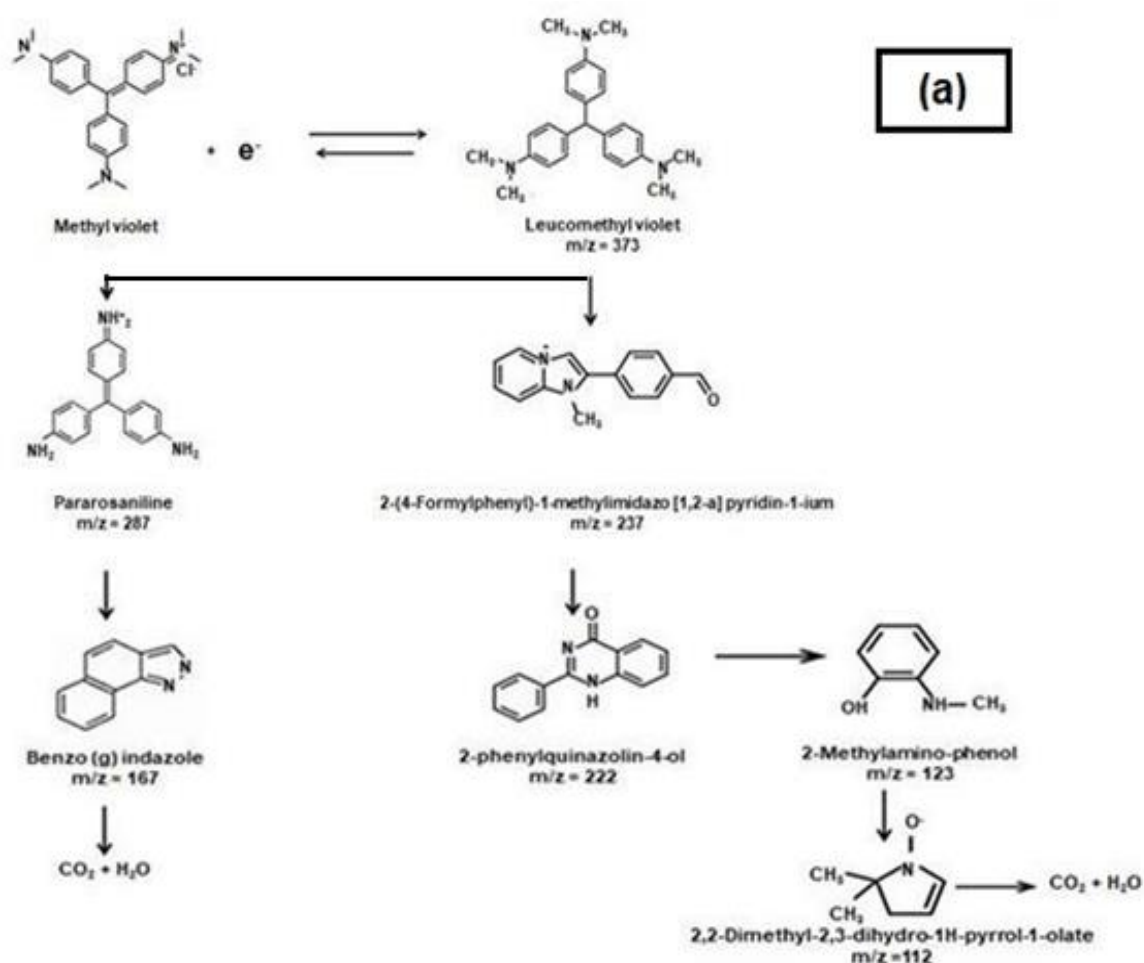
Figure 4.41: Intermediate products of (a) MV sample after 120 min degradation
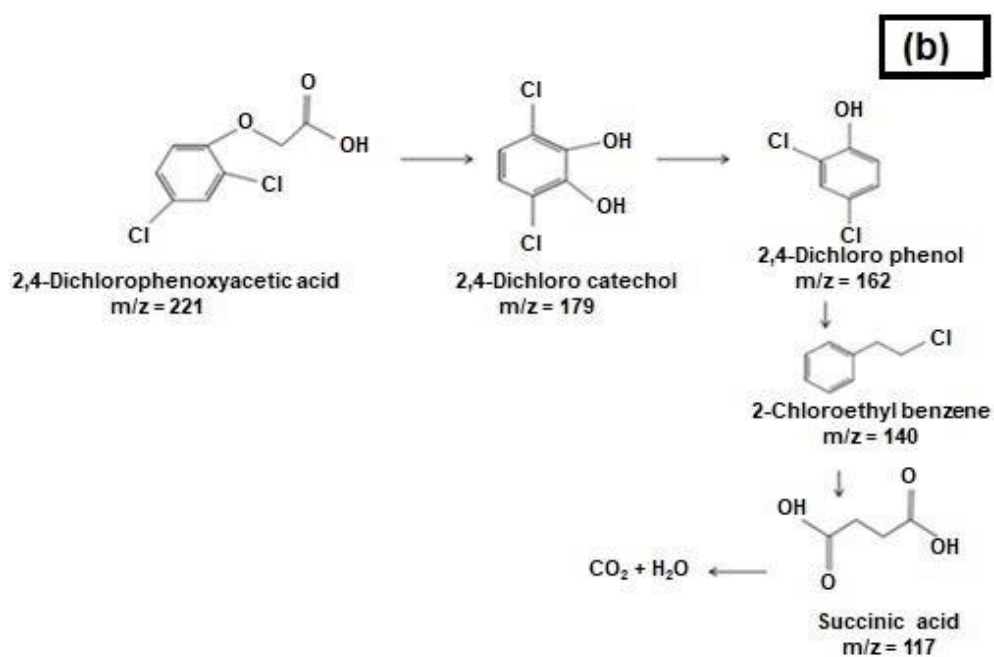
Figure 4.39: Intermediate products of (b) 2,4-D sample after 270 min degradation
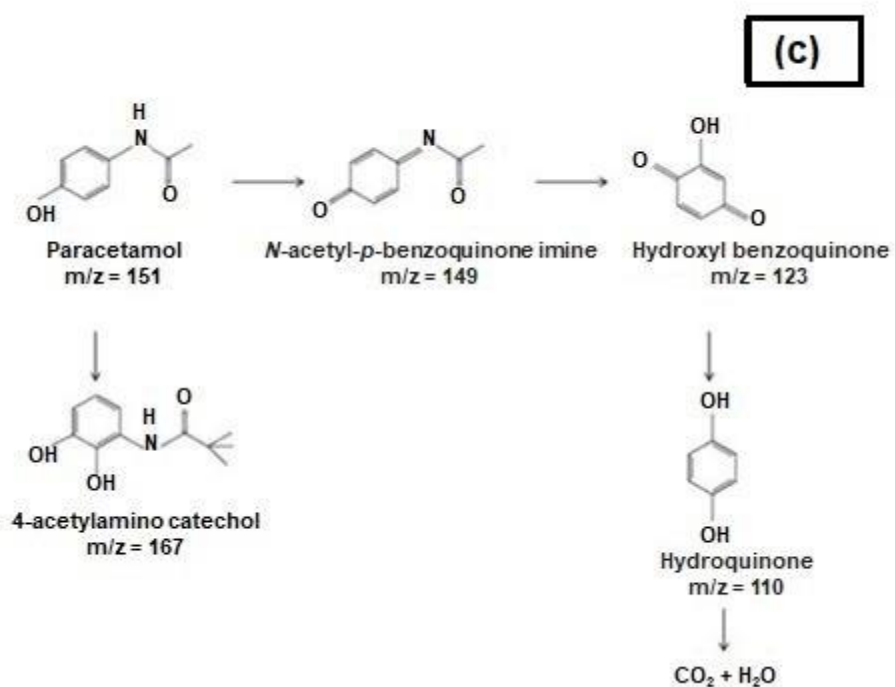
Figure 4.39: Intermediate products of (c) PARA sample after 240 min degradation

4.10. Stirred tank reactor studies

4.10.1. Effect of on biomass growth rate

From Figure: 4.40 it is evident that 2 % (w/v) inoculum volume settled at the bottom of the reactor and 20 % (w/v) culture inhibits the agitation process and 72 h culture yielded better results. The decrease in the growth rate with an increase in inoculum size can be attributed to the limitation of key nutrients including oxygen, for cells at higher densities (Lee et al. 2011). Looking into the second parameter, working volume of the reactor has a significant was varied as 1 L, 1.5 L and 2 L for which biomass dry weight of 40 g/L, 33 g/L, 24 g/L is obtained. The increase in the volume, lead to an improved mixing condition and oxygen transfer and found to have increased host cell growth. However, the increase in the working volume to 2 L showed an effect on biomass growth indicating the possibility of decrease in the oxygen transfer to cells (Collins et al. 2013; Schiefelbein et al. 2013). Although the biomass concentration profiles as shown in Figure: 4.41 are not affected by the agitation speed significantly, stirring at 120 rpm had a negative impact on growth due to the shear stress and ultimately reduced the formation of NPs which reflected in the measured absorbance values. However, the reduction in agitation speed resulted in the formation of biofilm in the bioreactor, therefore a minimal stirring of 80 rpm is considered (Rodríguez et al. 2005; Byrne et al. 2015).
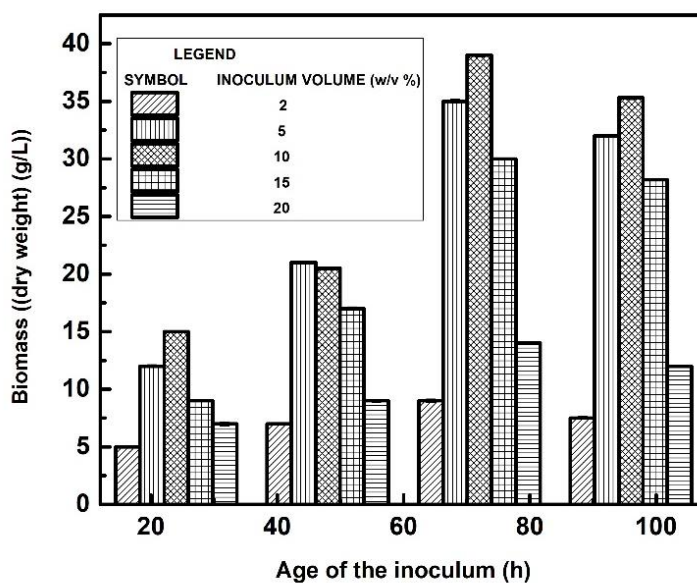
Figure 4.40: Biomass dry weight (g/L) with respect to the age of the inoculum for different inoculum volume
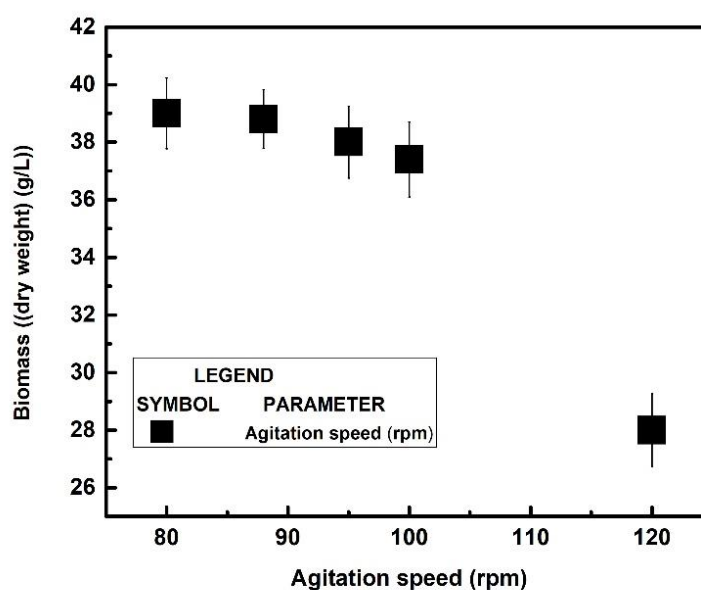
Figure 4.41: Biomass dry weight (g/L) with respect to agitation speed

4.10.2. Effect of precursor concentration and incubation time on NPs formation

From the above studies it is concluded that 72 h biomass, inoculum volume 10 % (w/v), working volume 1 L and agitation speed of 80 rpm are optimum. Based on these results, the effect of concentration of precursor and reaction time are studied. From Figure: 4.42 (a) the optimum concentration of precursor was found to be 30 mM. Even though the ratio of active nucleation sites to the number of atoms decreased with increasing concentration of ionic zinc, the intensity remained constant at 40 mM and 50 mM. At 10 mM and 20 mM, did not exhibit higher intensities suggesting an insufficient amount of reducing bio-molecules against available metal ions (Bhargava et al. 2016). The higher intensity is found on the 3rd day after the addition of precursor as given in Figure: 4.42 (b) this might be because of the metal reduction and eventual NPs synthesis are time-dependent reactions, longer incubation times allow the reaction equilibrium to shift towards the reduced form of metals and results in the formation of more nucleation sites leading to higher numbers of particles (Erasmus et al. 2014) however, the intensity remained constant on 4th and 5th day .
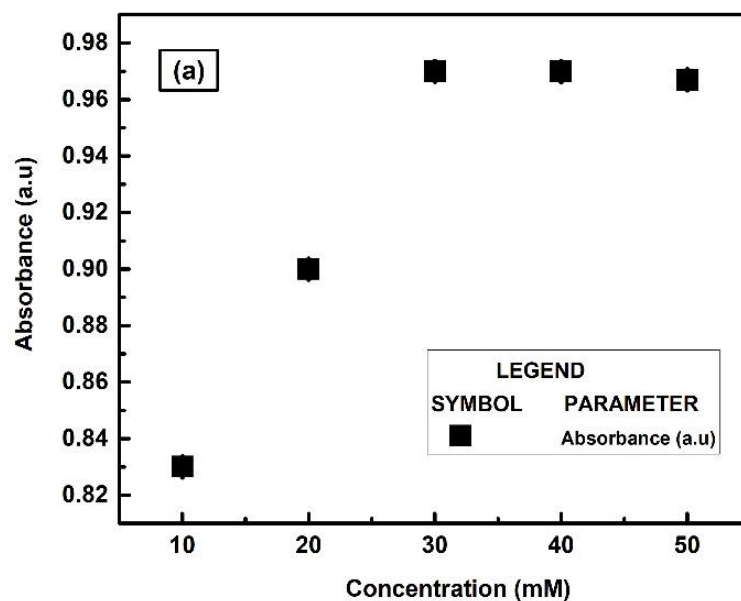
Figure 4.42: Effect of (a) precursor concentration on NPs formation
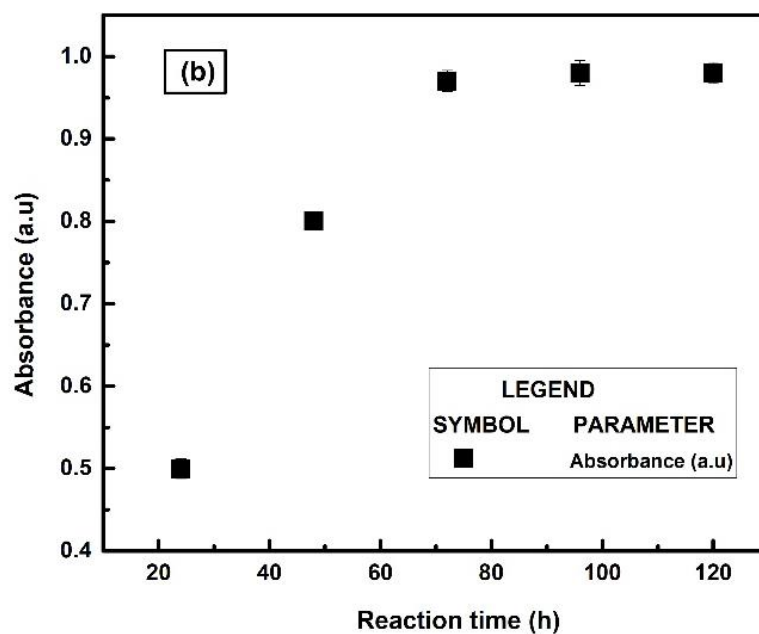
Figure 4.42: Effect of (b) reaction time on NPs formation

The diffraction peaks with maximum and minimum intensity is centered at 26°, 28°, 30°, 47° (2θ) can be attributed to (100), (002), (101) and (110) respectively, this is well-indexed to the hexagonal phase of ZnS, which are in good agreement with standard (Figure: 4.43 (a)) (ICDD card No. 00-036-1450). The synthesized ZnS NPs has a diameter range of 10-15 nm as

shown in Figure: 4.43 (b). Compared to batch studies, the crystallite size is observed to smaller which may be due to large medium volume as justified by Moon et al. 2010, in a study on crystallite size with respect to reactor volumes. The prominent lattice fringes observed in Figure: 4.43 (c), TEM image with 5nm magnification reveals the crystalline nature of the NPs and the SAED pattern exhibiting concentric rings confirm the polycrystallinity of the material supported by Figure: 4.43 (d). The SAED patterns are indexed to correspond with the (100), (101) and (110) planes in accordance with the hexagonal wurtzite structure and diffraction rings matched well with corresponding XRD patterns of the ZnS NPs reported by Bai et al. 2006; Chen et al. 2014.
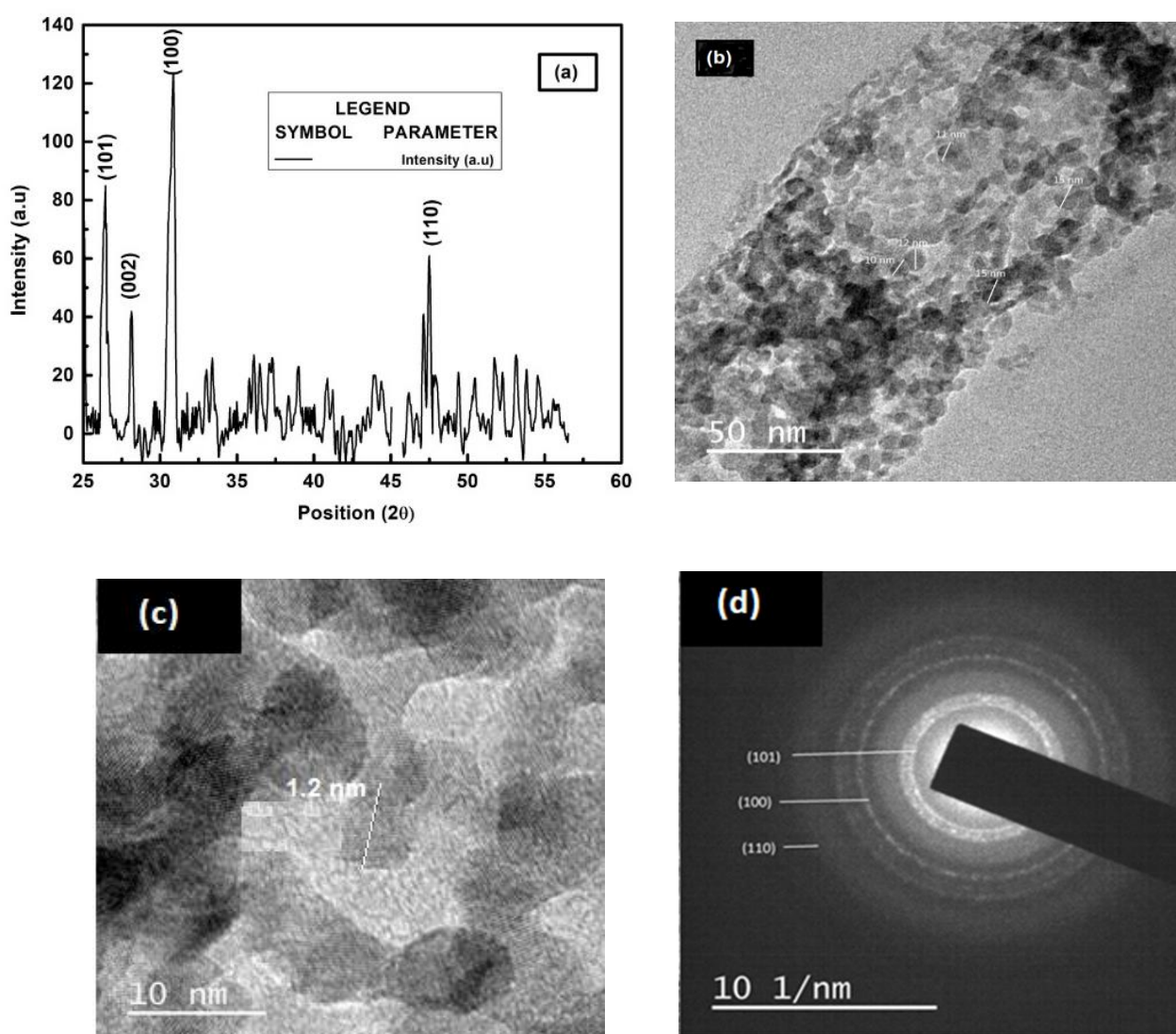
Figure 4.43: (a) XRD (b) TEM images (c) SAED pattern and (d) Lattice -fringe finger print image of ZnS NPs

CHAPTER 5

5. CONCLUSIONS

5.1. Summary and significant findings

The fungal species *Aspergillus flavus,* isolated from **a** medicinal plant *Nothapodytes foetida*, collected from Agumbe forest of Karnataka, India was used in the biosynthesis of ZnS NPs. *Aspergillus flavus* was selected as the most suitable fungus for the biosynthesis of ZnS NPs based on screening studies. Optimization of the operating variables for the biomass growth rate of *Aspergillus flavus* was done. The effects of precursor concentration and reaction time for the biosynthesis of ZnS NPs were assessed using a statistical method, CCD of RSM. The characterisation studies of the ZnS NPs (quantum dots) for its, morphology, optical, electrochemical and stability properties were carried out using various characterization studies such as TEM, DLS, EDAX, UV-Vis, DRS, FT-IR and Raman spectroscopy. The degradation potential of ZnS NPs under natural solar irradiation was evaluated for Methyl Violet (dye), 2,4-D - pesticide and pharmaceutical drug (PARA) for 120 min, 270 min and 240 min, respectively. To confirm the interaction of ZnS NPs with organic pollutants, fluorescence and AFM studies were conducted. COD, TOC and LC-MS studies for confirmation of mineralization of these pollutants and the intermediates formed in the degradation process was done. The mechanism of the NPs synthesis process was studied and the results suggest that the machinery required for the synthesis was similar to fungal metal detoxification. The NPs synthesis in the stirred tank reactor is assessed by various parameters such as inoculum volume, the age of the inoculum, working volume, agitation speed, precursor concentration and reaction time.

In summary, the biologically synthesized ZnS NPs isolated from an endophytic fungus *Aspergillus flavus* from a medicinal plant *Nothapodytes foetida* was evaluated for its photocatalytic degradation and mineralization potential over three different classes of organic pollutants under solar irradiation. The following conclusions are derived from the degradation studies of MV, 2,4-D and PARA:

- Initial studies revealed appreciable ZnS tolerance towards endophytic fungus *Aspergillus flavus* on this basis, the fungus was utilized for the extracellular biosynthesis of ZnS NPs.
- TEM and DLS images revealed that the average diameter of NPs to be 18 nm and 58.9 nm respectively.
- The biosynthesized ZnS NPs was found to have a hexagonal phase with peaks centered at 28.45º, 47.54º, 57º.

- UV and DRS spectrum revealed that there is a shift in the peak position compared to the bulk and the band gap thus obtained is found to be 3.75 eV

- FTIR revealed the functional groups present on the NPs which corresponds to amine groups of sulphur bearing proteins and the Raman spectroscopy reveals the vibrational, rotational and frequency modes

- ZnS NPs exhibited a strong photoluminescence peak at 420 nm which can be ascribed to the high-level energy transition in the ZnS semiconductor.

- From, the thermal properties it is concluded that TGA and TGA-DTG to be 72 % and 53.86 % respectively.

- As per DSC analysis, exothermic and endothermic peaks are found to be at 80 °C, 120 °C, 250 °C and 280 °C respectively.

- The cyclic voltammetry (CV) analysis obtained by sweeping the potential rate of 25 mV/s showed similar reduction and oxidation peaks indicating the stable state of the NPs.

- The zeta potential examination further confirmed the maximum stability at pH 9 i.e., at −22.3 mV.

- The degradation efficiency of ZnS NPs for degradation of MV, 2,4-D and PARA is 87 %, 33 % and 51 % respectively.

- COD and TOC analysis confirmed that the percentage of mineralization of the above organic pollutants as 78 % and 74 % for MV; 55.5 % and 57.2 % for 2,4-D; 47.6 % and 44.5 % for PARA respectively.

- The fluorescence studies revealed that MV/PARA had a quenching effect on the ZnS NPs whereas 2,4-D had fluorescence enhancement with time.

- The major intermediate products generated during the photocatalytic reaction for MV, 2,4-D and PARA were assessed by Mass Spectrophotometer.

- Investigations of SEM and AFM micrographs revealed that an extracellular mechanism being involved in the biosynthesis process of ZnS NPs.

- The retention time, 6-10 min and the peaks at 149, 301 and 579 of the filtrate free from NPs and biomass under the chromatogram analysis confirmed the presence of residual proteins such as metallothioneins and phytochelatins that are responsible for the formation of the ZnS NPs.

- For the stirred tank reactor studies, an optimum biomass growth yield was obtained at inoculum volume of 10 % (w/v), working volume of 1 L and agitation speed 80 rpm.

- XRD and TEM analysis confirmed the hexagonal phase of NPs with the average diameter of 10-15 nm at an optimum concentration of 30 mM for 72 h.

In conclusion, the isolated species endophytic fungus *Aspergillus flavus* can effectively synthesize NPs by an ecofriendly/economical one-step synthesis method. It has the ability to produce a narrow size range diameter of ZnS NPs and the synthesized NPs exhibited strong quantum confinement effect. The presence of functional groups and the mass chromatogram indicated the presence of thiol bearing compounds which are the residues of cysteine and methionine, moreover, the morphological studies revealed the extracellular synthesis mechanism of NPs. These bioactive compounds sustain the stability and it is affirmed by voltammetry studies. The encapsulation on ZnS NPs via endophytic fungus isolated from the medicinal plant *Nothapodytes foetida* offered a promising scope for fungal nano-catalysts to exploit their degradation potential. The present findings elucidate the catalytic activity towards pollutant degradation and mineralization using ZnS NPs and in presence of solar irradiation their activity enhanced because of its oxidized state during the reaction by enhancing their electron transfer capacity and the plasmonic effects. Hence, this work provided new insights for understanding the degradation of organic pollutants using biological ZnS nanophotocatalyst. In the stirred tank reactor, the work presented demonstrates the operation of the bioreactor systems for the scale-up of the NPs further the process variables were found to play a major role for enhancing the biomass growth and the NPs formation.

5.2. Scope of the work

The nano-biosynthesis of NPs from endophytic fungi *Aspergillus flavus* could be used in developing catalysts which may find potential applications in the wastewater treatment and heavy metal removal. Moreover, the challenges for redressal include optimal production and minimal time to obtain the desired size and shape, to enhance the stability of NPs and optimization of specific microorganisms for a specific application. In the context of the energy crisis, environmental considerations such renewable energy sources are rapidly increasing their contribution globally, for sustainable technologies such as the utility of solar energy for solar desalination/detoxification/disinfection to solve energy and water scarcity. Direct reuse systems envisioned, treatment of industrial wastewater seems to be one of the most promising fields of application of solar photocatalysis. The present work can be extended for degradation of various aromatic compounds such as benzene, toluene, phenol, catechol, volatile organic compounds (VOCs) and decontamination of benzene, degradation of benzene, toluene, and xylene (BTX), alkanes, haloalkanes, aliphatic alcohols, carboxylic acids, alkenes, aromatics,

haloaromatics, polymers, surfactants, herbicides, pesticides and dyes (Blanco et al. 2009; Soonchul et al. 2009; Malato et al. 2009). The synthesized ZnS NPs can be modified by encapsulation in silica shell and immobilized by a polymer matrix, composites of ZnS and rare earth metals doped ZnS which can be used as efficient entities for degradation, further, these can be immobilized in hydrogel-based catalytic systems. The scale-up is a procedure for designing and building a large-scale system on the basis of the results of experiments with small-scale models. To improve the cost of production the configuration and the design parameters should be optimised based on the simulation and computational methods. Additionally, fungal-biofilm based methods can be adopted for the synthesis of nanoparticles to avoid stirring. Thus, the future studies can explore the potential of these biological nano-catalysts as a novel catalytic and biological model in the field of material, energy and environmental science.

REFERENCES

Abdennouri, M., Elhalil, A., Farnane, M., Tounsadi, H., and Mahjoubi, F. Z. (2015). "Photocatalytic degradation of 2,4-D and 2,4-DP herbicides on Pt / TiO$_2$ nanoparticles." *J Saudi Chem Soc*., 19, 485–493.

Afzal K, S., Hamayun, M., and Ahmed, S. (2006). "Degradation of 4-aminophenol by newly isolated *Pseudomonas* sp. strain ST-4." *Enzyme Microb. Technol.*, 38(1–2), 10–13.

Ahluwalia, S., Prakash, N. T., Prakash, R., and Pal, B. (2016). "Improved degradation of methyl orange dye using bio-co-catalyst Se nanoparticles impregnated ZnS photocatalyst under UV irradiation." *Chem. Eng. J.*, 306, 1041–1048.

Ahmad, I., Ahmad, F. and Pichtel, J. (2011). "Microbes and Microbial Technology: Agricultural and Environmental Applications." *Springer.*, 1-27

Akir, S., Barras, A., Cof, Y., Bououdina, M., Boukherroub, R., and Dakhlaoui, A. (2016). "Eco-friendly synthesis of ZnO nanoparticles with different morphologies and their visible light photocatalytic performance for the degradation of Rhodamine B." *J Alloy Compd*., 42, 10259–10265.

Akpan, U. G., and Hameed, B. H. (2009). "Parameters affecting the photocatalytic degradation of dyes using TiO$_2$ -based photocatalysts : A review." *J Environ Sci*.,170, 520–529.

Akpan, U. G., and Hameed, B. H. (2011). "Photocatalytic degradation of 2,4-dichlorophenoxyacetic acid by Ca-Ce -W-TiO$_2$ composite photocatalyst." *Chem. Eng. J.*, 173(2), 369–375.

Alfano, O. M., Brandi, R. J., and Cassano, A. E. (2001). "Degradation kinetics of 2,4-dichlorophenoxyacetic acid in water employing hydrogen peroxide and UV radiation." *Chem. Eng. J.*, 82, 209–218.

Almeida, L. C., Garcia-Segura, S., Bocchi, N., and Brillas, E. (2011). "Solar photoelectro-Fenton degradation of paracetamol using a flow plant with a Pt/air-diffusion cell coupled with a compound parabolic collector: Process optimization by response surface methodology." *Appl. Catal. B Environ.*,

103(1–2), 21–30.

Alvin, A., Miller, K. I., and Neilan, B. A. (2014). "Exploring the potential of endophytes from medicinal plants as sources of antimycobacterial compounds." *Microbiol. Res.*, 169(7–8), 483–495.

Anand, K. V. (2015). "Optical and photoluminescence properties of HMTA capped transition metals (Cu , Co and Mn) doped ZnS nanoparticles." *J Chem Pharm Res.,*7(3), 286–290.

Andreozzi, R., Caprio, V., Marotta, R., and Vogna, D. (2003). "Paracetamol oxidation from aqueous solutions by means of ozonation and H_2O_2 /UV system." *Water Res.*, 37(5), 993–1004.

Arredondo, V. H. C., García, J. G., Granados, S. G., and Ponce, D. L. C. (2012). "Degradation of paracetamol by advance oxidation processes using modified reticulated vitreous carbon electrodes with TiO_2 and CuO/TiO_2 /Al_2O_3." *Chemosphere*, 89, 1195–1201.

Asif, S., Chaudhari, A., Gireesh-Babu, P., Roy Chaudhuri, P., and Sen, R. (2016). "Immobilization of fluorescent whole cell biosensors for the improved detection of heavy metal pollutants present in aquatic environment." *Mater. Today Proc.*, 3(10), 3492–3497.

Ayodhya, D., Venkatesham, M., Santoshi kumari, A., Reddy, G. B., Ramakrishna, D., and Veerabhadram, G. (2016). "Photocatalytic degradation of dye pollutants under solar, visible and UV lights using green synthesised CuS nanoparticles." *J. Exp. Nanosci.*, 11(6), 418–432.

Bai, H. J., Zhang, Z. M., and Gong, J. (2006). "Biological synthesis of semiconductor Zinc Sulfide nanoparticles by immobilized *Rhodobacter sphaeroides*." *Biotechnol. Lett.*, 28(14), 1135–1139.

Ballottin, D., Fulaz, S., Souza, M.L., Corio, P., Rodrigues, A.G., Souza, A.O., Gaspari, P.M., Gomes, A.F., Gozzo, F., and Tasic, L. (2016). "Elucidating Protein Involvement in the Stabilization of the Biogenic Silver Nanoparticles." *Nanoscale Res. Lett.* 11, 313

Baker, S., and Satish, S. (2012). "Endophytes : Toward a Vision in Synthesis of Nanoparticle for Future Therapeutic Agents." *Int J Bio-Inorg Hybrid.,* 1(2), 67–77.

Baker, S., and Satish, S. (2015). "Biosynthesis of gold nanoparticles by *Pseudomonas veronii* AS41G inhabiting *Annona squamosa* L." *Spectrochim. Acta - Part A Mol. Biomol. Spectrosc.*, 150, 691–695.

Bhainsa, K. C., and Souza, S. F. D. (2006). "Extracellular biosynthesis of silver nanoparticles using the fungus *Aspergillus fumigatus*." *Colloids and Surfaces B: Biointerfaces.,* 47, 160–164.

Bhattacharjee, A., Ahmaruzzaman, M., and Sinha, T. (2015). "A novel approach for the synthesis of SnO_2 nanoparticles and its application as a catalyst in the reduction and photodegradation of organic compounds." *Spectrochim. Acta - Part A Mol. Biomol. Spectrosc.*,136, 751–760.

Bhargava, R.N., Gallagher, D., Hong, X. and Nurmikko, A. (1994). "Optical properties of manganese-doped nanocrystals of ZnS." *Phys Rev Lett*, 72, 416–419.

Bhavani, R., and Sivasamy, A. (2016). "Sonocatalytic degradation of malachite green oxalate by a semiconductor metal oxide nanocatalyst." *Ecotoxicol. Environ. Saf.*, 134, 403–411.

Bhuyan, B., Paul, B., Dhar, D., and Sankar, S. (2016). "Facile synthesis and characterization of zinc oxide nanoparticles and studies of their catalytic activity towards ultrasound-assisted degradation of metronidazole." *Mater. Lett.*, 168, 158–162.

Bo, Y., Guolin, L., Lanshu, J., Yuting, Z., Tao, Z., and Jiaxi, Tang. (2015). "Adsorption and degradation of 2,4-dichlorophenoxyacetic acid in spiked soil with Fe^o nanoparticles supported by biochar." *Acta Agriculturae Scandinavica, Section B — Soil & Plant Science* 65 (3), 215-221.

Bogireddy, N. K. R., Kiran Kumar, H. A., and Mandal, B. K. (2016). "Biofabricated silver nanoparticles as green catalyst in the degradation of different textile dyes." *J. Environ. Chem. Eng.*, 4(1), 56–64.

Bokare, A. D., Chikate, R. C., Rode, C. V., and Paknikar, K. M. (2008). "Iron-nickel bimetallic nanoparticles for reductive degradation of azo dye Orange G in aqueous solution." *Appl. Catal. B Environ.*, 79(3), 270–278.

Boruah, P. K., Sharma, B., Karbhal, I., Shelke, M. V., and Das, M. R. (2017). "Ammonia-modified graphene sheets decorated with magnetic Fe_3O_4 nanoparticles for the photocatalytic and photo-Fenton

degradation of phenolic compounds under sunlight irradiation." *J. Hazard. Mater.*, 325, 90–100.

Byrne, J. M., Muhamadali, H., Coker, V. S., Cooper, J., and Llioyd, J. R. (2015). "Scale-up of the production of highly reactive biogenic magnetite nanoparticles using *Geobacter sulfurreducens.*" *J. Real Soc. Interface*, 12, 1–10.

Cai, C., Zhang, Z., Liu, J., Shan, N., Zhang, H., and Dionysiou, D. D. (2016). "Visible light-assisted heterogeneous Fenton with $ZnFe_2O_4$ for the degradation of Orange II in water." *Appl. Catal. B Environ.*, 182, 456–468.

Cao, G., and Wang, Y. (2004). "Fundamentals of homogeneous nucleation.

"*Nanostructures Nanomater. Synth. Prop. Appl.* 3, 68–69.

Castellote, M., and Bengtsson, N. (2011). "Principles of TiO_2 Photocatalysis." Application of Titanium Dioxide Photocatalysis to Construction Materials, RILEM State-of-the-Art Reports., 5-10

Chauhan, R., Kumar, A., and Chaudhary, R. P. (2013). "Photocatalytic degradation of methylene blue with Fe doped ZnS nanoparticles." *Spectrochim. Acta - Part A Mol. Biomol. Spectrosc.*, 113, 250–256.

Chauhan, R., Kumar, A., and Pal, R. (2014). "Photocatalytic degradation of methylene blue with Cu doped ZnS nanoparticles." *J. Lumin.*, 145, 6–12.

Chen, C. H., Chang, C. F., and Liu, S. M. (2010). "Partial degradation mechanisms of malachite green and methyl violet B by *Shewanella decolorationis* NTOU1 under anaerobic conditions." *J. Hazard. Mater.*, 177(1–3), 281–289.

Chen, F., Cao, Y., and Jia, D. (2015). "Facile synthesis of ZnS nanoparticles and their excellent photocatalytic performance." *Ceram. Int.*, 41(5), 6645–6652.

Chen, H., Kou, X., Yang, Z., Ni, W., and Wang, J. (2008). "Shape and Size-Dependent Refractive Index Sensitivity of Gold Nanoparticles." *Langmuir.*, 24(10), 5233–5237.

Chen, J., Hu, B., and Zhi, J. (2016). "Optical and photocatalytic properties of *Corymbia citriodora* leaf extract synthesized ZnS nanoparticles." *Phys. E Low-Dimensional Syst. Nanostructures*, 79, 103–106.

Chen, Z., Li, X. X., Du, G., Yu, Q., Li, B., and Huang, X. (2014). "Luminescence properties of chlorine and oxygen co-doped ZnS nanoparticles synthesized by a solid-state reaction." *Ceram. Int.*, 40(8), 13151–13157.

Choina, J., Bagabas, A., Fischer, C., Flechsig, G., and Kosslick, H. (2015). "The influence of the textural properties of ZnO nanoparticles on adsorption and photocatalytic remediation of water from pharmaceuticals." *Catalysis Today.*, 241, 47–54.

Conte, L. O., Schenone, A. V, and Alfano, O. M. (2016). "Photo-Fenton degradation of the herbicide 2 , 4-D in aqueous medium at pH conditions close to neutrality." *J. Environ. Manage.*, 170, 60–69.

Colpaert, J. V., Wevers, J. H. L., Krznaric, E., and Adriaensen, K. (2011). "How metal-tolerant ecotypes of ectomycorrhizal fungi protect plants from heavy metal pollution." *Ann. For. Sci.*, 68(1), 17–24.

Collins, T., Azevedo-silva, J., Costa, A., Branca, F., Machado, R., and Casal, M. (2013). "Batch production of a silk-elastin-like protein in E . coli BL21 (DE3): key parameters for optimisation." *Microb. Cell Fact.*, 12(21), 1–16.

Couteau, E., Hernadi, K., Seo, J. W., Thiên-Nga, L., Mikó, C., Gaál, R., and Forró, L. (2003). "CVD synthesis of high-purity multiwalled carbon nanotubes using $CaCO_3$ catalyst support for large-scale production." *Chem. Phys. Lett.*, 378(1–2), 9–17.

Darezereshki, E., Alizadeh, M., Bakhtiari, F., Schaffie, M., and Ranjbar, M. (2011). "A novel thermal decomposition method for the synthesis of ZnO nanoparticles from low concentration $ZnSO_4$ solutions." *Applied Clay Science.*, 54(1), 107-111.

Damodaran, D., Balakrishnan, R.M., and Shetty, V.K. (2013). "The Uptake Mechanism of Cd (II), Cr (VI), Cu (II), Pb (II), and Zn (II) by Mycelia and Fruiting Bodies of *Galerina vittiformis*" *BioMed Research International.*, 2013, 1-11

De Bary., A (1866)., Hofmeister's Handbook of Physiological Botany, Volume II, Engelmann, Leipzig, Germany

Dejonghe, W., Goris, J., Fantroussi, S. E, Vos, P. D, Verstraete, W., and Top, E. M., (2000). "Effect of Dissemination of of 2,4-D Degradation Plasmids on 2,4-D Degradation and on Bacterial Community Structure in Two Different Soil Horizons." *Appl Environ Microbiol.,* 66(8), 3297–3304.

Devi, L. S., and Joshi, S. R. (2015). "Ultrastructures of silver nanoparticles biosynthesized using endophytic fungi." *J. Microsc. Ultrastruct.*, 3(1), 29–37.

Dhiman, N., Singh, A., Verma, N. K., Ajaria, N., and Patnaik, S. (2017). "Statistical optimization and artificial neural network modeling for acridine orange dye degradation using in-situ synthesized polymer capped ZnO nanoparticles." *J. Colloid Interface Sci.*, 493, 295–306.

Du, J., Yu, X., Wu, Y., and Di, J. (2013). "ZnS nanoparticles electrodeposited onto ITO electrode as a platform for fabrication of enzyme-based biosensors of glucose." *Mater. Sci. Eng. C*, 33(4), 2031–2036.

Dubertret, B., Skourides, P., Norris, D.J., Noireaux, V., Brivanlou, A.H, and Libchaber, A. (2002). "In vivo imaging of quantum dots encapsulated in phospholipid micells." *Science.*, 298, 1759–1762.

Durán, N., Marcato, P.D., Alves, O.L., Souza, G.I.H..D., and Esposito, E. (2005). "Mechanistic aspects of biosynthesis of silver nanoparticles by several *Fusarium oxysporum* strains." *J. Nanobiotechnology.,* 3, 8.

Elizabeth, A., Zuleyka, M., Gregory, S. G., Phyllis D. C., and Thomas, A.K. (2000). "Are tropical fungal endophytes hyperdiverse ?" *Ecology letters*, 3,267-274.

El-Gamal, S. M. A., Amin, M. S., and Ahmed, M. A. (2015). "Removal of methyl orange and bromophenol blue dyes from aqueous solution using Sorel's cement nanoparticles." *J. Environ. Chem. Eng.*, 3(3), 1702–1712.

El-Kamash, A. M., Zaki, A. A., and El, M. A. (2005). "Modeling batch kinetics and thermodynamics of zinc and cadmium ions removal from waste solutions using synthetic zeolite A." 127, 211–220.

El-Kemary, M., and El-Shamy, H. (2009). "Fluorescence modulation and photodegradation

characteristics of safranin O dye in the presence of ZnS nanoparticles." *J. Photochem. Photobiol. A Chem.*, 205(2–3), 151–155.

El-Zomrawy, A. A. (2013). "Kinetic studies of photoelectrocatalytic degradation of Ponceau 6R dye with ammonium persulfate." *Journal of Saudi Chemical Society*, 17(4), 397-402.

Erasmus, M., Cason, E.D., Van Marwijk, J., Botes, E., Gericke, M., Van Heerden, E. (2014). "Gold nanoparticle synthesis using the thermophilic bacterium *Thermus scotoductus* SA-01 and the purification and characterization of its unusual gold reducing protein." *Gold Bull.,* 47, 245–253

Fan, H. J., Huang, S. T., Chung, W. H., Jan, J. L., Lin, W. Y., and Chen, C. C. (2009). "Degradation pathways of crystal violet by Fenton and Fenton-like systems: Condition optimization and intermediate separation and identification." *J. Hazard. Mater.*, 171(1–3), 1032–1044.

Fang, X., Zhai, T., Gautam, U. K., Li, L., Wu, L., Bando, Y., and Golberg, D. (2011). "ZnS nanostructures : From synthesis to applications." *Prog. Mater. Sci.*, 56(2), 175–287.

Feldman, Y., Zak, A., Popovitz-Biro, R., and Tenne, R. (2000). "New reactor for production of tungsten disulfide hollow onion-like (inorganic fullerene-like) nanoparticles." *Solid State Sci.*, 2(6), 663–672.

Fowsiya, J., Madhumitha, G., Al-dhabi, N. A., and Valan, M. (2016). "Photocatalytic degradation of Congo red using *Carissa edulis* extract capped zinc oxide nanoparticles." J*ournal of Photochemistry & Photobiology B : Biology.,* 162, 395–401.

Frasco, M. F., and Chaniotakis, N. (2009). "Semiconductor quantum dots in chemical sensors and biosensors." *Sensors*, 9(9), 7266–7286.

Gan, L., Cheng, Y., and Palanisami, T. (2014). "Pathways of reductive degradation of crystal violet in wastewater using free-strain *Burkholderia vietnamiensis* C09V." *Environ Sci Pollut Res.,* 21, 10339–10348.

Gaunt, J. A., Knight, A. E., Windsor, S. A., and Chechik, V. (2005). "Stability and quantum yield effects

of small molecule additives on solutions of semiconductor nanoparticles." *J.Colloid Interface Sci.*, 290, 437–443.

Goharshadi, E. K., Mehrkhah, R., and Nancarrow, P. (2013). "Synthesis, characterization, and measurement of structural, optical, and phtotoluminescent properties of zinc sulfide quantum dots." *Mater. Sci. Semicond. Process.*, 16(2), 356–362.

Georgiev, P., Bojinova, A., Kostova, B., Momekova, D., Bjornholm, T., and Balashev, K. (2013). "Implementing atomic force microscopy (AFM) for studying kinetics of gold nanoparticle ' s growth." *Colloids Surf A Physicochem Eng Asp.,* 434, 154–163.

Gekeler, W., Grill, E., Winnacker, E. L., and Zenk, M. H. (1988). "Algae sequester heavy metals via synthesis of phytochelatin complexes." *Arch. Microbiol.*, 150(2), 197–202.

Graham, N., Jiang, C. C., Li, X. Z., Jiang, J. Q., and Ma, J. (2004). "The influence of pH on the degradation of phenol and chlorophenols by potassium ferrate." *Chemosphere*, 56(10), 949–956.

Grant, D. J., de Szöcs , J., and Wilson, J. V., (1970). "Utilization of acetylsalicylic acid as sole carbon source and the induction of its enzymatic hydrolysis by an isolated strain of *Acinetobacter lwoffii*" *J Pharm Pharmacol,* 22(6), 461-4

Greert, L. E., and Shelton, D. R. (1992). "Effect of Inoculant Strain and Organic Matter Content on Kinetics of 2, 4-Dichlorophenoxyacetic Acid Degradation in Soil." *American Society for Microbiology.,* 58(5), 1459–1465.

Goharshadi, E. K., Mehrkhah, R., and Nancarrow, P. (2013). "Synthesis, characterization, and measurement of structural, optical, and phtotoluminescent properties of zinc sulfide quantum dots." *Mater. Sci. Semicond. Process.*, 16(2), 356–362.

Gupta, A. K., Pal, A., and Sahoo, C. (2006). "Photocatalytic degradation of a mixture of Crystal Violet (Basic Violet 3) and Methyl Red dye in aqueous suspensions using Ag C doped TiO$_2$." *Dyes and Pigments.,* 69, 224–232.

Gupta, S. Sen., and Bhattacharyya, K. G. (2008). "Immobilization of Pb(II), Cd(II) and Ni(II) ions on kaolinite and montmorillonite surfaces from aqueous medium." *J. Environ. Manage.*, 87(1), 46–58.

Gusseme, B. De, Vanhaecke, L., Verstraete, W., and Boon, N. (2011). "Degradation of acetaminophen by *Delftia tsuruhatensis* and *Pseudomonas aeruginosa* in a membrane bioreactor." *Water Res.*, 45(4), 1829–1837.

Han, Z., Zheng, X., Hu, F., Qu, F., Umar, A., and Wu, X. (2015). "Facile synthesis of hollow ZnS nanospheres for environmental remediation." *Mater. Lett.*, 160, 271–274.

Hart, A., and Orr, D. L. J. (1974). "The degradation of paracetamol (4-hydroxyacetanilide) and other substituted acetanilides by a *Penicillium species*." *Antonie Van Leeuwenhoek*, 41(1), 239–247

Haugland, R. A., Schlemm, D. J., and Sferra, P. R. (1990). "Degradation of the Chlorinated Phenoxyacetate Herbicides." *Appl. Environ. Microbiol.*, 56(5), 1357–1362.

Hennebel, T., Nevel, S. Van, Verschuere, S., Corte, S. De, Gusseme, B. De, Cuvelier, C., Fitts, J. P., Lelie, D. Van Der, Boon, N., and Verstraete, W. (2011). "Palladium nanoparticles produced by fermentatively cultivated bacteria as catalyst for diatrizoate removal with biogenic hydrogen." *Appl. Microbiol. Biotechnol.*, 91(5), 1435–1445.

Hedberg, Y. S., Pradhan, S., Cappellini, F., Karlsson, M.E., Blomberg, E., Karlsson, H. L., Odnevall, W. I., and Hedberg, J. F. (2016). "Electrochemical surface oxide characteristics of metal nanoparticles (Mn, Cu and Al) and the relation to toxicity." *Electrochim. Acta.*, 212, 360–371.

Hisaindee, S., Meetani, M. A., and Rauf, M. A. (2013). "Application of LC-MS to the analysis of advanced oxidation process (AOP) degradation of dye products and reaction mechanisms." *Trends in Analytical Chemistry.,* 49, 31–44.

Huang, C., Lo, S., and Lien, H. (2013). "Synergistic effect of zero-valent copper nanoparticles on dichloromethane degradation by vitamin B 12 under reducing condition." *Chemical Engineering Journal.,* 219, 311–318.

Hudlikar, M., Joglekar, S., Dhaygude, M., and Kodam, K. (2012). "Latex-mediated synthesis of ZnS nanoparticles: Green synthesis approach." *J. Nanoparticle Res.*, 14 (5) 865.

Hulkoti, N.I., and Taranath, T.C. (2014). "Biosynthesis of nanoparticles using microbes-A review." *Colloids Surfaces B Biointerfaces.*, 121, 474–483.

Ibhadon, A. O., and Fitzpatrick, P. (2013). "Heterogeneous Photocatalysis: Recent Advances and Applications." *Catalysts.*, 3, 189–218.

Jaafarzadeh, N., Ghanbari, F., and Ahmadi, M. (2017). "Efficient degradation of 2,4-D by peroxymonosulfate / magnetic copper ferrite nanoparticles / ozone : A novel combination of advanced oxidation processes." *Chemical Engineering Journal.*, 320, 436–447.

Jabeen, U., Mujtaba, S., and Ullah, S. (2017). "Photo catalytic degradation of Alizarin red S using ZnS and cadmium doped ZnS nanoparticles under unfiltered sunlight." *Surfaces and Interfaces*, 6, 40–49.

Jafari, S., Azizian, S., and Jaleh, B. (2012). " Enhancement of methyl violet removal by modification of TiO_2 nanoparticles with AgI." *J. Ind. Eng. Chem.*, 18(6), 2124–2128.

Jain, N., Bhargava, A., Majumdar, S., Tarafdar, J. C., and Panwar, J. (2011). "Extracellular biosynthesis and characterization of silver nanoparticles using *Aspergillus flavus* NJP08: a mechanism perspective." *Nanoscale*, 3(2), 635–641.

Jagannathan, M., Grieser, F., and Ashokkumar, M. (2013). "Sonophotocatalytic degradation of paracetamol using TiO_2 and Fe^{3+}." *Sep. Purif. Technol.*, 103, 114–118.

Jallouli, N., Elghniji, K., Trabelsi, H., and Ksibi, M. (2017). "Photocatalytic degradation of paracetamol on TiO_2 nanoparticles and TiO_2/cellulosic fiber under UV and sunlight irradiation." *Arab. J. Chem.*, 10, 3640–3645.

Jayavel, G. M. R., and Kumar, M. R. (2016). "Synthesis , optical , photocatalytic , and electrochemical studies on Ag_2S / ZnS and ZnS / Ag_2S nanocomposites." *Applied Nanoscience.*, 4 (6) 503–510.

Jalgaonwala, R. E., Mohite, B. V., and Mahajan, R. T. (2011). "A review : Natural products from

plant associated endophytic fungi." *J. Microbiol. Biotech. Res.,* 1(2), 21–32.

Jeyasubramanian, K., Hikku, G. S., and Sharma, R. K. (2015). " Photo-catalytic degradation of methyl violet dye using zinc oxide nano particles prepared by a novel precipitation method and its anti-bacterial activities." *J. Water Process Eng.*, 8, 35–44.

Jha, A. K., and Prasad, K. (2012). "Biological synthesis of cobalt ferrite nanoparticles." *Nanotechnol. Dev.*, 2(1), 1-9.

Juan, Y., Jun, D. A. I., Jincai, Z., and Juan, M. (2010). "Mechanism of photocatalytic degradation of dye MG by TiO$_2$ -film electrode with cathodic bias potential." *Chinese Science Bulletin.,* 55(2), 131–139.

Kaneva, N., Bojinova, A., Papazova, K., and Dimitrov, D. (2016). "Effect of thermal and mechano-chemical activation on the photocatalytic efficiency of ZnO for drugs degradation."*Arch Pharm Res.,* 39(10) 1418-1425

Kaur, S., Sharma, S., and Kumar, S. (2016). "Synthesis of ZnS / CQDs nanocomposite and its application as a photocatalyst for the degradation of an anionic dye , ARS." *Superlattices and Microstructures.,* 98, 86–95.

Kaul, S., Gupta, S., Ahmed, M., and Dhar, M. K. (2012). "Endophytic fungi from medicinal plants : a treasure hunt for bioactive metabolites." 11 (2) 487–505.

Kavitha, S. R., Umadevi, M., Janani, S. R., Balakrishnan, T., and Ramanibai, R. (2014). "Fluorescence quenching and photocatalytic degradation of textile dyeing waste water by silver nanoparticles." *Spectrochim. Acta - Part A Mol. Biomol. Spectrosc.*, 127, 115–121.

Khan, J. A., He, X., Shah, N. S., Khan, H. M., Hapeshi, E., Fatta-Kassinos, D., and Dionysiou, D. D. (2014). "Kinetic and mechanism investigation on the photochemical degradation of atrazine with activated H$_2$O$_2$, S$_2$O8^{2-} and HSO$_5^-$." *Chem. Eng. J.*, 252, 393–403.

Khataee, A., Karimi, A., Arefi-oskoui, S., Darvishi, R., Soltani, C., Hanifehpour, Y., Soltani, B., and Woo, S. (2015). "Sonochemical synthesis of Pr-doped ZnO nanoparticles for sonocatalytic degradation

of Acid Red 17." *Ultrasonics Sonochemistry.,* 22, 371–381.

Kooh, M.R.R., Dahri, M.K., and Lim, L.B.L. (2017). "Removal of methyl violet 2B dye from aqueous solution using *Nepenthes rafflesiana* pitcher and leaves." *Appl. Water Sci.,* 7, 3859-3868.

Kuo, W., and Chen, W. (2012). "Solar Photocatalytic Degradation of Azo Dye in Aqueous TiO_2 Suspension Assisted by Fresnel Lens." *International Journal of Photoenergy.,* 2012(1), 1–8.

Kim, J., and Grate, J. W. (2003). "Single-enzyme nanoparticles armoured by a nanometer-scale organic/inorganic network." *Nano Letters.,* 3, 1219–1222

Kitching, M., Ramani, M., and Marsili, E. (2015). "Fungal biosynthesis of gold nanoparticles: Mechanism and scale up." *Microb. Biotechnol.*, 8(6), 904–917.

Kumar, S., Sood, S., Umar, A., and Mehta, S. K. (2013). "Photocatalytic degradation of Eriochrome Black T dye using well-crystalline anatase TiO_2 nanoparticles." 581, 392–397.

Lee, H., Hoon, S., Park, Y., Kim, S., Seo, S., Jin, S., and Jung, S. (2015). "Photocatalytic reactions of 2,4-dichlorophenoxyacetic acid using a microwave-assisted photocatalysis system." *Chemical Engineering Journal.,* 278, 259–264.

Lee, J. B., Kim, H. Y., Jang, Y. M., Song, J. Y., Woo, S. M., Park, M. S., Lee, H. S., Lee, S. K., and Kim, M. (2016). "Determination of malachite green and crystal violet in processed fish products." *Food Addit Contam Part A Chem Anal Control Expo Risk Assess.,* 27 (7) 953-61

Lee, J., Lim, J., Velmurugan, P., Park, Y., Park, Y., Bang, K., and Oh, B. (2016). "Photobiologic-mediated fabrication of silver nanoparticles with antibacterial activity." *Journal of Photochemistry & Photobiology B : Biology*., 162, 93–99.

Lee, E.J., Moh, S.H., and Paek, K.Y. (2011). "Influence of inoculum density and aeration volume on biomass and bioactive compound production in bulb-type bubble bioreactor cultures of *Eleutherococcus koreanum* Nakai." *Bioresour. Technol.,* 102, 7165–7170.

Li, J., Ng, D. H. L., Song, P., Kong, C., and Song, Y. (2015). "Synthesis of SnO₂ activated carbon fiber hybrid catalyst for the removal of methyl violet from water." *Mater. Sci. Eng. B*, 194, 1–8.

Li, J., Yu, Y., Wang, Y., Qian, J., and Zhi, J. (2013). "The benzoquinone-mediated electrochemical microbial biosensor for water biotoxicity assay." *Electrochim. Acta*, 97, 52–57.

Li, X., Huang, Y., Chen, J., and Tao, X. (2012). "Visible light-driven binary dyes synergic degradation by iodine-doped TiO₂ nanocrystal film." *Catalysis Communications.*, 20, 94–98.

Liu, B., Zhao, X., Terashima, C., Fujishima, A., and Nakata, K. (2014). "Thermodynamic and kinetic analysis of heterogeneous photocatalysis for semiconductor systems." *Phys. Chem. Chem. Phys.*, 16(19), 8751–8760.

Liu, C., Zhang, L., Liu, R., Gao, Z., Yang, X., Tu, Z., Yang, F., Ye, Z., Cui, L., Xu, C., and Li, Y. (2016). "Hydrothermal synthesis of N-doped TiO₂ nanowires and N-doped graphene heterostructures with enhanced photocatalytic properties." *J. Alloys Compd.,* 656, 24-32

Luna, A. J., Chiavone-filho, O., Machulek, A., Ermírio, J., Moraes, F. De, and Nascimento, C. A. O. (2012). "Photo-Fenton oxidation of phenol and organichlorides (2,4-DCP and 2,4-D) in aqueous alkaline medium with high chloride concentration." *J. Environ Manage.,* 111, 10–17.

Malarkodi, C., Rajeshkumar, S., Paulkumar, K., Jobitha, G. G., and Vanaja, M. (2013). "Biosynthesis of semiconductor nanoparticles by using sulfur reducing bacteria *Serratia nematodiphila*." *Advances in nano research.,* 1(2), 83–91.

Maltseva, O., Mcgowan, C., Fulthorpet, R., and Oriel, P. (1996). "Degradation of 2,4-dichlorophenoxyacetic acid by haloalkaliphilic bacteria." *Microbiology., 1*42, 1115-22

Mandal, D., Bolander, M.E., Mukhopadhyay, D., Sarkar, G. and Mukherjee, P. (2006). "The use of microorganisms for the formation of metal nanoparticles and their application." *Appl. Microbiol.,* 69, 485-92.

Manirethan, V., Raval, K., Rajan, R., Thaira, H., and Balakrishnan, R. M. (2018). "Kinetic and

thermodynamic studies on the adsorption of heavy metals from aqueous solution by melanin nanopigment obtained from marine source: *Pseudomonas stutzeri.*" *J. Environ. Manage.*, 214, 315–324.

Mansur, A. A. P., Mansur, H. S., Ramanery, F. P., Carlos, L., and Souza, P. P. (2014). " Green colloidal ZnS quantum dots / chitosan nano-photocatalysts for advanced oxidation processes : Study of the photodegradation of organic dye pollutants." *"Applied Catal. B, Environ.*, 158–159, 269–279.

Mantzouridou, F. T., and Naziri, E. (2017). "Scale translation from shaken to diffused bubble aerated systems for lycopene production by *Blakeslea trispora* under stimulated conditions." *Appl. Microbiol. Biotechnol.*, 101(5), 1845–1856.

Mary, J. J., Raj, M. B., and Bardhan, S.K (2013). "Selenium and lead tolerance in fungi isolated from sea water." *Int. J. Inno. Res. Sc. Eng. Tech.,* 2(7), 2975–2982.

Mary, J. J., Mohan, R., and Bhat, U. (2014). "Biosynthesis of lead selenide quantum rods in marine *Aspergillus terreus.*" *Mater. Lett.*, 124, 279–281.

Maya-treviño, M. L., Guzmán-mar, J. L., Hinojosa-reyes, L., and Ramos-delgado, N. A. (2014). "Activity of the ZnO – Fe$_2$O$_3$ catalyst on the degradation of Dicamba and 2 , 4-D herbicides using simulated solar light." *Ceram. Int.*, 40(6), 8701–8708.

Mehra, R.K., and Winge, D.R. (1991). "Metal ion resistance in fungi: Molecular mechanisms and their regulated expression." *J. Cell. Biochem.,* 45, 30–40.

Mehta, S. K., Kumar, S., and Gradzielski, M. (2011). "Growth, stability , optical and photoluminescent properties of aqueous colloidal ZnS nanoparticles in relation to surfactant molecular structure." *J. Colloid Interface Sci..,* 360, 497–507.

Mirzadeh, S., Darezereshki, E., Bakhtiari, F., Fazaelipoor, M. H., and Hosseini, M. R. (2013). "Characterization of zinc sulfide (ZnS) nanoparticles Biosynthesized by *Fusarium oxysporum.*" *Mater. Sci. Semicond. Process.*, 16(2), 374–378.

Mittal, A.K., Chisti, Y., and Banerjee, U.C. (2013). "Synthesis of metallic nanoparticles using

 plant extracts." *Biotechnol. Adv.,* 31, 346–356.

Moctezuma, E., Leyva, E., Aguilar, C. A., Luna, R. A., and Montalvo, C. (2012). "Photocatalytic degradation of paracetamol : Intermediates and total reaction mechanism." *J. Hazard. Mater.*, 243, 130–138.

Mohanpuria, P., Rana, N. K., and Yadav, S. K. (2008). "Biosynthesis of nanoparticles: Technological concepts and future applications." *J. Nanoparticle Res.*, 10(3), 507–517.

Moon, J.-W., Rawn, C. J., Rondinone, A. J., Love, L. J., Roh, Y., Everett, S. M., Lauf, R. J., and Phelps, T. J. (2010). "Large-scale production of magnetic nanoparticles using bacterial fermentation." *J. Ind. Microbiol. Biotechnol.*, 37, 1023–1031.

Moritz, M., and Geszke-moritz, M. (2013). "The newest achievements in synthesis , immobilization and practical applications of antibacterial nanoparticles." *Chem Eng J.,* 228, 596–613.

Moteshafi, H., Mousavi, S. M., and Shojaosadati, S. A. (2012). "The possible mechanisms involved in nanoparticles biosynthesis." *J. Ind. Eng. Chem.*, 18(6), 2046–2050.

Murugadoss, G., Jayavel, R., Thangamuthu, R., and Kumar, M. R. (2016). "PbO/CdO/ZnO and PbS/CdS/ZnS nanocomposites: Studies on optical, electrochemical and thermal properties." *J. Lumin.*, 170, 78–89.

Musavi, S. F., and Balakrishnan, R. M. (2013). "Placement of an Endophytic *Fusarium oxysporum* NFX 06 Isolated from *Nothapodytes foetida.*" *Journal of Mycology.,* 2013,1-10

Naeimi, H., and Kiani, F. (2015). "Ultrasound-promoted one-pot three component synthesis of tetrazoles catalyzed by zinc sulfide nanoparticles as a recyclable heterogeneous catalyst." *Ultrason. Sonochem.*, 27, 408–415.

Nezamzadeh-Ejhieh, A., and Banan, Z. (2012). "Sunlight assisted photodecolorization of crystal violet catalyzed by CdS nanoparticles embedded on zeolite A." *Desalination*, 284, 157–166.

Nomura, T., Kuriyama, Y., Tokumoto, H., and Konishi, Y. (2015). "Cytotoxicity of functionalized

polystyrene latex nanoparticles toward lactic acid bacteria, and comparison with model microbes." *J. Nanoparticle Res.*, 17(2), 1–10

Nichols, W. T., Keto, J. W., Henneke, D. E., Brock, J. R., Malyavanatham, G., Becker, M. F., and Glicksman, H. D. (2001). "Large-scale production of nanocrystals by laser ablation of microparticles in a flowing aerosol." *Appl. Phys. Lett.*, 78(8), 1128–1130.

Nikitin, N., Trifonova, E., Evtushenko, E., Kirpichnikov, M., Atabekov, J., and Karpova, O. (2015). "Comparative Study of Non-Enveloped Icosahedral Viruses Size." 10, 1–11.

Nisa, H., Kamili, A. N., Nawchoo, I. A., Shafi, S., Shameem, N., and Bandh, S. A. (2015). "Fungal endophytes as prolific source of phytochemicals and other bioactive natural products: A review." *Microb. Pathog.*, 82 50–59.

Ogram, A. V, Jessup, R. E., Ou, L. T., and Rao, P. S. C. (1985). "Effects of sorption on biological degradation rates of 2,4- Dichlorophenoxy acetic acid in soils." *Appl. Environ. Microbiol.*, 49(3), 582–587.

Onwudiwe, D. C., Krüger, T. P. J., Jordaan, A., and Strydom, C. A. (2014). "Laser-assisted synthesis, and structural and thermal properties of ZnS nanoparticles stabilised in polyvinylpyrrolidone." *Appl. Surf. Sci.*, 321, 197–204.

Onwudiwe, D. C., Krüger, T. P. J., and Strydom, C. A. (2014). "Laser assisted solid state reaction for the synthesis of ZnS and CdS nanoparticles from metal xanthate." *Mater. Lett.*, 116, 154–159.

Onwudiwe, D. C., and Strydom, C. A. (2015). "The bipyridine adducts of N-phenyldithiocarbamato complexes of Zn (II) and Cd (II); synthesis, spectral, thermal decomposition studies and use as precursors for ZnS and CdS nanoparticles." *Spectrochim. Acta Part A Mol. Biomol. Spectrosc.*, 135, 1080–1089.

Paraszkiewicz, K., Bernat, P., Naliwajski, M., and Długoński, J. (2010). "Lipid peroxidation in the fungus *Curvularia lunata* exposed to nickel." *Arch. Microbiol.* 192, 135–141. doi:10.1007/s00203-009-0542-3

Pal, S., Patra, A. S., Ghorai, S., Sarkar, A. K., Mahato, V., Sarkar, S., and Singh, R. P. (2015). "Efficient and rapid adsorption characteristics of templating modified guar gum and silica nanocomposite toward removal of toxic reactive blue and Congo red dyes." *Bioresour. Technol.*, 191, 291–299.

Perales-Vela, H. V., Peña-Castro, J. M., and Cañizares-Villanueva, R. O. (2006). "Heavy metal detoxification in eukaryotic microalgae." *Chemosphere*, 64(1), 1–10.

Poornaprakash, B., Reddy, D. A., Murali, G., Rao, N. M., Vijayalakshmi, R. P., and Reddy, B. K. (2013). "Composition dependent room temperature ferromagnetism and PL intensity of cobalt doped ZnS nanoparticles." *J. Alloys Compd.*, 577, 79–85.

Prasanth, S., Irshad, P., Raj, D. R., Vineeshkumar, T. V., Philip, R., and Sudarsanakumar, C. (2015). "Nonlinear optical property and fluorescence quenching behavior of PVP capped ZnS nanoparticles co-doped with Mn^{2+} and Sm^{3+}." *J. Lumin.*, 166, 167–175.

Pimentel, M. R., Molina, G., Dionísio, A. P., Maróstica Junior, M. R., and Pastore, G. M. (2011). "The Use of Endophytes to Obtain Bioactive Compounds and Their Application in Biotransformation Process." *Biotechnol. Res. Int.*, 2011, 1–11.

Qian, Y., Yu, H., He, D., and Yang, H. (2013). "Biosynthesis of silver nanoparticles by the endophytic fungus *Epicoccum nigrum* and their activity against pathogenic fungi." *Bioprocess Biosyst Eng.,* 36 (11)1613–1619.

Qutub, N., Pirzada, B. M., Umar, K., Mehraj, O., Muneer, M., and Sabir, S. (2015). "Synthesis , characterization and visible-light driven photocatalysis by differently structured CdS / ZnS sandwich and core – shell nanocomposites." *Physica E Low Dimens Syst Nanostruct.,*74, 74–86.

Rad, L. R., Irani, M., Divsar, F., Pourahmad, H., Sayyafan, M. S., and Haririan, I. (2015). "Simultaneous

degradation of phenol and paracetamol during photo-Fenton process: Design and optimization." *J. Taiwan Inst. Chem. Eng.*, 47, 190–196.

Radhu, S., and Vijayan, C. (2011) "Observation of red emission in wurtzite ZnS nanoparticles and the investigation of phonon modes by Raman spectroscopy." *Mater. Chem. Phys*., (129)1132–1137.

Ray, T.R., Lettiere, B., Rutte, J., and Pennathur,S. (2015). "Quantitative characterization of the colloidal stability of metallic nanoparticles using UV–vis absorbance spectroscopy."*Langmuir,* 31, 3577–3586.

Ryan, R. P., Germaine, K., Franks, A., Ryan, D. J., and Dowling, D. N. (2008). "Bacterial endophytes : Recent developments and applications." *FEMS Microbiol. Lett.*, 278(1), 1–9.

Raheman, F., Deshmukh, S., Ingle, A., Gade, A., and Rai, M. (2011). "Silver Nanoparticles : Novel Antimicrobial Agent Synthesized from an Endophytic Fungus *Pestalotia* sp . Isolated from leaves of *Syzygium*" 3(3), 174-178

Reddy, D. A., Liu, C., Vijayalakshmi, R. P., and Reddy, B. K. (2014). "Effect of Al doping on the structural , optical and photoluminescence properties of ZnS nanoparticles." *J. Alloys Compd.*, 582, 257–264.

Rodríguez Porcel, E. M., Casas López, J. L., Sánchez Pérez, J. A., Fernández Sevilla, J. M., and Chisti, Y. (2005). "Effects of pellet morphology on broth rheology in fermentations of Aspergillus terreus." *Biochem. Eng. J.*, 26(2–3), 139–144.

Sadeghi, R., Etemad, S. G., Keshavarzi, E., and Haghshenasfard, M. (2015). "Investigation of alumina nanofluid stability by UV–vis spectrum." *Microfluid. Nanofluidics*, 18(5–6), 1023–1030.

Sandmann, E . R . I . C ., and Loos, M.A, (1984) "Enumeration of 2 , 4-D degrading microorganisms in soils and crop plant rhizospheres using indicator media ; high populations associated with sugarcane (*Saccharum Officinarum*) ." *Chemosphere.,* 13(9), 1073–1084.

Saharan, P., Chaudhary, G. R., Lata, S., Mehta, S. K., and Mor, S. (2015). "Ultra fast and effective treatment of dyes from water with the synergistic effect of Ni doped ZnO nanoparticles and ultrasonication." *Ultrason. Sonochem.*, 22, 317–325.

Sakthivel, S., Neppolian, B., Shankar, M. V, Arabindoo, B., Palanichamy, M., and Murugesan, V. (2003). "Solar photocatalytic degradation of azo dye: comparison of photocatalytic efficiency of ZnO and TiO$_2$." *Sol. Energy Mater. Sol. Cells*, 77(1), 65–82.

Salvadori, M.R., Nascimento, C.A.O., and Corrêa, B. (2014). "Nickel oxide nanoparticles film produced by dead biomass of filamentous fungus." *Sci. Rep*. 4, 6404.

Samir, R., Essam, T., Ragab, Y., and Hashem, A. (2015). "Enhanced photocatalytic-biological degradation of 2 , 4 dichlorophenoxyacetic acid." *Bull. Fac. Pharmacy, Cairo Univ.*, 53(2), 77–82.

Sandana M. J. G., and Rose, C. (2014). "Facile production of ZnS quantum dot nanoparticles by *Saccharomyces cerevisiae* MTCC 2918." *J. Biotechnol.*, 170(1), 73–78.

Sanghi, R., and Verma, P. (2009). "A facile green extracellular biosynthesis of CdS nanoparticles by immobilized fungus." *Chem. Eng. J.*, 155(3), 886–891.

Saraswathi, V. S., Tatsugi, J., Shin, P., and Santhakumar, K. (2017). "Facile biosynthesis , characterization , and solar assisted photocatalytic effect of ZnO nanoparticles mediated by leaves of L . speciosa." *J. Photochem. Photobiol. B Biol.*, 167, 89–98.

Saikkonen, K., Young, C. A., Helander, M., and Schardl, C. L. (2016). "Endophytic Epichloë species and their grass hosts: from evolution to applications." *Plant Mol. Biol.*, 90(6), 665–675

Schenone, A. V., Conte, L. O., Botta, M. A., and Alfano, O. M. (2015). "Modeling and optimization of photo-Fenton degradation of 2,4-D using ferrioxalate complex and response surface methodology (RSM)." *J. Environ. Manage.*, 155, 177–183.

Schiefelbein, S., Fröhlich, A., John, G.T., Beutler, F., Wittmann, C., Becker, J. (2013). "Oxygen supply in disposable shake-flasks: Prediction of oxygen transfer rate, oxygen saturation and maximum cell

concentration during aerobic growth." *Biotechnol. Lett.,*. 35, 1223–1230.

Shah, M. (2014). "Biodegradation of Azo Dyes by Three Isolated Bacterial Strains : An Environmental Bioremedial Approach." *J. Microb. Biochem Technol*, S3-007,1948-5948.

Shakir, M., Faraz, M., Asif, M., and Al-resayes, S. I. (2016). "Photocatalytic degradation of the Paracetamol drug using Lanthanum doped ZnO nanoparticles and their in-vitro cytotoxicity assay." *J. Lumin.*, 176, 159–167.

Shamsipur, M., and Rajabi, H. R. (2014). "Study of photocatalytic activity of ZnS quantum dots as efficient nanoparticles for removal of methyl violet: Effect of ferric ion doping." *Spectrochim. Acta - Part A Mol. Biomol. Spectrosc.*, 122, 260–267.

Sheela, T., Nayaka, Y. A., Viswanatha, R., Basavanna, S., and Venkatesha, T. G. (2012). "Kinetics and thermodynamics studies on the adsorption of Zn (II), Cd (II) and Hg (II) from aqueous solution using zinc oxide nanoparticles." *Powder Technol.*, 217, 163–170.

Singh, D., Rathod, V., Ninganagouda, S., Herimath, J., and Kulkarni, P. (2013). "Biosynthesis of silver nanoparticle by endophytic fungi *Pencillium* sp . isolated from *Curcuma longa* (turmeric) and its antibacterial activity against pathogenic gram negative bacteria." *J. Pharm. Res.*, 7(5), 448–453.

Singh, K. P., Gupta, S., Singh, A. K., and Sinha, S. (2011). "Optimizing adsorption of crystal violet dye from water by magnetic nanocomposite using response surface modeling approach." *J. Hazard. Mater.,* 186, 1462–1473.

Singh, R., and Bishnoi, N.R. (2015). "Biotransformation dynamics of chromium(VI) detoxification using *Aspergillus flavus* system." *Ecol. Eng.,* 75, 103–109.

Singh, R., Kumar, M., and Bishnoi, N.R. (2016). "Development of biomaterial for chromium (VI) detoxification using *Aspergillus flavus* system supported with iron." *Ecol. Eng.* 91, 31–40.

Sinha, T., and Ahmaruzzaman, M. (2015). "Biogenic synthesis of Cu nanoparticles and its degradation behavior for methyl red." *Mater. Lett.*, 159, 168–171.

Sinha, T., Ahmaruzzaman, M., and Bhattacharjee, A. (2014). "A simple approach for the synthesis of silver nanoparticles and their application as a catalyst for the photodegradation of methyl violet 6B dye under solar irradiation." *J Environ Chem.,* 2(4), 2269–2279.

Soltani, N., Saion, E., Mat, W. M., Navasery, M., Bahmanrokh, G., Erfani, M., Reza, M., and Gharibshahi, E. (2013). "Photocatalytic degradation of methylene blue under visible light using PVP-capped ZnS and CdS nanoparticles." *Sol. Energy*, 97, 147–154.

Soltani, T., and Entezari, M. H. (2013). "Solar photocatalytic degradation of RB5 by ferrite bismuth nanoparticles synthesized via ultrasound." *Ultrasonics Sonochemistry.,* 20, 1245–1253.

Stark, W. J., and Pratsinis, S. E. (2002). "Aerosol flame reactors for manufacture of nanoparticles." *Powder Technol.*, 126(2), 103–108.

Sun, Y., and Pignatello, J. J. (1993). "Photochemical Reactions Involved in the Total Mineralization of 2,4-D by $Fe^{3+}/H_2O_2/UV$." *Environ. Sci. Technol.*, 27(2), 304–310.

Suganthi, K.S., and Rajan, K.S. (2012)." Temperature induced changes in ZnO–water nanofluid:zeta potential, size distribution and viscosity profiles." *Int. J. Heat Mass Transf.*, 55, 7969–7980.

Tantra, R., Schulze, P., and Quincey, P. (2010). "Effect of nanoparticle concentration on zeta-potential measurement results and reproducibility." *Particuology*, 8(3), 279-285.

Tang, Y., Zhang, G., Liu, C., Luo, S., Xu, X., Chen, L., and Wang, B. (2013). "Magnetic TiO_2 -graphene composite as a high-performance and recyclable platform for efficient photocatalytic removal of herbicides from water." *J. Hazard. Mater.,* 253, 115–122.

Taylor, P., Ying, B., and Lin, G. (2015). "Adsorption and degradation of 2 , 4- dichlorophenoxyacetic acid in spiked soil with Fe nanoparticles supported by biochar." *Acta Agriculturae Scandinavica , Section B — Soil & Plant Science .,* 65, 37–41.

Thakkar, K.N., Mhatre, S.S., and Parikh, R.Y. (2010). "Biological synthesis of metallic nanoparticles." *Nanomedicine Nanotechnology, Biol. Med.* 6, 257–262.

Thi, U., Thuy, D., Quang, N., Parlett, C. M. A., Lalev, G. M., and Wilson, K. (2014). "Synthesis of CuS and CuS / ZnS core / shell nanocrystals for photocatalytic degradation of dyes under visible light." *Catalysis Communications.*, 44, 62–67.

Thi, V. H. T., and Lee, B. K. (2016). "Effective photocatalytic degradation of paracetamol using La-doped ZnO photocatalyst under visible light irradiation." *Mater. Res. Bull.*, 96, 171–182.

Tichonovas, M., Krugly, E., Racys, V., Hippler, R., Kauneliene, V., Stasiulaitiene, I., and Martuzevicius, D. (2013). "Degradation of various textile dyes as wastewater pollutants under dielectric barrier discharge plasma treatment." *Chem. Eng. J.*, 229, 9–19.

Tiya-Djowe, A., Acayanka, E., Lontio-Nkouongfo, G., Laminsi, S., and Gaigneaux, E. M. (2015). "Enhanced discolouration of methyl violet 10B in a gliding arc plasma reactor by the maghemite nanoparticles used as heterogeneous catalyst." *J. Environ. Chem. Eng.*, 3(2), 953–960.

Trajić, J., Kostić, R., Romčević, N., Romčević, M., Mitrić, M., Lazović, V., Balaž, P., and Stojanović, D. (2015) " Raman spectroscopy of ZnS quantum dots." *J. Alloys Compd.*, 637,401–406.

Turchi, C. (1990). "Photocatalytic degradation of organic water contaminants: Mechanisms involving hydroxyl radical attack." *J. Catal.*, 122(1), 178–192.

Velmurugan, R., Krishnakumar, B., Subash, B., and Swaminathan, M. (2013). "Preparation and characterization of carbon nanoparticles loaded TiO_2 and its catalytic activity driven by natural sunlight." *Sol. Energy Mater. Sol. Cells*, 108, 205–212.

Vogna, D., Marotta, R., Napolitano, A., and Ischia, M. (2002). "Advanced Oxidation Chemistry of Paracetamol . UV / H_2O_2 - Induced Hydroxylation / Degradation Pathways and ^{15}N-Aided Inventory of Nitrogenous Breakdown Products ." *J. Org. Chem.*, 67(17), 6143–6151.

Vicentini, F. C., Garcia, L. L. C., Figueiredo-Filho, L. C. S., Janegitz, B. C., and Fatibello-Filho, O. (2016). "A biosensor based on gold nanoparticles, dihexadecylphosphate, and tyrosinase for the determination of catechol in natural water." *Enzyme Microb. Technol.*, 84, 17–23.

Viet, H.T.T., and Lee, B.K. (2017). "Effective photocatalytic degradation of paracetamol using La-doped ZnO photocatalyst under visible light irradiation" *Materials Research Bulletin.,* 96(3), 171-182

Wang, N., Zhu, L., Wang, D., Wang, M., Lin, Z., and Tang, H. (2010). "Sono-assisted preparation of highly-efficient peroxidase-like Fe_3O_4 magnetic nanoparticles for catalytic removal of organic pollutants with H_2O_2." *Ultrason. - Sonochemistry*, 17(3), 526–533.

Warrier, M., Lo, K., Monbouquette, G., and Garcia-garibay, M. A. (2004). "Photocatalytic Reduction of Aromatic Azides to Amines using CdS and CdSe Nanoparticles." *Photochem Photobiol Sci.,* 3 (9), 859-63.

Waterborg, J. H., and Matthews, H. R. (1984). "The lowry method for protein quantitation." *Methods Mol. Biol.*, 1, 1–3.

Wesselinowa, J. M., and Apostolov, A. (1997). "On the origin of the central peak in hydrogen-bonded ferroelectrics." *J. Phys.: Condens. Matter.*, 17(19):3001–3014.

Wu, S., Zhang, L., and Chen, J. (2012). "Paracetamol in the environment and its degradation by microorganisms." *Appl. Microbiol. Biotechnol.*, 96(4), 875–884.

Wu, X., Li, K., and Wang, H. (2009). "Facile synthesis of ZnS nanostructured spheres and their photocatalytic properties." *J Alloy Comp.*, 487, 537–544.

Wu, Y., Zhang, J., Xiao, L., and Chen, F. (2009). "Preparation and characterization of TiO_2 photocatalysts by Fe^{3+} doping together with Au deposition for the degradation of organic pollutants."*Appl Catal B.,* 88, 525–532.

Xiao, X., Ma, X. B., Yuan, H., Liu, P. C., Lei, Y. Bin, Xu, H., Du, D. L., Sun, J. F., and Feng, Y. J. (2015). "Photocatalytic properties of zinc sulfide nanocrystals biofabricated by metal-reducing bacterium *Shewanella oneidensis* MR-1." *J. Hazard. Mater.*, 288, 134–139.

Yao, W. F. W., Guohua L., and Hao Y. G. G., (2002). "The large-scale production of carbon nanotubes in a nano-agglomerate fluidized-bed reactor." *Chem. Phys. Lett.*, 364, 568–572.

Zehentbauer, F. M., Moretto, C., Stephen, R., Thevar, T., Gilchrist, J. R., Pokrajac, D., Richard, K. L., and Kiefer, J. (2014). "Fluorescence spectroscopy of Rhodamine 6G : Concentration and solvent effects." *Spectrochim. Acta - Part A Mol. Biomol. Spectrosc.*, 121, 147–151.

Zhang, L., Hu, J., Zhu, R., Zhou, Q., and Chen, J. (2013). "Degradation of paracetamol by pure bacterial cultures and their microbial consortium." *Appl. Microbiol. Biotechnol.*, 97(8), 3687–3698.

Zhang, Y., Han, C., Nadagouda, M. N., and Dionysiou, D. D. (2015). "The fabrication of innovative single crystal N,F-codoped titanium dioxide nanowires with enhanced photocatalytic activity for degradation of atrazine." *Appl. Catal. B Environ.*, 168–169, 550–558.

Ziylan-Yavaş, A., and Ince, N. H. (2016). "Enhanced photo-degradation of paracetamol on n-platinum-loaded TiO_2: The effect of ultrasound and OH/hole scavengers." *Chemosphere*, 162, 324–332.

Ziylan-yavas, A., Mizukoshi, Y., Maeda, Y., and Ince, N. H. (2015). "Supporting of pristine TiO_2 with noble metals to enhance the oxidation and mineralization of paracetamol by sonolysis and sonophotolysis." *"Applied Catal. B, Environ.*, 172–173, 7–17.

LIST OF PUBLICATIONS

Publications:

- Uddandarao, P., Tina Arun Hingnekar., Balakrishnan, R. M., Eldon R, Rene. (2019). **"Solar assisted photocatalytic degradation of organic pollutants in the presence of biogenic fluorescent ZnS nanocolloids"** Chemosphere (In press).https://doi.org/10.1016/j.chemosphere.2019.05.265

- Uddandarao, P., Balakrishnan, R. M. (2017). **"Thermal and optical characterization of biologically synthesized ZnS nanoparticles synthesized from an endophytic fungus *Aspergillus flavus*: A colorimetric probe in metal detection"**. Spectrochimica Acta Part A: Molecular and Biomolecular Spectroscopy. Vol. 175, Pages 200–207.

- Uddandarao, P., Balakrishnan, R. M. (2016). **"ZnS semiconductor quantum dots production by an endophytic fungus *Aspergillus flavus*"** Materials Science and Engineering: B . 207, 26–32. doi.org/10.1016/j.mseb.2016.01.013

Conferences:

- Raj, M.B., Priyanka, U. and Seenivasaperumal, A. **"Studies on microbial synthesis of ZnS nanocolloids in a stirred tank reactor"** was accepted and presented for "11th CESE conference, International Conference in Challenges in Environmental Science and Engineering" which was conducted from Bangkok, Thailand, 4th -8th November, 2018

- Priyanka, U., Tina, A.H. and Raj, M.B. (2016) **"Solar photocatalysis of methyl violet dye using biological ZnS nanoparticles synthesized from an endophytic fungi *Aspergillus flavus*"** *In:* Rene, E.R., Balakrishnan, R.M., Kiran, M.G., Behera, R.N. and Lens, P.N.L (eds.), In: Abstract book from the 5th International Conference on Research Frontiers in Chalcogen Cycle Science & Technology, Goa, India, December 19-21, pp: 28-29, pp: 14.

UDDANDARAO PRIYANKA

MIG Plot no: 16, Sector: 1, MVP colony, Visakhapatnam Andhra Pradesh, India - 530017

Email ID: uddandaropriyanka@gmail.com , Mobile no: +919591855221

PhD area of research:

"Biosynthesis of ZnS nanoparticles from endophytic fungus Aspergillus flavus for degradation of organic pollutants"

Internship Experience:

- **Water Advanced Research and Innovation (WARI) Internship** at United States of America for a period of 6 months from May 1st to November 1st, 2018 funded by University of Nebraska Lincoln Department of Science and Technology, Govt. of India, the University of Nebraska-Lincoln (UNL), the Daugherty Water for Food Institute (DWFI) and the Indo-U.S. Science and Technology Forum (IUSSTF) on the topic "*Fabrication of TiO$_2$ nanowire membrane for their photocatalytic/antibacterial activity*"

- Summer Course Programme on the topic *"Sensors and Nanotechnology"* at The Russell Berrie Nanotechnology Institute and the faculty of Mechanical Engineering, Technion Israel Institute of Technology, Israel from July 26th to August 24th, 2017 and International Travel Grant for this program is funded by Department of Science and Technology-Science and Engineering Research Board (Application No. - ITS/Off-387/2017-18)

- Summer Research Fellowship Programme on the topic *"Identification of Beijing Strains of Mycobacterium Tuberculosis Using Multiplex PCR"* at National Center for Disease Control, Delhi in collaboration with Indian Academy of Sciences, Bangalore funded by Department of Science and Technology from May and July, 2011

Academic Qualifications:

- Doctorate from National Institute of Technology Karnataka, Surathkal, Karnataka, India from 2014 to 2019 in the Department of Chemical Engineering

- Master's from Pondicherry Central University, Puducherry, India from 2012 to 2014 in the Department of Environmental Engineering and Management with an aggregate of 87 %

- Bachelor's from Andhra University, Visakhapatnam, Andhra Pradesh, India from 2008 to 2012 in the Department of Biotechnology with an aggregate of 80 %

Book Chapters:

- Balakrishnan, R. M., <u>Uddandarao, P.,</u> Keyur, Raval., Ritu, Raval. (2019). **"A perspective of advanced biosensors for environmental monitoring"** in Tools, Techniques and Protocols for Monitoring Environmental Contaminants pp. 19-51 Publisher: Joe Hayton
https://doi.org/10.1016/B978-0-12-814679-8.00002-9

Publications:

- <u>Uddandarao, P.,</u> Tina Arun Hingnekar., Balakrishnan, R. M., Eldon R, Rene. (2019). **"Solar assisted photocatalytic degradation of organic pollutants in the presence of biogenic fluorescent ZnS nanocolloids"** Chemosphere (In press).
https://doi.org/10.1016/j.chemosphere.2019.05.265

- Shiljashree Vijay., Balakrishnan, R. M., Eldon R, Rene., Uddandarao, P. (2019) **"Photocatalytic Degradation of Irgalite Violet Dye using Nickel Ferrite Nanoparticles"** Aqua (In press).

- <u>Uddandarao, P.,</u> Balakrishnan, R. M., Ashok, A., Swarup, S., & Sinha, P. (2019). **"Bioinspired ZnS: Gd Nanoparticles Synthesized from an Endophytic Fungi *Aspergillus flavus* for Fluorescence-Based Metal Detection".** Biomimetics, *4*(1), 11. https://doi.org/10.3390/biomimetics4010011

- <u>Uddandarao, P.,</u> Balakrishnan, R. M. (2017). **"Thermal and optical characterization of biologically synthesized ZnS nanoparticles synthesized from an endophytic fungus *Aspergillus flavus*: A colorimetric probe in metal detection"**. Spectrochimica Acta Part A: Molecular and Biomolecular Spectroscopy. Vol. 175, Pages 200–207.

- <u>Uddandarao, P.,</u> Akshay Gowda, K M., Elisha, M G., Surya Teja, B., Nitish, N., Balakrishnan, R. M. (2016). **"Biologically synthesized PbS nanoparticles for the detection of Arsenic in water"** International Biodeterioration & Biodegradation. DOI No. 10.1016/j.ibiod. 2016.10.009

- <u>Uddandarao, P.,</u> Balakrishnan, R. M. (2016). **"ZnS semiconductor quantum dots production by an endophytic fungus *Aspergillus flavus*"** Materials Science and Engineering: B . 207, 26–32. doi.org/10.1016/j.mseb.2016.01.013

Conferences:

- <u>Priyanka, U.,</u> Raj, M.B., Anurag and Yenduri B.Y. **"Studies on Photocatalytic degradation of methyl violet dye using ZnS nanocolloids and the influence of metal ions"** was accepted and presented for "11th CESE conference, International Conference in Challenges in Environmental Science and Engineering" which was conducted from Bangkok, Thailand, 4th - 8th November, 2018

- Raj, M.B., <u>Priyanka, U.</u> and Seenivasaperumal, A. "**Studies on microbial synthesis of ZnS nanocolloids in a stirred tank reactor**" was accepted and presented for "11th CESE conference, International Conference in Challenges in Environmental Science and Engineering" which was conducted from Bangkok, Thailand, 4th -8th November, 2018

- Priyanka, U. **"Photocatalytic performance of ZnS@CNT nanocomposite membranes for inactivation of emerging pollutants and drug resistant bacteria"** was presented as poster at "Sci-ROI Annual Event, 2018" which is held at University of Chicago, Chicago, USA on September 8-9, 2018.

- Priyanka, U., Banajarani, P., Daniel., S and Siamak., N **"Mitigation of surface and groundwater pollutants of Missouri and Arkansas River Basins"** was presented as poster at "National Institutes for Water Resources Regional Symposium Water Resources of the US Great Plains Region: Status and Future" held at Nebraska Water Center at University of Nebreska Lincoln, Lincoln, USA form October 24-26,2018.

- Priyanka, U., Tina, A.H. and Raj, M.B. (2016) **"Solar photocatalysis of methyl violet dye using biological ZnS nanoparticles synthesized from an endophytic fungi *Aspergillus flavus*"** *In:* Rene, E.R., Balakrishnan, R.M., Kiran, M.G., Behera, R.N. and Lens, P.N.L (eds.), In: Abstract book from the 5th International Conference on Research Frontiers in Chalcogen Cycle Science & Technology, Goa, India, December 19-21, pp: 28-29, pp: 14.

- Laurens, V.H., Priyanka, U., Bram, V., Jo V.C., Raj, M.B. and Abhishek , D. (2016) **"Biosorption of selenium (IV) by *Chlorella vulgaris* using a column reactor."** *In:* Rene, E.R., Balakrishnan, R.M., Kiran, M.G., Behera, R.N. and Lens, P.N.L (eds.), In: Abstract book from the 5th International Conference on Research Frontiers in Chalcogen Cycle Science & Technology, Goa, India, December 19-21, pp: 28-29, pp: 35.

- Priyanka, U., Tasneem, A. and Abbasi, S.A."**Treatment of the wastewater of a typical canteen with a novel bioreactor SHEFROL$^®$** " was accepted and presented for "National conference on Multidisciplinary approaches in Public Health: Innovations Practices and Future Strategies" which was conducted from 21st -23rd Feb,2014

- Priyanka, U., Tasneem, A. and Abbasi, S.A. **"SHEFROL$^®$: A new bioreactor for clean-green and rapid treatment of sewage and other biodegradable wastewater**" was accepted and presented for "National Conference on Hydrology with Special Emphasis on Rain Water Harvesting" which was conducted on 15th -16th Nov,2013

- Priyanka, U., Megha, S. and Aravind, Rai. **"Identification of Beijing strains of *Mycobacterium tuberculosis* using Multiplex PCR"** was accepted and presented for international conference on New Horizons in Biotechnology jointly organized by The Biotech Research Society and CSIR at Trivandrum from 21st to 24th Nov,2011

Technical/Scientific skills:

- Isolation and identification of microbial species
- Expertise in the microbial biosynthesis/hydrothermal synthesis of nanoparticles
- Analysis and data interpretation based on UV-Visible spectroscopy, Photoluminescence spectroscopy, FTIR, SEM, TEM, DLS and XRD
- Handling TOC, HPLC and LC-MS instruments

Interpersonal skills:

- Capability to work independently as well as in group
- Leadership in handling projects
- Demonstrating lab protocols and mentoring students

Declaration:

I hereby declare that all the above given information are true and correct to best of my knowledge and belief.

DATE: 26/06/2019   UDDANDARAO PRIYANKA

PLACE: Visakhapatnam